Fall 2014

Analysis of the Impact of Early Exhaust Valve Opening and Cylinder Deactivation on Aftertreatment Thermal Management and Efficiency for Compression Ignition Engines

Leighton Edward Roberts
Purdue University

Graduate School ETD Form 9
(Revised 01/14)

PURDUE UNIVERSITY
GRADUATE SCHOOL
Thesis/Dissertation Acceptance

This is to certify that the thesis/dissertation prepared

By Leighton E. Roberts

Entitled
Analysis of the Impact of Early Exhaust Valve Opening and Cylinder Deactivation on Aftertreatment Thermal Management and Efficiency for Compression Ignition Engines

For the degree of Master of Science in Mechanical Engineering

Is approved by the final examining committee:

Gregory M. Shaver

Peter H. Meckl

Robert P. Lucht

To the best of my knowledge and as understood by the student in the *Thesis/Dissertation Agreement. Publication Delay, and Certification/Disclaimer (Graduate School Form 32)*, this thesis/dissertation adheres to the provisions of Purdue University's "Policy on Integrity in Research" and the use of copyrighted material.

Gregory M. Shaver

Approved by Major Professor(s): _____

_____

Approved by: David C. Anderson 07/30/2014

Head of the Department Graduate Program Date

ANALYSIS OF THE IMPACT OF EARLY EXHAUST VALVE OPENING AND CYLINDER DEACTIVATION ON AFTERTREATMENT THERMAL MANAGEMENT AND EFFICIENCY FOR COMPRESSION IGNITION ENGINES

A Thesis

Submitted to the Faculty

of

Purdue University

by

Leighton E. Roberts

In Partial Fulfillment of the

Requirements for the Degree

of

Master of Science in Mechanical Engineering

December 2014

Purdue University

West Lafayette, Indiana

Dedicated to my wife and children: Tamara, Stahs, and Ksenia

ACKNOWLEDGMENTS

Most of all, I would like to thank my wife for her love and support she has given to me and for her understanding for all the time spent away from my family to finish this work.

I would like to extend my appreciation for my advisor, Dr. Greg Shaver, for the opportunity to work on such an exciting, cutting-edge research project and for the help and support that he provided to me to accomplish this work. I would like to thank my current and former colleagues in my research team for their help and support, especially Dan Van Alstine, Mark Magee, David Fain, Akash Garg, Chuan Ding, and Aswin Ramesh.

My thanks are extended to the technical staff at Herrick Laboratories, Bob Brown, Ron Evans, Dave Meyer, and Frank Lee for their assistance, as well as to our collaborators at Cummins Inc. and Eaton Corporation: Ed Koeberlein, Ray Shute, Mike Ruth, David Koeberlein, James McCarthy, Jr., and Douglas Nielsen.

TABLE OF CONTENTS

Page

LIST OF TABLES

LIST OF FIGURES

ABSTRACT

Roberts, Leighton E. MSME, Purdue University, December 2014. Analysis of the Impact of Early Exhaust Valve Opening and Cylinder Deactivation on Aftertreatment Thermal Management and Efficiency for Compression Ignition Engines. Major Professor: Gregory M. Shaver, School of Mechanical Engineering.

In order to meet strict emissions regulations, engine manufacturers have implemented aftertreatment technologies which reduce the tailpipe emissions from diesel engines. The effectiveness of most of these systems is limited when exhaust temperatures are low (usually below 200°C to 250°C). This is a problem for extended low load operation, such as idling and during cold start. Use of variable valve actuation, including early exhaust valve opening (EEVO) and cylinder deactivation (CDA), has been proposed as a means to elevate exhaust temperatures. This thesis discusses a research effort focused on EEVO and CDA as potential enablers of exhaust gas temperature increase for aftertreatment thermal management.

EEVO results in hotter exhaust gas, however, more fueling is needed to maintain brake power output. The first study outlines an analysis of the impact of EEVO on exhaust temperature (measured at the turbine outlet) and required fueling. An experimentally validated model is developed which relates fueling increase with EVO timing. This model is used to generate expressions for brake thermal efficiency and turbine out temperature as a function of EVO. Using these expressions the impact of EEVO is evaluated over the entire low-load operating space of the engine. Considering the earliest EVO studied, the model predicts an approximate 30°C to 100°C increase in turbine out temperature, which is sufficient to raise many low-load operating conditions to exhaust temperatures above 250°C. However, the analysis also predicts penalties in brake thermal efficiency as large as 5%.

The second study focuses on the impact of 3-cylinder CDA on exhaust temperature and efficiency at both "loaded" and "unloaded" idle conditions. CDA at idle results in a reduction in air-to-fuel ratio, and heat transfer surface area. This enables an increase in exhaust temperature for aftertreatment thermal management, and an increase in efficiency via reduced pumping and heat transfer losses. At the loaded idle condition, deactivating 3 cylinders provides an increase in exhaust temperature from about 200°C (6-cylinders) to approximately 300°C (3-cylinders), with no fuel economy penalty. Additionally, at the unloaded condition, CDA provides an increase in exhaust temperature of about 20°C, from about 117°C to about 135°C, with a fuel consumption reduction of 15%-26%.

The third study includes additional research motivating CDA as a thermal management strategy. Results of an experimental load sweep with CDA show an increase of about 5% to 7% BTE at low load (1.3 bar) with an increase in exhaust temperature from 166°C to about 245°C. By about 2.5 bar, there is no significant change in BTE, yet an exhaust temperature increase is observed from 215°C to about 340°C. At 6.4 bar, a reduction of about 10% to 15% BTE is observed with a temperature increase from 354°C to about 512°C. As noted above, these are desirable benefits during steady-state; however, when an engine transitions from low to higher load, more air is needed to accompany the additional fuel. During transient operation, the reduced air-fuel ratio as a result of CDA limits the rate at which the load can be increased, as well as the maximum load that can be achieved. In addition to demonstrating the benefits of CDA during steady state operation, this paper identifies challenges with respect to transient operation of CDA for engines incorporating conventional air handling systems - high pressure EGR and variable geometry turbocharging. The transient Federal Test Procedure (FTP) cycle requires a load transition from near zero load to about 6 bar BMEP within approximately one second. This study shows that at low speed (800 rpm), the test engine operating in CDA mode cannot meet the load transition required by the FTP without mode transitioning to conventional 6 cylinder operation. At a moderate speed consistent with highway cruise conditions

(1200 rpm), the transient FTP heavy-duty cycle can be met only by increasing the higher load air-fuel ratio target from ∼18 to ∼21, which reduces the temperature benefit seen from CDA by ∼60°C (from 512°C to 450°C) and increases the NOx from 3.2 to 10.3 g/hp-hr. The load response required for the mid-range cycle cannot be met with CDA due to low air-fuel ratios causing large soot emissions, even when air-fuel ratio is increased to ∼23.

The work presented here provides insight into the thermal management capabilities of EEVO and CDA. EEVO can significantly raise exhaust temperatures; however, this comes at a large efficiency penalty. CDA provides large exhaust temperature increase accompanied by fuel consumption benefits at low load. This thesis demonstrates the benefit of CDA, but illustrates that remaining challenges exist with enabling transient operation.

1. INTRODUCTION

1.1 Motivation

Over the past several decades, the U.S. Environmental Protection Agency (EPA) has tightened regulations on nitrogen oxides (NOx) and particulate matter (PM) from diesel engines. Fig. 1.1 shows the history of these emissions regulations over the past 20 years. Modern regulations demand that these tailpipe emissions be near zero. The most recent regulations (EPA 2010) require that PM be no more than 0.01 g/hp-hr (0.013 g/kWh) and that NOx not exceed 0.2 g/hp-hr (0.27 g/kWh) [1]. CO_2 is also regulated as a greenhouse gas which is reduced by more efficient fuel consumption. Additionally, energy use in the transportation sector is projected to increase over the next four decades, while oil prices are expected to remain high [2]. This is further motivation for engine manufacturers to improve engine efficiencies; higher efficiency engines reduce overall fuel consumption leading to lower CO_2 emissions. However, future improvements in diesel engine efficiency must not compromise the ability to meet the EPA 2010 criteria pollutant regulations.

In the past, engine manufacturers have developed several "on-engine" strategies to meet tailpipe emissions limits. Such strategies include high fuel injection pressure, late fuel injection, and exhaust gas recirculation (EGR) [4]. To meet the present regulations, these strategies must be combined with modern aftertreatment technologies. Typical aftertreatment systems include Selective Catalytic Reduction (SCR) to reduce NOx emissions, a Diesel Oxidation Catalyst (DOC) to reduce unburned hydrocarbons (HC) and carbon monoxide (CO), and a Diesel Particulate Filter (DPF) to reduce PM emissions.

A major drawback with even the most advanced aftertreatment systems is the need to operate within a certain temperature range for emissions conversion efficiency. This

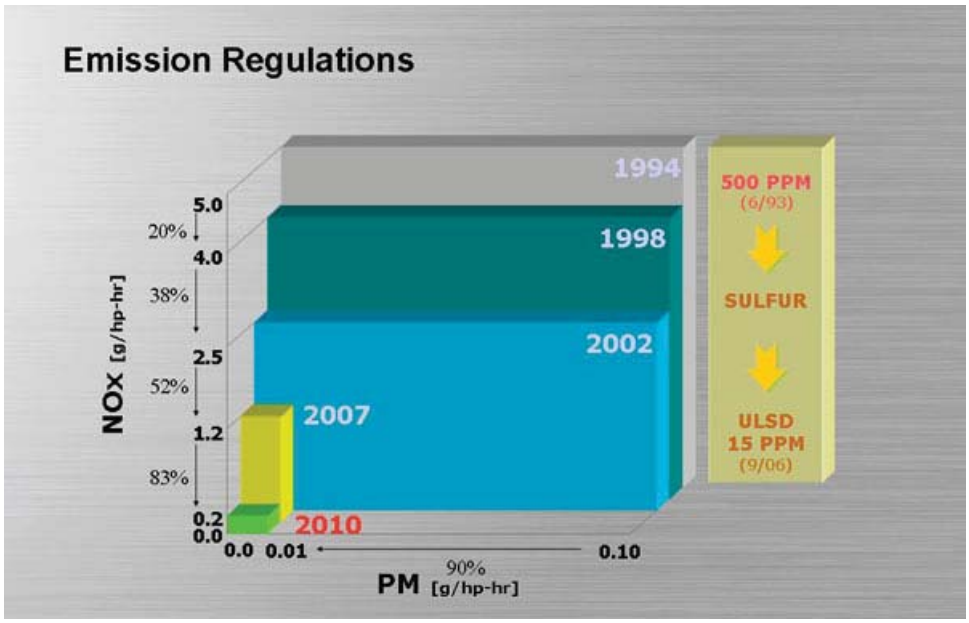

Figure 1.1. Overview of the change to 2010 EPA emissions regulations [3].

is problematic during cold start and at low load engine operation when the exhaust gas temperature is too low to keep the aftertreatment working effectively. Therefore, thermal management is needed for efficient aftertreatment operation over a wide range of duty cycles [5, 6].

Many aftertreatment thermal management strategies penalize fuel consumption. This can be a significant detriment to overall fuel economy for a drive cycle that spends a lot of time in idle. For example, one report from industry shows that operation at idle to meet a particular NOx target on a line haul truck required a 12.5% fuel consumption increase from nominal idle operation [7]. Discovering more efficient thermal management methods would demonstrate a significant fuel consumption improvement. However, maximizing aftertreatment efficiency allows the engine to be operated more efficiently (via increased engine out NOx operation) [2, 5]. The ideal thermal management solution would increase temperature enough to improve the aftertreatment effectiveness while minimizing the fuel consumption penalty.

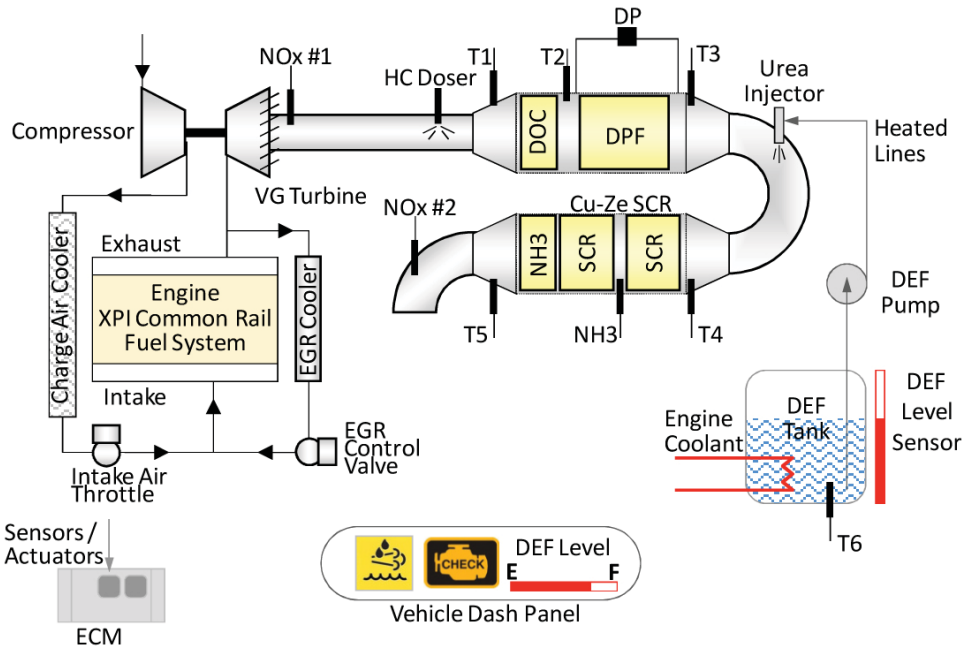

Figure 1.2. Schematic of aftertreatment architecture solution used by Cummins [6].

As will be demonstrated in this thesis, variable valve actuation (VVA) technology is an attractive solution to thermal management. There are many approaches to VVA which have significant thermal management potential. Among these are early exhaust valve opening (EEVO), and cylinder deactivation (CDA).

1.2 Literature Review

1.2.1 Modern Aftertreatment Technology

Fig. 1.2 shows an example of an arrangement of modern aftertreatment catalysts used by Cummins. This solution includes a DOC followed by a DPF. Two copper zeolite SCR units are preceded by a urea injector. All these catalysts are followed by an ammonia oxidation catalyst (AMOx), labeled NH3, used to control ammonia slip [2]. Additionally, a HC doser is placed upstream of the DOC for thermal management.

There are three main functions of the DOC: the conversion of CO to CO_2, the oxidation of HC, and the conversion of NO to NO_2. The main chemical equations that take place supporting each of these functions are listed in order [8]:

$$CO + \frac{1}{2}O_2 \longrightarrow CO_2 \tag{1.1}$$

$$H_xC_y + \left(\frac{x}{4} + y\right) O_2 \longrightarrow yCO_2 + \frac{x}{2}H_2O \tag{1.2}$$

$$NO + \frac{1}{2}O_2 \longrightarrow NO_2. \tag{1.3}$$

The efficiencies of these reactions are different for various catalyst temperatures. HC oxidation is more efficient at higher temperatures (∼400°C) whereas NO conversion is most efficient (∼70%) around 325°C [9, 10]. CO conversion is almost 100% efficient when the DOC is above 200°C. The ability to burn HC is useful, and is utilized in modern systems by injecting additional fuel into the exhaust to heat up the aftertreatment system. This can only take place, however, when the DOC is up to a proper operating temperature. The conversion of NO to NO_2 is desirable for both DPF passive regeneration and SCR NOx conversion efficiencies [8].

A DPF filters the PM out of the exhaust gas by allowing air to pass through a porous material which traps the soot particles. As soot builds up on the filter, the back pressure on the engine increases, reducing the efficiency of the engine. This necessitates regeneration of the DPF, or burning of the carbon particles, to reduce this back pressure [11]. Most often this occurs via passive regeneration, which is the oxidation of soot with NO_2. Passive regeneration occurs at temperatures between 250°C and 400°C and takes place continuously provided there is enough NO_2 available [12]. Fig. 1.3 illustrates how the DOC assists in providing NO_2 for passive regeneration. It should be noted, however, that the total NOx fraction is not reduced through these

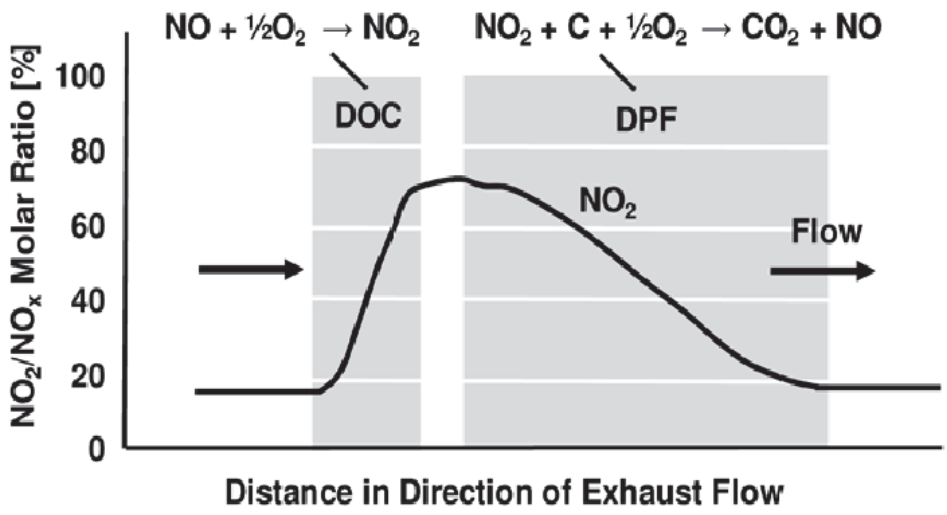

Figure 1.3. NO_2/NOx species ratio through DOC and DPF [1].

catalysts. Occasionally, active regeneration of a DPF might be necessary when conditions are not right for passive regeneration. This involves carbon oxidation using O_2 and requires higher exhaust temperatures (above 550°C). Thermal management solutions are usually required to achieve active regeneration temperatures [1].

The SCR catalysts are effective in converting NOx into N_2 and H_2O with the following main reactions [13]:

$$2NH_3 + NO + NO_2 \longrightarrow 2N_2 + 3H_2O \tag{1.4}$$

$$4NH_3 + 4NO + O_2 \longrightarrow 4N_2 + 6H_2O \tag{1.5}$$

$$8NH_3 + 6NO_2 \longrightarrow 7N_2 + 12H_2O. \tag{1.6}$$

Each of these equations shows the NOx reacting with NH_3. Urea, or diesel exhaust fluid (DEF), is injected upstream of the SCR which decomposes into ammonia and

carbon dioxide in order to deliver the necessary amount of ammonia to the catalysts. This urea can only be injected with catalyst temperatures above 200°C to avoid build up of solid deposits [2,14]. Copper zeolite catalysts are common because they provide high efficiency conversion at relatively low temperatures [2]. Typical operating range for maximum efficiency is between 200°C to 400°C [15]. In order to meet EPA standards, a very high consistent NOx conversion is necessary. Additionally, operation of the SCR to achieve very high NOx conversion efficiencies allows the engine to be run with relaxed engine out NOx constraints which generally improves efficiency [6].

A study performed by Naseri et al. [5] compared four different arrangements of aftertreatment systems from the most basic including DOC, DPF and SCR. The most advanced configuration included an SCR coated DPF, a high porosity high cell density SCR and an ammonia slip catalyst. Each aftertreatment configuration was tested using a cold and hot FTP cycle on a 6 cylinder 9.0 liter HD diesel engine. The researchers reported that the advanced system showed lower than desired NOx conversion performance when subjected to the cold FTP cycle. A thermal management strategy was simulated by preheating the system. The results showed a considerable improvement was possible if thermal management could be used.

Even with most advanced aftertreatment systems, a major drawback is the need to operate the aftertreatment system within a certain temperature range. This is especially problematic at cold start and low loads and idle conditions. Thermal management strategies are needed for efficient aftertreatment operation over a wide range of duty cycles [5, 6].

1.2.2 Thermal Management

Thermal management is engine operation aimed at optimization of aftertreatment effectiveness, including earlier light-off of catalysts and reduced cooling effects of idling during stop-and-go operation [1].

While many exhaust thermal management strategies penalize fuel consumption [1, 8, 16], maximizing aftertreatment efficiency has the potential to improve overall (engine and aftertreatment) system efficiency. This could be accomplished by more efficient engine operation (via relaxed engine out NOx constraint) [2, 5]. However, in general, the ideal thermal management solution would increase temperature enough to improve the aftertreatment effectiveness while minimizing the fuel consumption penalty.

Conventional Approaches

One of the more common approaches to thermal management is modulation of main or post fuel injection timings. Another related option is the dosing of fuel in the exhaust pipe upstream of the DOC for increased HC oxidation in the catalyst, provided the DOC is already operating at a sufficient temperature [11]. Singh et al. [17] showed that dosing of fuel upstream of the DOC does effectively increase temperatures enough for active regeneration in the particulate filter. 99% of the injected HC was oxidized over the DOC and catalyzed particulate filter. Parks et al. [18] compared HC dosing in the exhaust with extended main and post injections in the cylinders in a 4 cylinder 1.7 L engine. They noted that during cold initial conditions, earlier injection strategies are more effective due to the inability of the DOC to oxidize fuel at cooler temperatures. [8] also investigated the use of post and main injection modifications in a 4 cylinder 7.0 L HD engine. The goal of this study was to increase the DOC temperature to increase the NO_2/NO ratio in order to improve the effectiveness of the SCR.

Charlton et al. [1] mentioned the inclusion of a VGT and a common rail high pressure fuel system allows for thermal management flexibility for fast warm-up of the aftertreatment catalysts.

Mayer et al. [19] studied the use of an intake throttle for exhaust temperature increase for the purpose of DPF active regeneration. Their study showed that an intake

throttle can reduce the air flow, such that air-fuel ratios and exhaust temperatures consistent with maximum load operation were achievable at part load. One drawback mentioned was that this method also caused an increase in engine out NOx.

Akiyoshi et al. [20] used a burner at the inlet of the aftertreatment systems to increase catalyst temperatures to meet the 2010 standards. A spark was used in the burner to ignite extra fuel injected upstream of the burner. This showed to be effective for improving SCR light-off time and for active regeneration of the DPF.

Another thermal management strategy has been to implement electrically heated catalysts (EHC). Kim et al. [21] studied the performance of an EHC placed upstream of the DOC. They claimed that nominally the test engine emitted 50% of the total NOx within the first 350 seconds of the FTP75 cycle. The use of the EHC improved NOx conversion to 90% between 150 and 350 seconds of the FTP75 cycle.

Variable Valve Actuation

The potential for variable valve actuation technology as an enabler of aftertreatment thermal management in diesel engines is being researched. VVA possibilities include early intake valve closing (EIVC) or late intake valve closing (LIVC), early exhaust valve opening (EEVO), internal EGR (IEGR) via negative valve overlap (NVO) or a secondary exhaust valve bump [22], as well as cylinder deactivation (CDA).

Both EIVC and LIVC reduce the amount of air trapped at valve closing. In the case of LIVC charge is pushed back into the intake manifold from the cylinder before closing. EIVC prevents charges from entering the cylinder. These methods reduce the effective compression ratio and volumetric efficiency. This results in lower NOx emissions and reduced air-fuel ratio, which results in hotter exhaust temperature. Opening the exhaust valve early reduces the work done on the piston during the expansion stroke resulting in a reduction in brake torque. With less energy extracted as work on the piston more energy remains in the form of heat which is expelled through the exhaust [23]. IEGR is accomplished by trapping hot exhaust gas with

NVO or by opening the exhaust valve for a brief time during the intake stroke to re-induct hot exhaust. This provides EGR without sending the exhaust through a cooler which provides hotter exhaust temperatures. CDA is accomplished by keeping the valves shut and injecting no fuel. This prevents the deactivated cylinders from breathing air. This reduction of airflow through the engine results in lower air-fuel ratios causing exhaust gas temperatures to increase.

Several studies have been performed researching the effects of these strategies. De Ojeda [24] studied EIVC on a 6.4 liter V8 diesel with a lost motion electro-hydraulic VVA device. He found that EIVC could achieve a 100°C increase in the exhaust manifold with a 5% improvement in fuel consumption and reduced soot at a constant NOx level. He claims that this method is more efficient than intake throttling or late post injection or HC dosing.

Garg et al. [25] used a 6 cylinder diesel equipped with an electro-hydraulic VVA system to study IVC modulation. They found that IVC modulation provides a substantial increase in exhaust temperature due to the reduced volumetric efficiency and air-fuel ratio. They also reported an improvement in fuel consumption due to a reduction in pumping losses. The experiments showed that NOx also decreased which was attributed to the lower compression ratio and in-cylinder temperature at the start of combustion.

Gehrke et al. [26] explored the use of VVA on a single cylinder research engine with the goal to quickly achieve and maintain aftertreatment system temperature between 200°C and 400°C. They compared LIVC/EIVC, NVO, and EEVO strategies in terms of effects on fuel consumption temperature and emissions. It was reported that LIVC had the largest temperature gain (∼120°C) with a small fuel consumption increase. NVO and EEVO both had moderate exhaust temperature increases of about 65°C; however, EEVO had the largest fuel consumption penalty.

Wickstrom [27] also studied and compared multiple VVA strategies including EIVC/LIVC, EEVO, secondary EV bump and IV and EV phase shifting. His research was conducted on a single cylinder diesel engine. It was reported that EIVC

and LIVC were both effective in raising exhaust temperature with little fuel consumption penalty. EEVO was not studied in detail due to the large fuel consumption penalty induced. An exhaust valve bump in the intake stroke proved to give a large temperature benefit with only a 6% increase in fuel consumption. This work was also compared to conventional thermal management strategies such as intake throttle, exhaust brake, and hot EGR. Wickstrom reported that the exhaust brake method showed the highest potential for heating the aftertreatment system.

Honardar et al. [28] compared exhaust valve (EV) phasing with post and main fuel injection modulation. This study was conducted on a 4 cylinder in-line research engine equipped with VVA technology. They reported that EV phasing increased fuel consumption by 11%; however, lower CO, HC and NOx emissions were measured when compared to late post injection. EV phasing yielded a small exhaust temperature increase for cold start conditions whereas more than 100°C increase was measured with a late post injection strategy.

There are not many public studies on the effectiveness of CDA on thermal management. Kitabatake et al. [29] studied the use of CDA on a 6 cylinder 9.84 liter 3-stage turbo charged diesel engine for efficiency benefit. The camless VVA system was driven by hydraulic pressure. This study showed that deactivation of three or four cylinders produced a fuel economy improvement of 8.9% at light load due to a reduction in heat loss. The researchers also describe that this is only viable at light loads; therefore, there is a need to switch to activating the cylinders during transient operation.

1.3 Experimental Setup

The experiments were conducted on a 2010 Cummins diesel engine at Purdue University's Herrick Laboratories. This engine has six in-line cylinders and is equipped with high-pressure common rail fuel injection system, variable geometry turbocharger (VGT), exhaust gas recirculation (EGR), a charge air cooler (CAC), and high resolu-

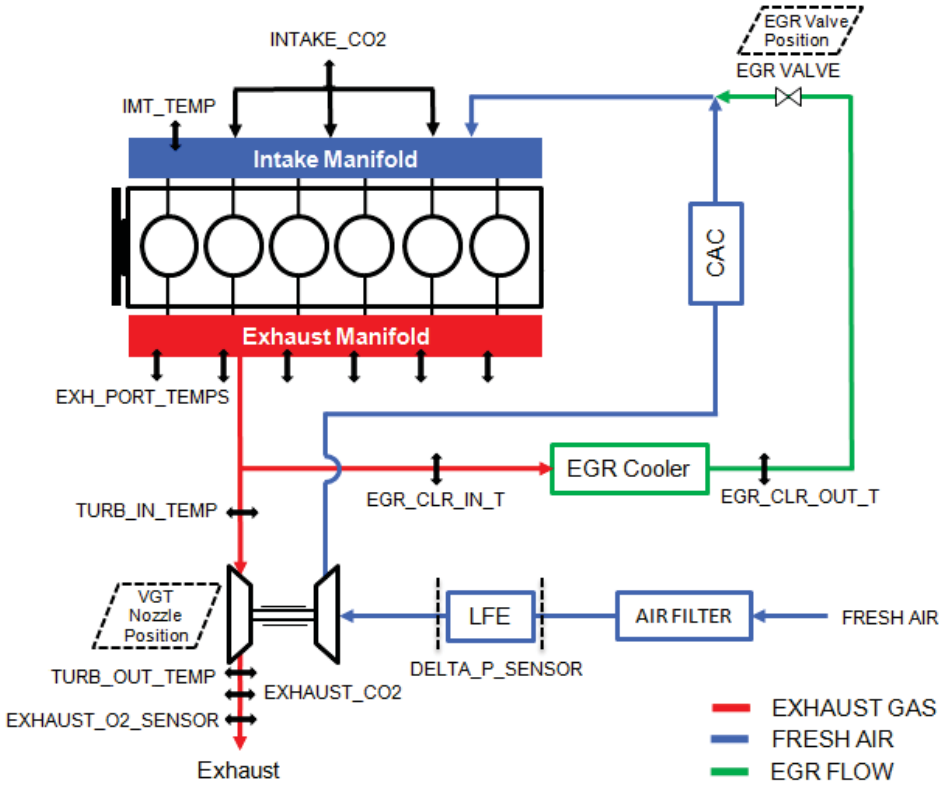

Figure 1.4. Schematic of Cummins multicylinder testbed.

tion emission analyzers for NOx, HC, and PM. A schematic of the engine architecture is presented in Fig. 1.4. The fresh air flows through the laminar flow element into the compressor and is then cooled in the CAC before being mixed with cooled recirculated exhaust gas. The exhaust that is not recirculated to the intake flows through the turbine to the exhaust pipe. The exhaust temperature is measured at the exit of the turbine, referred to in this paper as turbine outlet temperature (TOT). A mixture of two Kistler 6067 and four AVL QC34C in-cylinder pressure transducers in tandem with an AVL 365C crankshaft position encoder are used with an AVL 621 Indicom module for high-speed data acquisition. Laboratory-grade air flow and fuel flow measurements are also used.

There is no aftertreatment system installed on this testbed; however, a butterfly valve is used in the exhaust pipe to simulate the back pressure that would be caused by

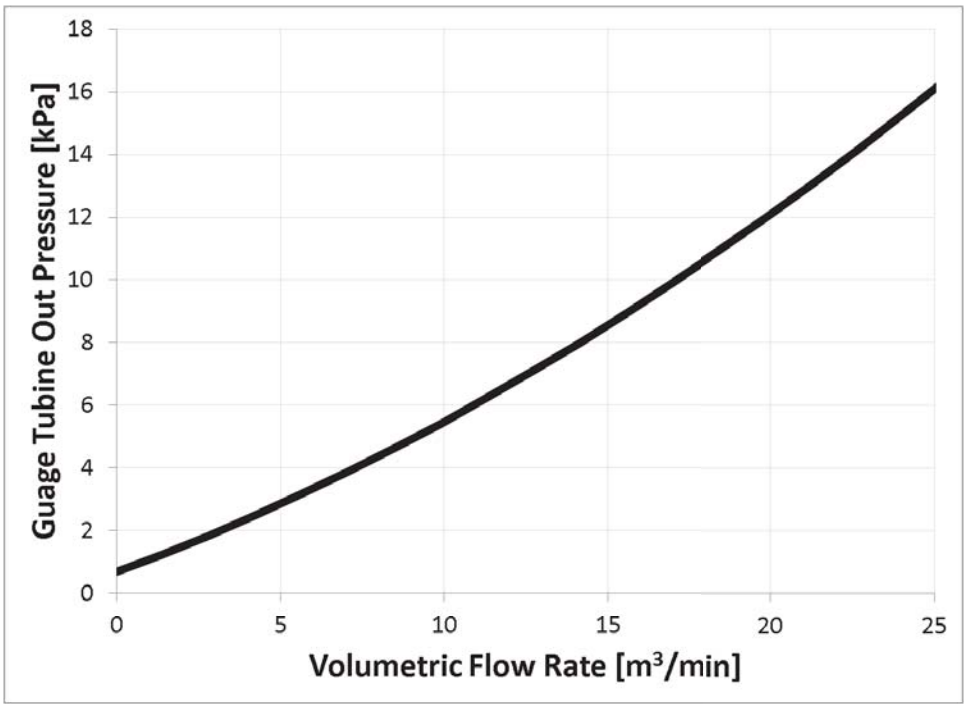

Figure 1.5. Exhaust pressure vs. volumetric flow rate relationship simulating aftertreatment back pressure.

a typical aftertreatment system. Fig. 1.5 shows the measurement-based relationship between the exhaust volumetric flow rate and the exhaust pressure at the turbine outlet to which the valve was controlled during this study.

This engine is also equipped with a fully flexible variable valve actuation (VVA) system. For each of the 6 cylinders, both the intake and exhaust valve pairs are driven by the VVA system. As such, the VVA system has a total of twelve actuators. Each actuator uses position feedback for closed-loop control, enabling cylinder independent, cycle-to-cycle operation of the system. The VVA system is able to control valve opening and closing timing and lift. Fig. 1.6 presents a schematic of the VVA system. The valve profiles are generated in dSPACE and sent to the servo valves via the controller and amplifier. The servo valves shuttle high pressure hydraulic oil to one side of the piston actuators. These actuators push on the valve pairs through a

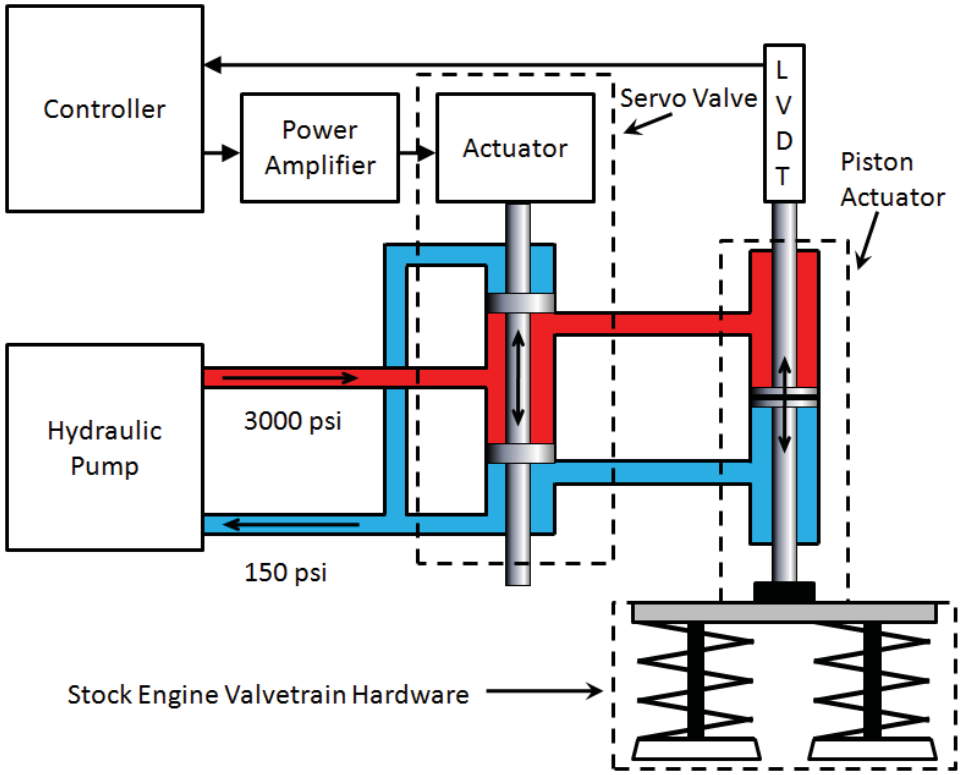

Figure 1.6. Schematic of Purdue variable valve actuation system.

valve bridge to open them. The return force from the valve springs close the valves as the actuators retract. Position feedback is obtained through LVDTs.

The aforementioned equipment, full access to the engine control module (ECM), and additional temperature and pressure sensors are integrated using a dSPACE system. The dSPACE system simultaneously controls the VVA system, sends commands and receives data with the ECM, and samples all of the external measurement channels.

The VVA system allows the early exhaust valve opening and cylinder deactivation operations that will be discussed in the subsequent chapters. Examples of EEVO valve profiles are shown in Fig. 1.7. Each has the same EVC and EVL but a different EVO. The nominal valve profile is adjusted to EEVO profiles like those shown in Fig. 1.7 by simply adjusting the EVO parameter.

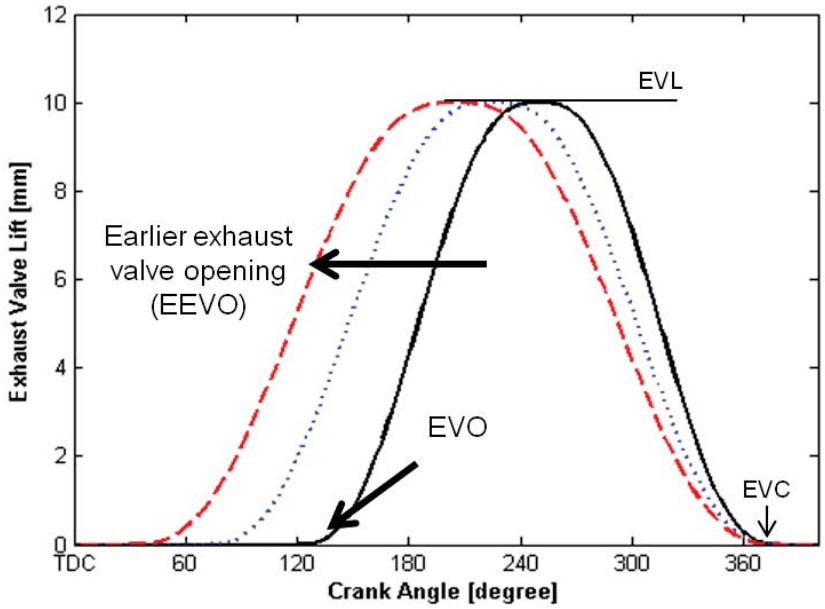

Figure 1.7. Exhaust valve profiles generated on VVA demonstrating EEVO.

Note that EVO here refers to the point in the crank angle domain at which the valve is commanded to open, not at which it actually begins to open. The difference between commanded and actual EVO timing varies with how advanced EVO is set. Figure 1.8 shows an example of the amount of EVO delay when the EVO is set 90 degrees crank angle before the nominal timing.

CDA in this study is performed by deactivating three of the six cylinders. Cylinders are deactivated by turning off valve actuation signals after the intake stroke and injecting no fuel. This method traps fresh charge air inside the cylinder. There is not a perfect seal around the piston rings, and some charge is lost from the deactivated cylinders during each compression. Periodically, the intake valves are opened for one cycle to recharge or allow a fresh charge into the cylinders in order to keep positive pressure and avoid oil accumulation around the piston rings. For steady state tests, this recharge event occurs every 100 cycles. For transient operation, the recharge event was set to occur every 400 cycles to prevent any interference with the transient response data collection.

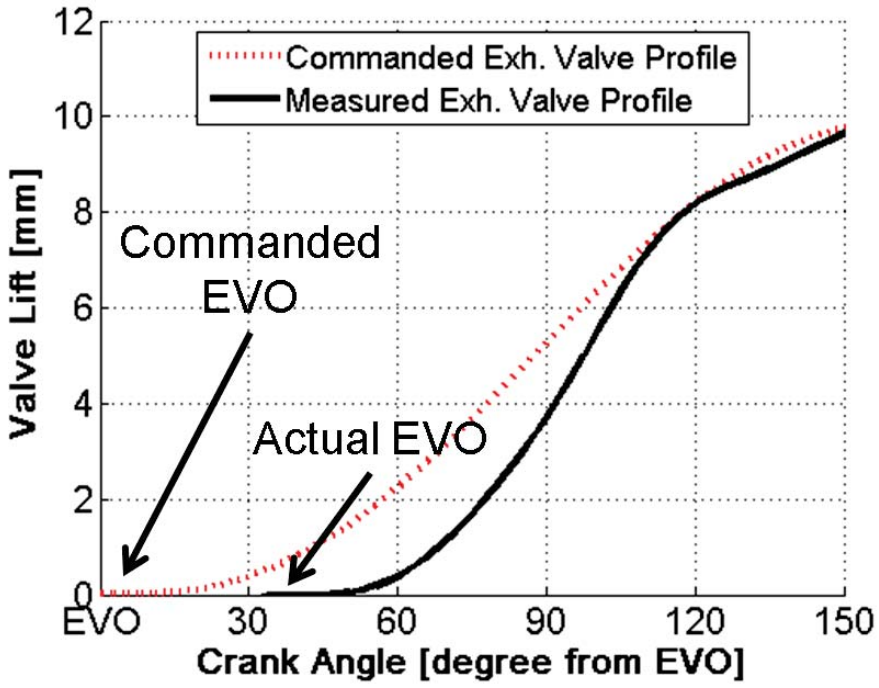

Figure 1.8. Commanded vs. measured exhaust valve profiles.

1.4 Contributions

The author led the work of several major research accomplishments some of which are discussed in this thesis. This work includes the study of two VVA-based strategies for diesel aftertreatment thermal management, EEVO and CDA. GT-Power simulations and experimental validation of EEVO operation was performed. Using experimental EEVO data, models were developed generalizing the relationship between EVO timing and exhaust temperature and fuel consumption.

Work was also performed on the investigation of the potential thermal management benefit of CDA operation at idle. This involved performing several designs of experiments on the research engine and performing a constrained optimization.

The transient capability and potential challenges of CDA were also explored. In order to experimentally study transient operation, the author led an effort to modify the SIMULINK model which communicates with the engine's ECM to enable simul-

taneous setting of all the engine input overrides. Additionally, modifications were made to the fueling input override to allow various fueling profiles during a load transition to be commanded. Utilizing this update to the engine software, experiments were performed involving load transitions with various fueling profile strategies for the characterization of potential challenges of transient operation with CDA.

In addition to the research discoveries and contributions mentioned above, the author also assisted colleagues in similar research efforts. Assistance was given to Akash Garg, Chuan Ding, and Mark Magee in the collection of experimental data for the analysis of VVA strategies on exhaust thermal management. These studies included intake valve closing timing modulation, negative valve overlap and cylinder deactivation.

Assistance was also given to Mark Magee and David Fain for the modification of the SIMULINK model to enable cylinder deactivation. This effort also enabled a cylinder recharge sequence which opens the intake valves for one cycle in the deactivated cylinders every 100 cycles to keep positive in-cylinder gauge pressure.

1.5 Outline

Chapter 2 discusses the effect of EEVO on raising TOT and also its effect on BTE. Models are developed for the relationships of how temperature and fueling change with varying EVO. Chapter 3 outlines an optimization effort comparing CDA operation to nominal 6-cylinder operation. Chapter 4 begins with motivating results of CDA at steady-state conditions at several engine loads at a cruising speed. The second part discusses the limits of CDA during transient load transitions. Chapter 5 gives a summary of the work presented in this thesis. Some discussion of future work is also included.

2. MODELING THE IMPACT OF EARLY EXHAUST VALVE OPENING ON EXHAUST THERMAL MANAGEMENT AND EFFICIENCY

As mentioned in the first chapter, previous studies have discussed the potential of EEVO to raise exhaust temperatures [27, 28]. However, the studies involving diesel engines are restricted to reporting data at one or two operating conditions. This chapter focuses on the modeling, generalization, and prediction of the effect of EEVO on exhaust gas temperature and the required fueling to maintain torque.

2.1 Experimental Data Collection

The experimental data for this study was conducted at three speed/BMEP conditions: 800 r/min at 1.3 bar, 2000 r/min at 1.3 bar, and 2200 r/min at 6.3 bar. The point at 800 r/min represents a loaded idle condition. The point at 2000 r/min and 1.3 bar is representative of a condition at a cruising speed without the accelerator pressed. The third condition was chosen at a moderate load (6.3 bar) and a slightly higher speed (2200 r/min) to represent the engine condition after the accelerator is pressed at a cruising speed. The TOTs at the 1.3 bar points are very low, ∼150°C and 200°C for the 800 and 2000 r/min points, respectively, and they are common operating conditions. The TOT at the 6.3 bar load point, another common condition, is nominally above 250°C; however, any increase in temperature would be beneficial for heating the aftertreatment system from cooler conditions.

EEVO sweeps were performed at each of these conditions to explore the primary impact of EVO modulation. Each EEVO sweep was performed by setting the engine to run at the desired speed/load condition then adjusting the commanded EVO timing from the nominal value to 90° crank angle before nominal. The experiments were performed at a constant torque; therefore, the fueling amount was increased as EVO

was advanced to make up for the torque loss resulting from earlier EVO. All other engine inputs (e.g. injection timings, rail pressure, VGT, and EGR actuator positions) were held constant during the sweep. Data was taken for each sweep at five different EVO values, listed in Table 2.1.

Table 2.1. EVO values studied with respect to nominal.

EVO values
Nominal
-30°
-50°
-70°
-90°

A total of seven constant-torque EEVO sweeps were performed. Table 2.2 lists each condition at which the EEVO sweeps were performed and the inputs associated with the sweep. TOT at nominal EVO (NEVO) is also listed for reference. It was necessary to isolate the effect of EEVO from the influences of other engine parameters in order to model the impact of EEVO on TOT and the required fueling increase. Therefore, three sweeps were conducted at both 2000 r/min at 1.3 bar and 2200 r/min at 6.3 bar but with other inputs (SOI, rail pressure, air/fuel ratio, and EGR fraction) adjusted. Conditions 1, 2a and 3a have engine parameters consistent with the production ECM calibration. Start of injection (SOI) and rail pressure were varied significantly between conditions 2a-c (2000 r/min at 1.3 bar) and between conditions 3a-c (2200 r/min at 6.3 bar). The starting values of air/fuel (A/F) ratios and EGR fractions for conditions 3a-c were set to values as listed in Table 2.2 using the VGT and EGR actuators. SOI and rail pressure were held constant during each sweep, and the VGT and EGR actuators were not adjusted; however, the A/F ratio and EGR fractions were allowed to float based on changes in the gas exchange process

caused by EEVO and fueling amounts (which, as noted previously, were adjusted to maintain torque).

Table 2.2. Engine conditions and inputs for experimental EVO sweeps.

Condition	Speed	BMEP	TOT at NEVO	SOI	Rail press.	A/F ratio	EGR frac.
	r/min	bar	deg C	deg bTDC	bar	-	-
1	800	1.3	147	2.1	900	40.8	0.63
2a	2000	1.3	186	-0.1	1263	83.4	0
2b	2000	1.3	201	-2.8	1800	78.0	0
2c	2000	1.3	213	-7.7	1800	74.5	0
3a	2200	6.3	344	1.4	1538	32.7	0.18
3b	2200	6.3	449	7.6	1593	25.8	0.20
3c	2200	6.3	459	6.6	1800	23.8	0.22

Each sweep was experimentally tested once; however, repeat data was collected each time the testbed was operated. A measurement uncertainty analysis was performed based on this data. Error bars are included for each variable shown in subsequent figures. These error bars represent +/- one standard deviation of this repeat data. Note that in some cases the error bars are too small to be be visible.

2.2 Experimental Results

The impact of the EEVO sweeps on the TOT is shown in Fig. 2.1. The EVO timing is displayed on the x-axis where negative numbers represent timings earlier than nominal. The speed and load of each condition (as specified in Table 2.2) is represented by different line and marker styles (per legend in Fig. 2.1). TOT increases by 30°C to 80°C with EVO set to the most advanced timing studied. The

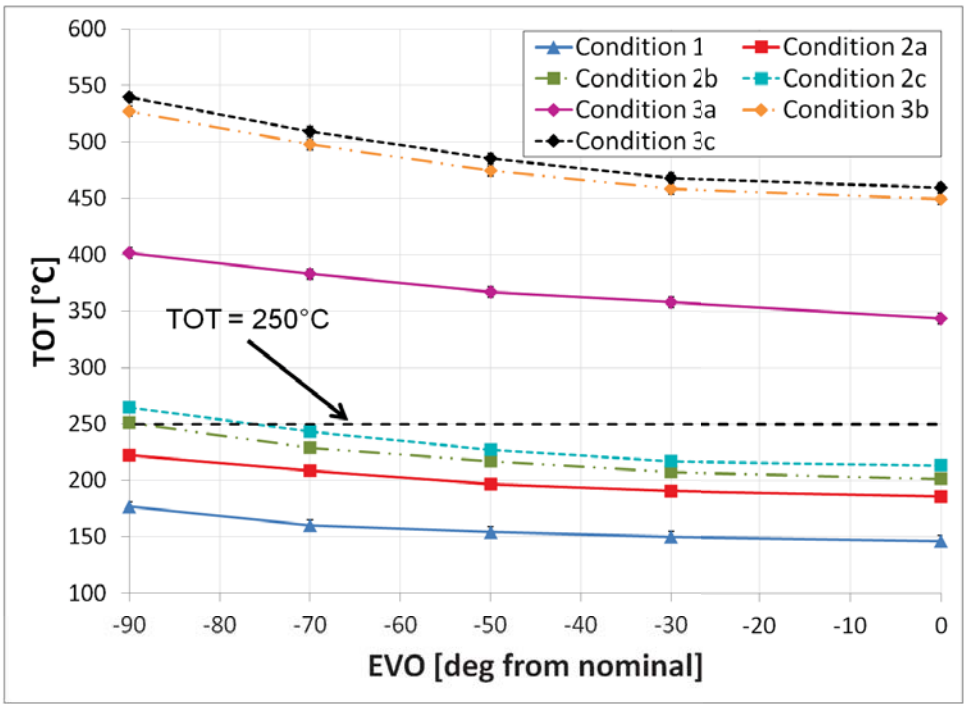

Figure 2.1. TOT vs. EVO for experimental EEVO sweeps (see Table 2.2 for condition details).

TOTs for conditions 1 and 2a-c are all below 250°C. Increasing these temperatures would be desirable for aftertreament effectiveness. The experiments demonstrate that the TOTs for conditions 2b and 2c are increased above 250°C. Conditions 3a-c, which nominally have the highest TOT, also have the largest temperature increases with EEVO. The larger temperature increases are caused by larger quantities of added fuel to maintain the torque. The TOT increases by about 80°C for conditions 3b and 3c. These conditions have nominal TOTs that are hot enough for aftertreatment effectiveness, however this increase in TOT would be beneficial for more rapid heating of the aftertreatment system.

The fueling increases measured relative to nominal EVO (NEVO) during the experimental EEVO sweeps are shown in Fig. 2.2. The highest fueling increase observed is about 22% at condition 1. The lowest fueling increase was calculated to be 13% at conditions 3a-c. Conditions 2b and 2c have a measured fuel increase of 18% to 21%.

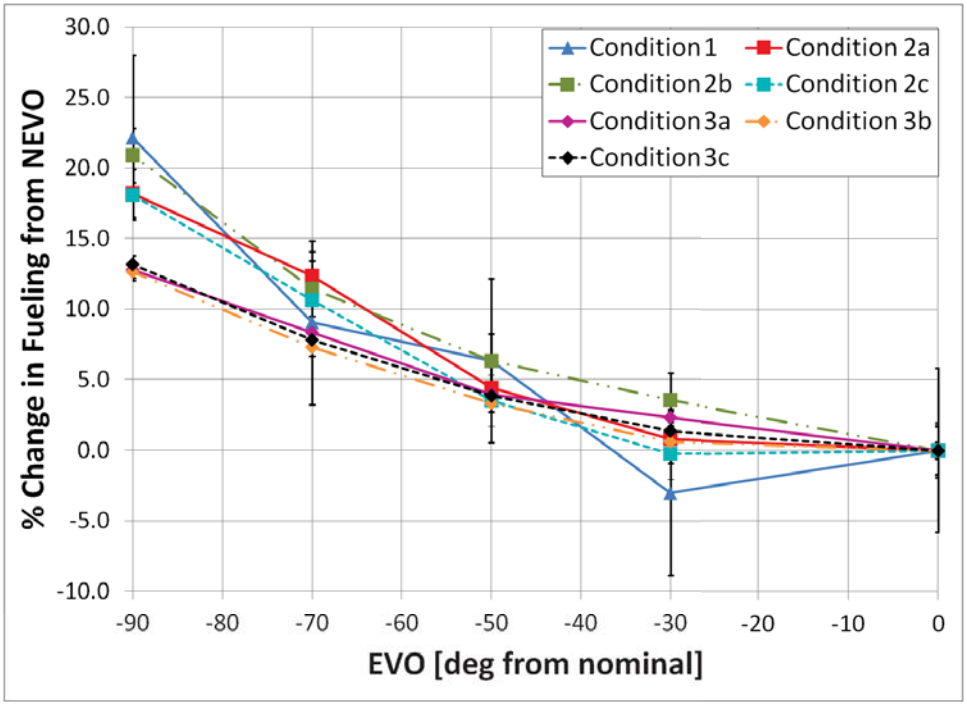

Figure 2.2. Fueling vs. EVO for experimental EEVO sweeps (see Table 2.2 for condition details).

The fueling increase directly affects the engine brake thermal efficiency (BTE), which is displayed in Fig. 2.3. The brake thermal efficiency represents the overall efficiency of the engine, or the ratio of the amount of usable power extracted to the injected fuel power. The experiments were run at a constant BMEP, as noted previously, which means that the amount of usable power output remained the same for a given EVO sweep. Therefore, the fueling increase is proportional to the decrease in BTE. The BTE penalties that were observed in this set of experiments at the earliest EVO timing were between 10-20%.

It is useful to visually demonstrate the effect of EEVO on the in-cylinder pressure and, therefore, the work done during a cycle. Figure 2.4 shows a logP-logV diagram of one of the cylinders at condition 2a, both at nominal valve timing and at the earliest EVO studied (-90°). The direct impact on the lost expansion work is manifest at the volume where the EEVO pressure drops below the nominal pressure. Additional fuel is

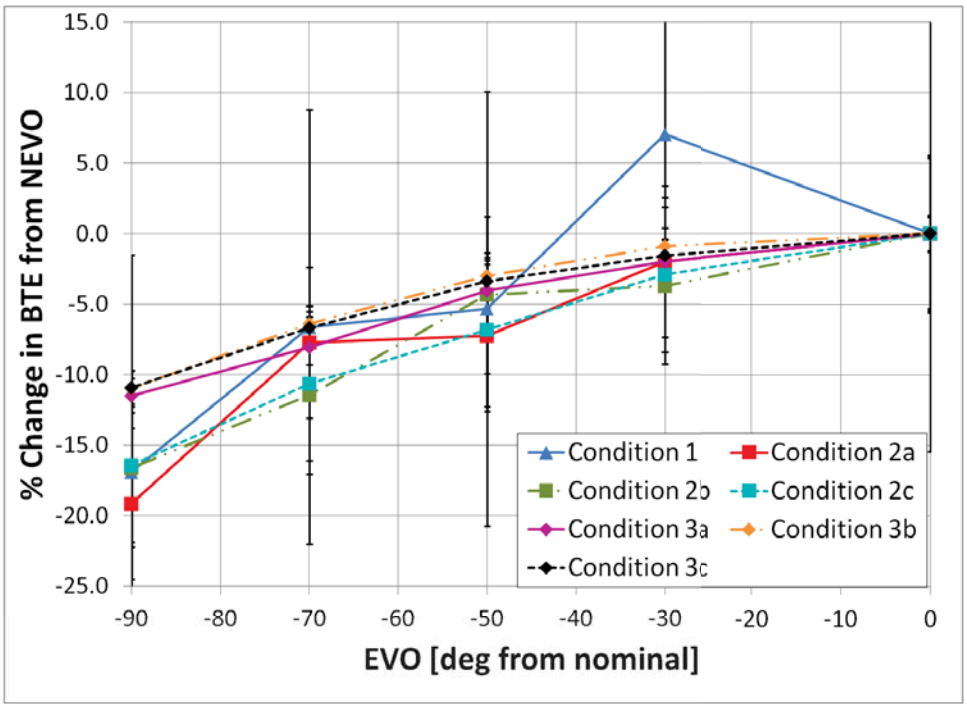

Figure 2.3. Normalized BTE values vs. EVO for experimental EEVO sweeps (see Table 2.2 for condition details).

added for the EEVO case in order to raise the cylinder pressure enough to compensate for the loss in gross work during the early blowdown. The re-compression at the end of the exhaust stroke is a side effect of the EEVO strategy developed on this VVA system. The closing edge of the profile is also slightly advanced for the EEVO cases (per Fig. 1.7). This does not significantly affect the fuel consumption results, as will be shown later.

The results of the experimental EEVO sweeps demonstrate, for the seven conditions discussed, the beneficial and negative impacts of EEVO on thermal management and fuel economy, respectively. The following section outlines an analysis that allows generalizable projections of EEVO impact at other operating conditions.

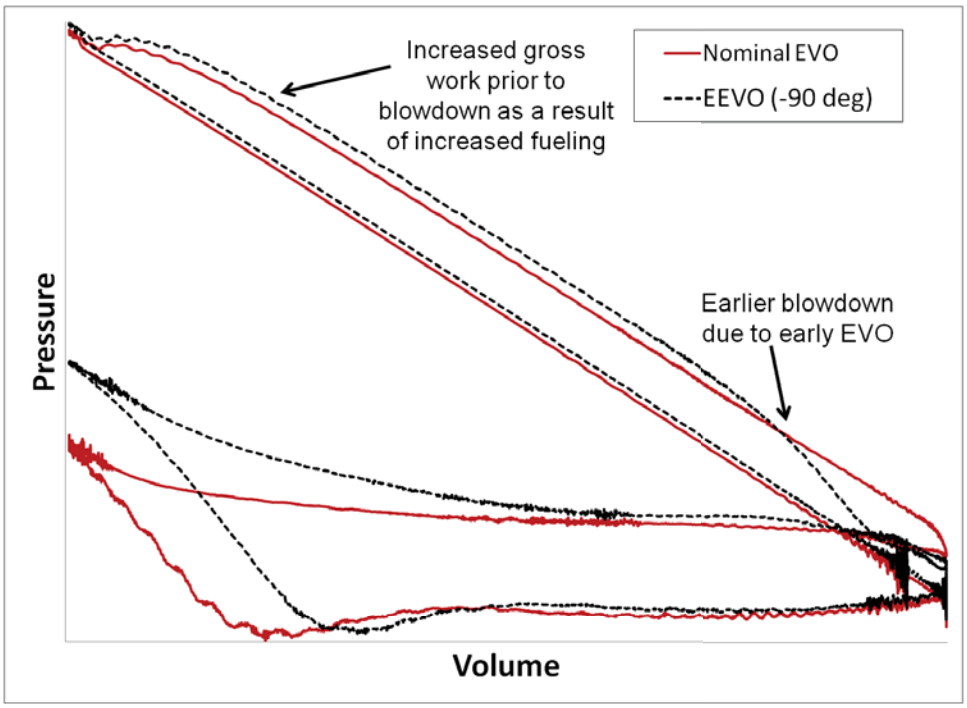

Figure 2.4. Log P-Log V diagram of nominal and early EVO timing at 2000 r/min / 1.3 bar.

2.3 Impact of EEVO on required fueling and exhaust temperature at constant torque

The experiments described in the previous section are useful for understanding the impact of EEVO at specific operating conditions. Models will be developed in this section to gain insight into the effect of EEVO at any operation condition where experiments have not been conducted. A model is developed in the first part of this analysis to estimate the quantity of fuel increase required during EEVO operation to maintain a given BMEP. This will lead to a prediction of TOT increase as a function of EVO. The experimental EEVO sweep data described in the prior section will be used to validate these models.

2.3.1 Required fueling at constant torque with EEVO

EEVO reduces the work output during the expansion stroke for a given fueling amount, and as such, directly affects the gross indicated mean effective pressure (GIMEP). GIMEP can be calculated as the sum of brake mean effective pressure (BMEP), pumping mean effective pressure (PMEP), and friction mean effective pressure (FMEP):

$$GIMEP = BMEP - PMEP + FMEP. \tag{2.1}$$

However, with torque constant (via increasing fueling for EEVO),

$$BMEP_{NEVO} = BMEP_{EEVO}. \tag{2.2}$$

Two key assumptions can be made regarding FMEP and PMEP:

1. EVO advancement has no significant effect on FMEP
2. EVO advancement has no significant effect on PMEP

Friction is primarily affected by speed and peak cylinder pressure. Speed does not change with a variation in EVO. Peak cylinder pressure only slightly increases with increased fueling to maintain torque (per Fig. 2.4). EEVO mostly affects the closed cycle, which includes the compression and expansion strokes of the cylinder. Therefore, it is not expected to disturb the gas exchange process and, therefore, the pumping work.

These assumptions can be validated using the experimental data described in Section 2.2. Fig. 2.5 shows the change in FMEP from the FMEP at nominal EVO timing versus EVO from the experimental EEVO sweep data. There is no direct measurement of FMEP on this testbed; therefore, it is calculated from equation 2.1 using measurements of BMEP, GIMEP, and PMEP. The figure shows that, for each EEVO sweep condition, FMEP varies minimally with EVO, specifically, less than $\sim$0.15 bar at an EVO of -90°. This is a small fraction of the GIMEP (per Fig. 2.6) and BMEP.

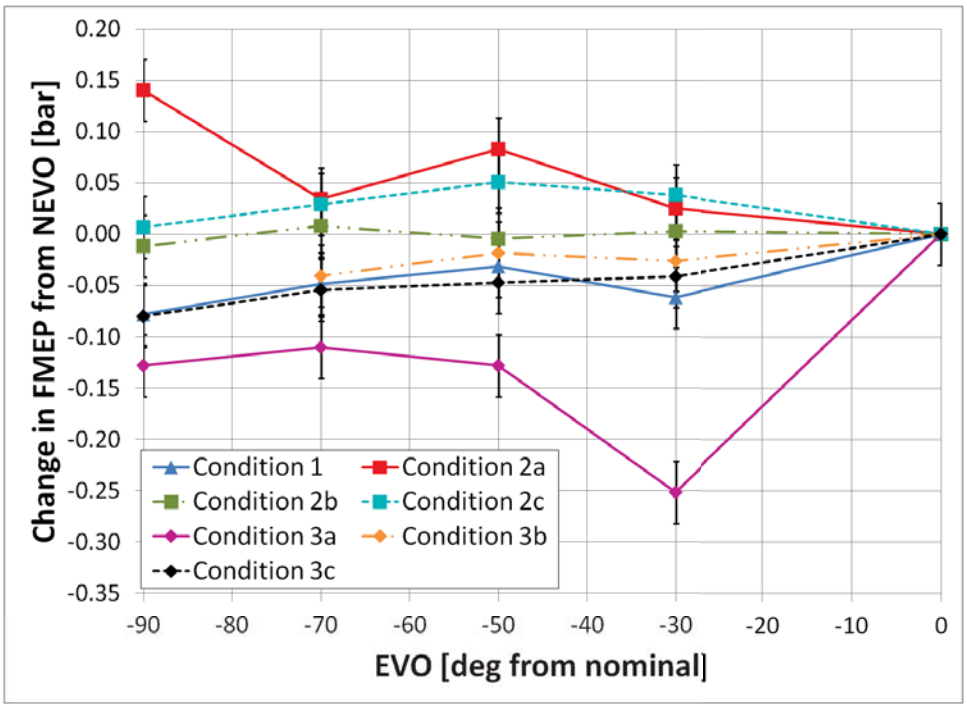

Figure 2.5. Change in FMEP values from nominal for experimental EEVO sweeps (see Table 2.2 for condition details).

The experimental data, shown in Fig. 2.7, indicates that there was a slight decreasing trend for PMEP as EVO was advanced; however, this change is minimal, specifically, less than ∼0.15 bar along the sweep, a small fraction of the GIMEP (per. Fig. 2.6) and BMEP. Earlier opening of the exhaust valves causes an elevated pressure of the the burned gases in the exhaust manifold, as shown in Fig. 2.4. The higher in-cylinder pressures at the intake valve opening event help to recover some of the work lost to the pumping penalty. This causes the minor increase in the pumping penalty. However, as stated, this increase is not significant and can be modeled as a constant with EEVO.

Applying these two key assumptions with equation 2.2 to equation 2.1 reveals that

$$GIMEP_{NEVO} \simeq GIMEP_{EEVO} \tag{2.3}$$

will hold as the fueling is increased to maintain a constant BMEP as EVO is modulated. Fig. 2.6 shows that there is almost no change in GIMEP with modulated

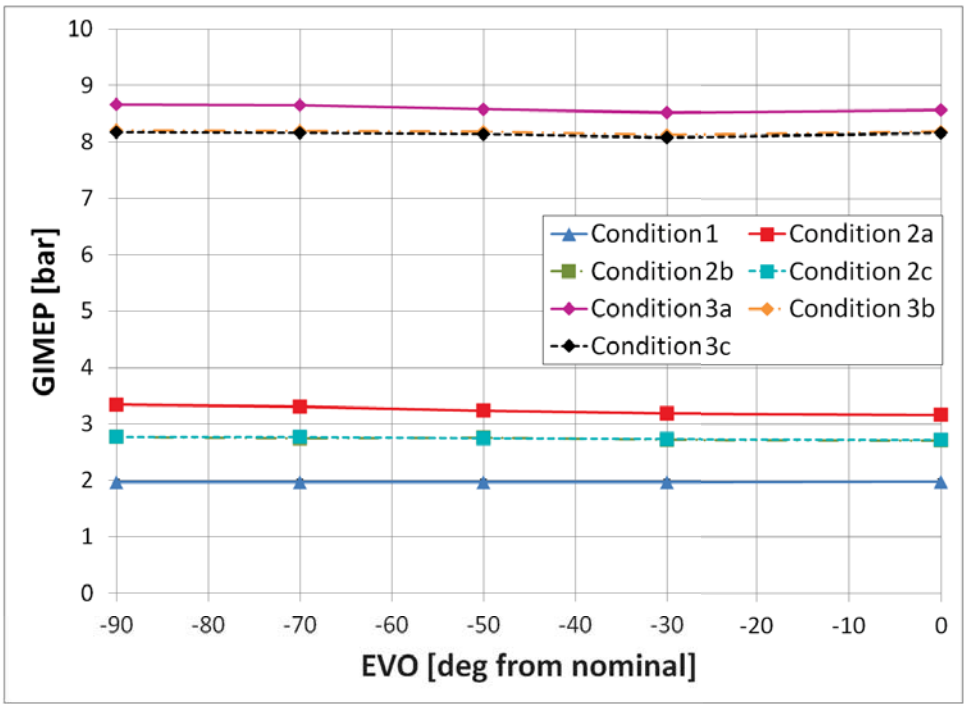

Figure 2.6. GIMEP values for experimental EEVO sweeps (see Table 2.2 for condition details).

EVO (per equation 2.3). Specifically, GIMEP varies no more than ~0.2 bar along each EVO sweep. This is consistent with constant BMEP engine operation, as well as the small variations in FMEP and PMEP, during each EVO sweep.

GIMEP can be converted into gross power using the speed, N, and engine geometry:

$$GrossPower = \frac{GIMEP * V_d * N}{n_R}. \tag{2.4}$$

where V_d is the displacement volume and n_R is the number of crankshaft revolutions for each power stroke (2 for a four-stroke engine). This term is used in calculating closed cycle efficiency:

$$\eta_c = \frac{GrossPower}{FuelPower}. \tag{2.5}$$

Closed cycle efficiency is a measure of the efficiency of the closed cylinder portion of the cycle and is defined as the ratio of the power released from the injected fuel

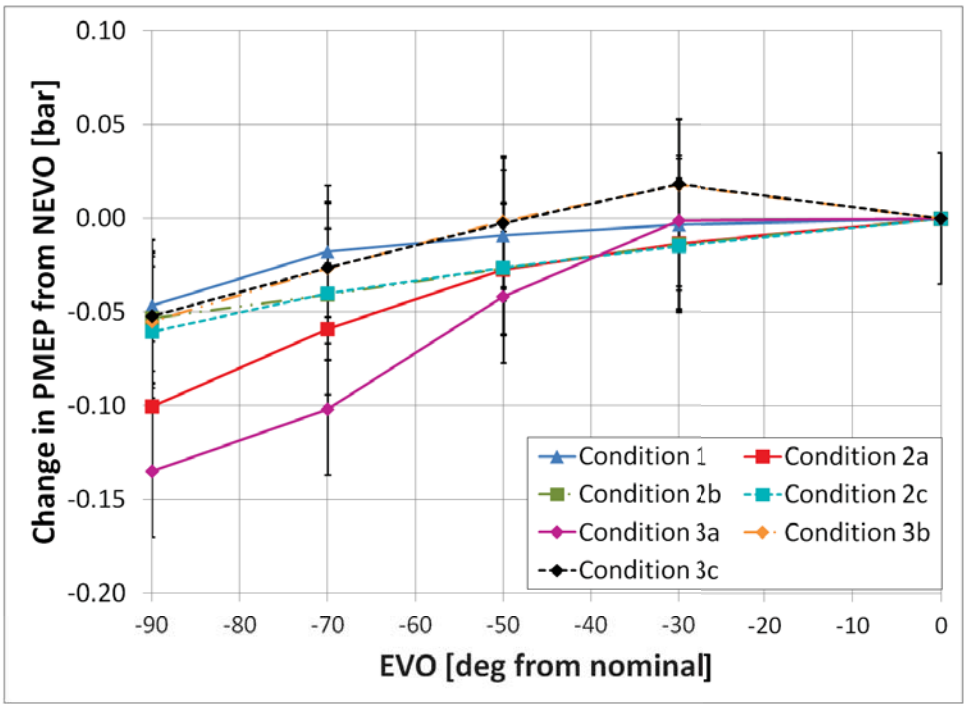

Figure 2.7. Change in PMEP values from nominal for experimental EEVO sweeps (see Table 2.2 for condition details).

(measured at the piston during the closed cycle) to the energy contained in the fuel. Fuel power is defined as the product of fuel mass flow rate and the lower heating value (LHV) of the fuel. The LHV of the fuel is 42.72 MJ/kg. The impact of EVO on the required fueling for constant brake power (and gross power) can be defined with the following:

$$f(EVO) \equiv \frac{\eta_{c_{EEVO}}}{\eta_{c_{NEVO}}} = \frac{\left(\frac{GrossPower}{FuelPower}\right)_{EEVO}}{\left(\frac{GrossPower}{FuelPower}\right)_{NEV0}}. \tag{2.6}$$

Gross power is constant per equation 2.3 when torque (and, therefore, BMEP) is held constant. Therefore, equation 2.6 can be written as

$$f(EVO) = \frac{FuelPower_{NEVO}}{FuelPower_{EEVO}} = \frac{\dot{m}_{f_{NEVO}}}{\dot{m}_{f_{EEVO}}}, \tag{2.7}$$

where $f(EVO)$ essentially scales the fuel power and mass flow for a particular commanded EVO. Rearranging equation 2.7 yields

$$\dot{m}_{f_{EEVO}} = \frac{\dot{m}_{f_{NEVO}}}{f(EVO)}. \tag{2.8}$$

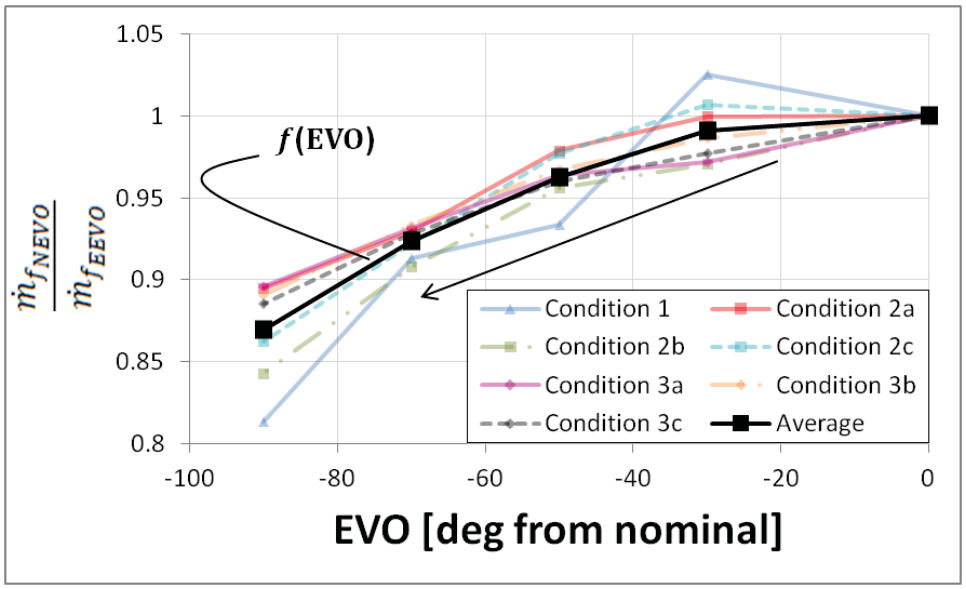

Figure 2.8. Function of the change of fuel flow rate as EVO is advanced (see Table 2.2 for condition details).

$f(EVO)$ can be approximated using the experimental EEVO sweep data described earlier. Fig. 2.8 illustrates the method used to generate $f(EVO)$. The ratio of the mass of fuel from the nominal case to the EEVO case (per equation 2.7), as shown on the y-axis, was averaged at each EVO value. The resulting function represents a fuel mass flow conversion from nominal to EEVO cases and confirms the expected trend: more fuel is needed to maintain torque as EVO is advanced. The average decrease of closed cycle efficiency is 13% at an EVO timing of 90° before nominal. This $f(EVO)$ relationship describes the overall effect on fueling increase from EEVO and will be used to predict the impact of EEVO on fueling at other operating conditions.

The nature of this generalization implies there is some amount of variation at each operating condition given that fueling increase is calculated solely with $f(EVO)$. However, the experiments used to generate $f(EVO)$ include multiple speeds and loads and various injection timings, rail pressures, air and EGR flow rates, all of which would be expected to change the rate of efficiency loss. The incorporation

of these variations in the sweeps allows all the effects on efficiency caused by these parameters to be approximately accounted for in $f(EVO)$.

Table 2.3 shows the generated values for $f(EVO)$. This fueling model, $f(EVO)$, is always smaller than 1 and decreases for earlier EVOs. This is consistent with an expected increase in required fueling to maintain constant torque as EVO is advanced, per equation 2.8.

Table 2.3. $f(EVO)$ values as EVO is advanced.

EVO	$f(EVO)$
Nominal	1
-30	0.991
-50	0.962
-70	0.924
-90	0.869

2.3.2 Fueling Model Validation

In order to demonstrate the accuracy of the $f(EVO)$ model, (equation 2.8), a comparison was made of actual fueling values obtained from the experimental sweeps with calculated values predicted by equation 2.8. A one-to-one comparison of values from all seven conditions is shown in Fig. 2.9. These values in the plot are normalized to the largest fueling amount. Figs. 2.10 and 2.11 show this same comparison with the residual percent errors and true errors in kg/hr at each EVO timing, respectively. The model shows accurate fueling values within 5% error, with the exception of one point at -90° EVO timing. The largest error shown is about 0.4 kg/hr.

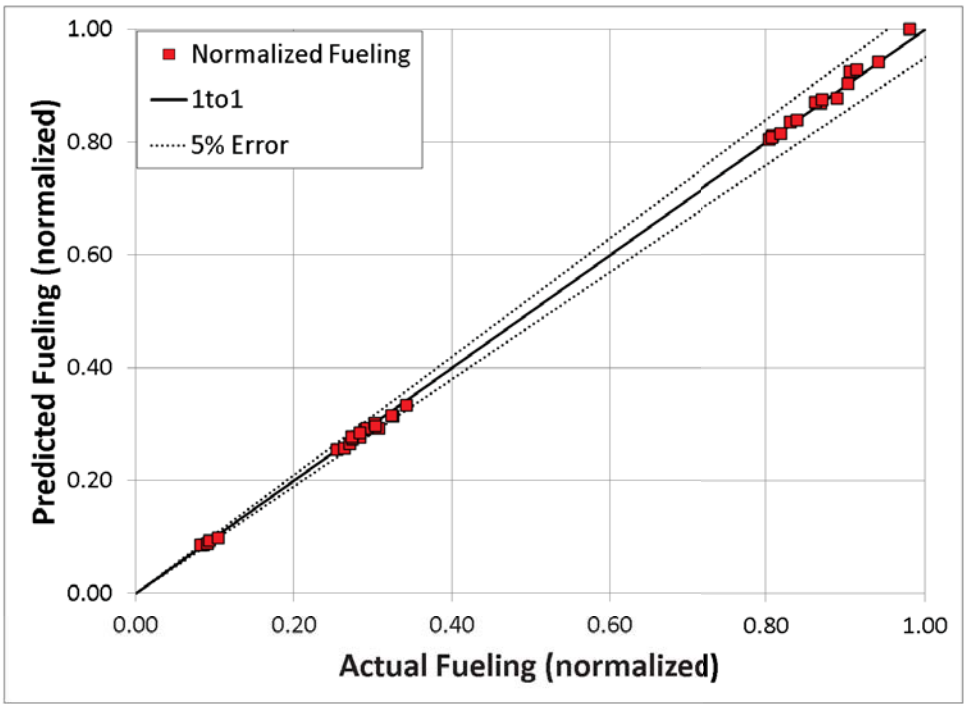

Figure 2.9. One-to-one comparison of normalized predicted vs. actual fueling values.

An accurate model for increased fuel flow with EEVO allows for the prediction of the effect of EEVO on the overall BTE. Incorporating equation 2.8 into the calculation for BTE yields

$$BTE = \frac{Torque}{\frac{\dot{m}_{f_{NEVO}}}{f(EVO)} * LHV}. \tag{2.9}$$

Predicted values of BTE were calculated based on the experimental sweeps performed using equation 2.9. A one-to-one comparison is made between these predicted values and the actual values obtained from experiment, as shown in Fig 2.12. The values are normalized to the largest measured BTE point. The residual percent and actual errors are also shown in Figs. 2.13 and 2.14. Almost all of the predicted values are within 5% error of the actual efficiencies, with the exception of 2 points at -90° EVO timing. All actual errors are less than 0.015 points BTE.

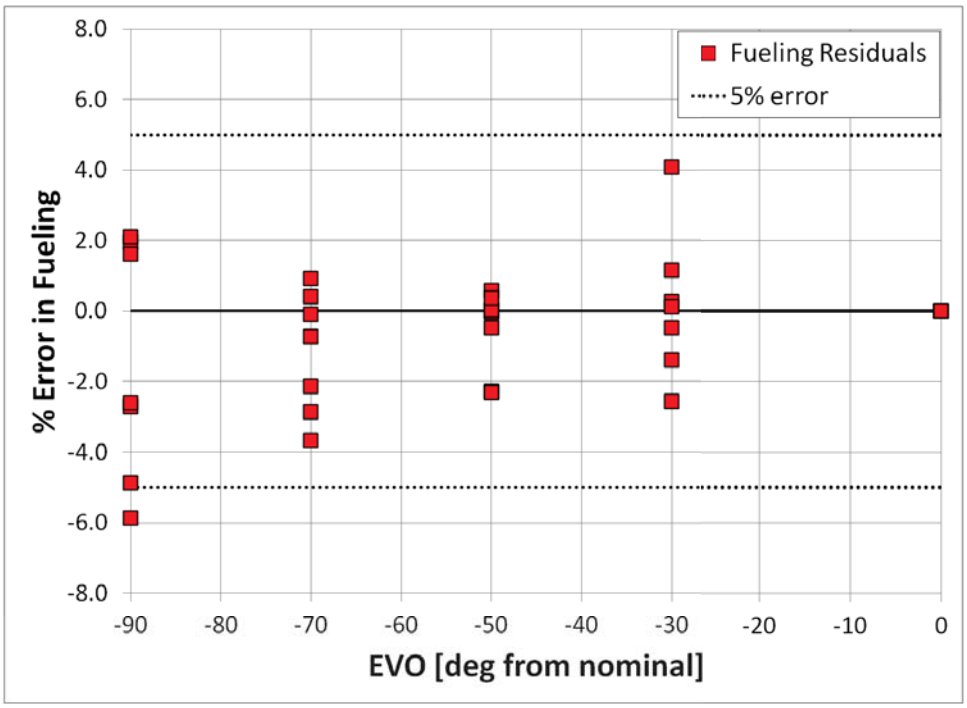

Figure 2.10. Percent residual error of predicted vs. actual fueling values.

A model for generalizing the effect of EEVO on the fueling required to maintain torque has been described. The following two sections describe the generation of a model for the impact of EEVO on turbine out temperature.

2.3.3 First Law Balance

A first law based analysis was completed and validated using the EEVO sweep experiments in order to generalize the impact of early EVO on exhaust temperature. This analysis also utilizes the fueling model described above.

The control volume for this analysis is defined as everything from the inlet of the compressor through the engine block to the exit of the turbine, as shown in Fig. 2.15. This analysis uses the following assumptions:

1. The engine is in steady-state and is an open system.

2. The reference temperature is taken to be ambient temperature.

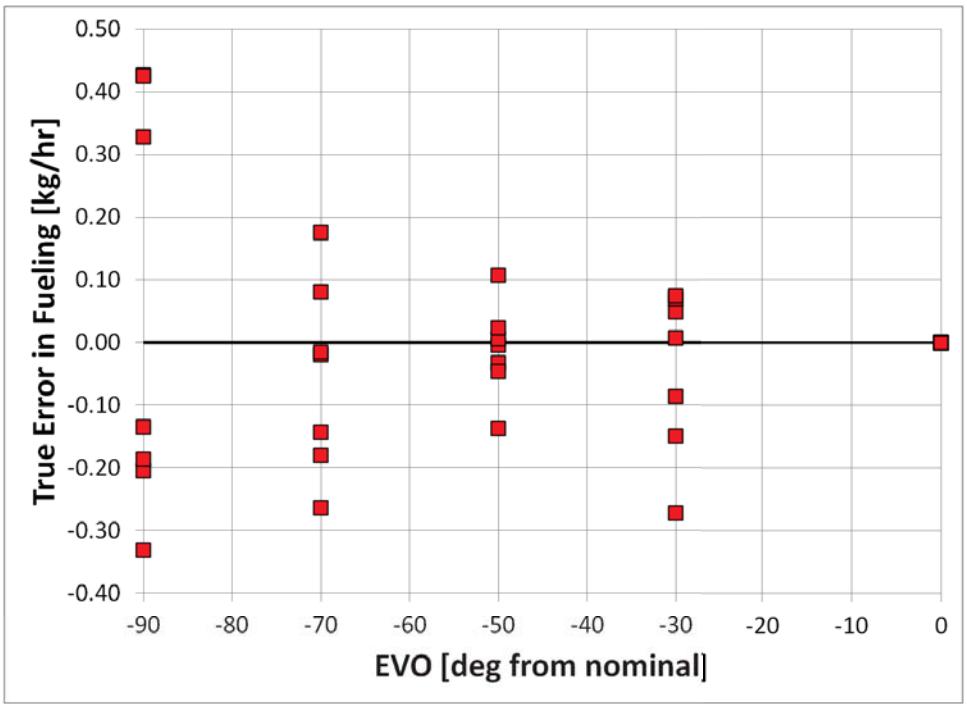

Figure 2.11. Actual residual error of predicted vs. actual fueling values in kg/hr.

3. The temperature of the exhaust gas is the turbine outlet temperature.

Based on the first assumption, the energy balance can be written as

$$\dot{Q} - \dot{W}_b + \dot{E}_f + \dot{E}_{air} - \dot{E}_{exh} = 0, \tag{2.10}$$

where $\dot{Q}$ is the heat transfer (heat loss), $\dot{W}_b$ is the brake power output, $\dot{E}_f$ is the fuel power, and $\dot{E}_{air}$ and $\dot{E}_{exh}$ are the powers associated with the fresh air flow and exhaust flow, respectively. Air flow (and exhaust flow) power is defined as

$$\dot{E}_{air} = \dot{m}_{air} c_p (T_{air} - T_{ref}), \tag{2.11}$$

where $\dot{m}_{air}$ is mass flow rate of air (exhaust), c_p is the constant pressure specific heat, T_{air} is the temperature of the fresh air (or exhaust) and T_{ref} is the reference temperature. The power associated with the fueling rate is defined as

$$\dot{E}_f = \dot{m}_f LHV. \tag{2.12}$$

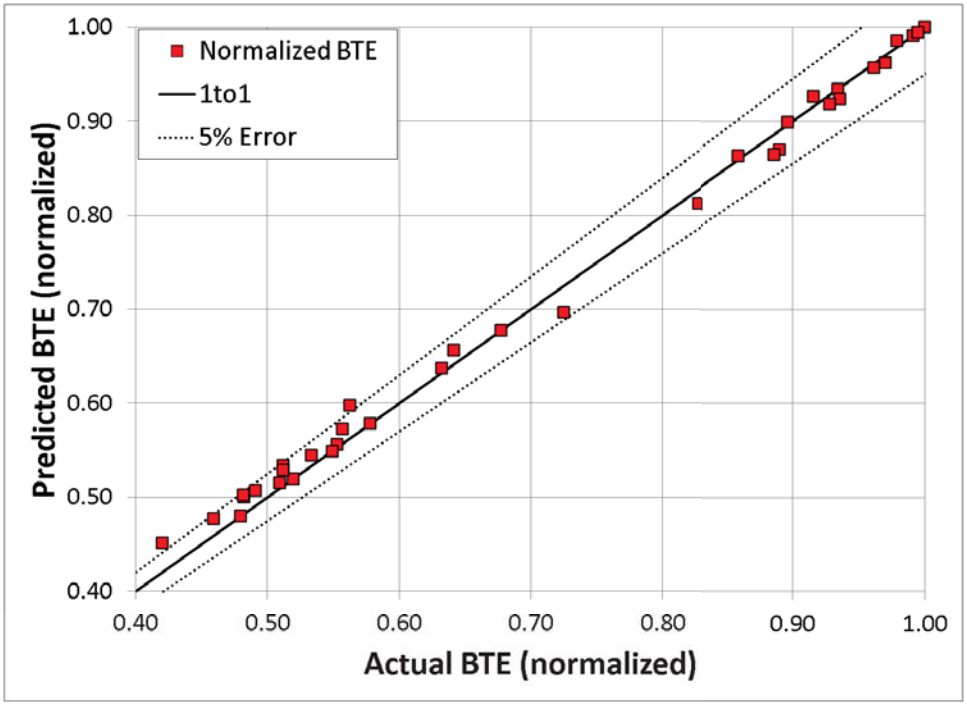

Figure 2.12. One-to-one comparison of normalized predicted vs. actual BTE values.

Applying all assumptions, the first law can be rewritten as

$$\dot{m}_f LHV - \dot{W}_b - \dot{Q} \quad = \quad \dot{m}_{exh} c_p (TOT - T_{ref}), \tag{2.13}$$

where $\dot{Q}$ is positive with heat transfer out of the system. Performing a mass balance on the same control volume shows that

$$\dot{m}_{exh} \quad = \quad \dot{m}_{air} + \dot{m}_f. \tag{2.14}$$

Combining equations 2.13 and 2.14 and rearranging for TOT yields

$$TOT \quad = \quad \frac{\dot{m}_f LHV - \dot{W}_b - \dot{Q}}{(\dot{m}_{air} + \dot{m}_f)\, c_p} + T_{ref}. \tag{2.15}$$

The impact of EEVO (during constant torque or brake work $\dot{W}_b$ operation) on the required fueling $\dot{m}_f$ has been generalized and modeled in Section A above. Equations 2.8 and 2.15 can be combined to generate an expression for TOT at an early EVO:

$$TOT_{EEVO} = \left(\frac{\frac{\dot{m}_{f_{NEVO}}}{f(EVO)} * LHV - \dot{W}_{b_{NEVO}} - \dot{Q}}{\left(\dot{m}_{air} + \frac{\dot{m}_{f_{NEVO}}}{f(EVO)} \right) * c_p} \right) + T_{ref}. \tag{2.16}$$

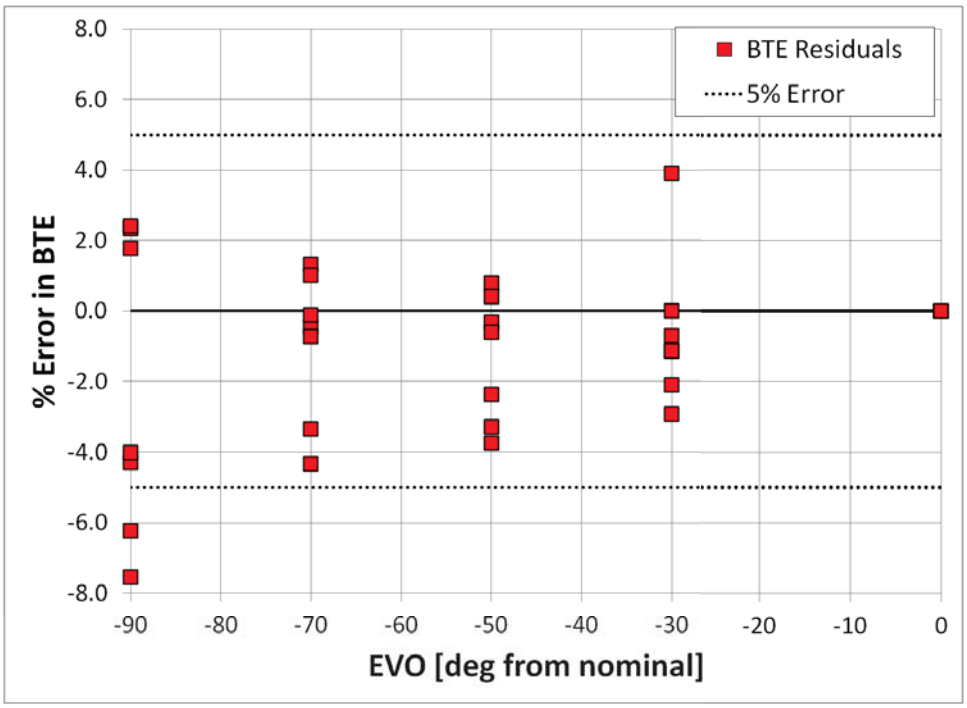

Figure 2.13. Percent residual error of predicted vs. actual BTE values.

The impact of EEVO on the air flow $\dot{m}_{air}$ and heat transfer $\dot{Q}$ is outlined and modeled in the following section. Those results, in combination with equation 2.15, will yield an equation for TOT during EEVO operation just in terms of EVO and the values of the parameters during nominal engine operation.

2.3.4 TOT increase with EEVO model

Equation 2.16, as mentioned above, calls for two additional generalizations to be made in order to predict TOT, specifically, how $\dot{Q}$ and $\dot{m}_{air}$ behave as EVO is advanced. The experimental EEVO sweep data collected was used to generate assumptions or relationships between EVO and these parameters. Fig. 2.16 shows change in measured air flow during the EVO sweeps. All values represent less than 7% increase in air flow at an EVO of -90°. This indicates that air flow is not significantly affected by EEVO and can be assumed as constant:

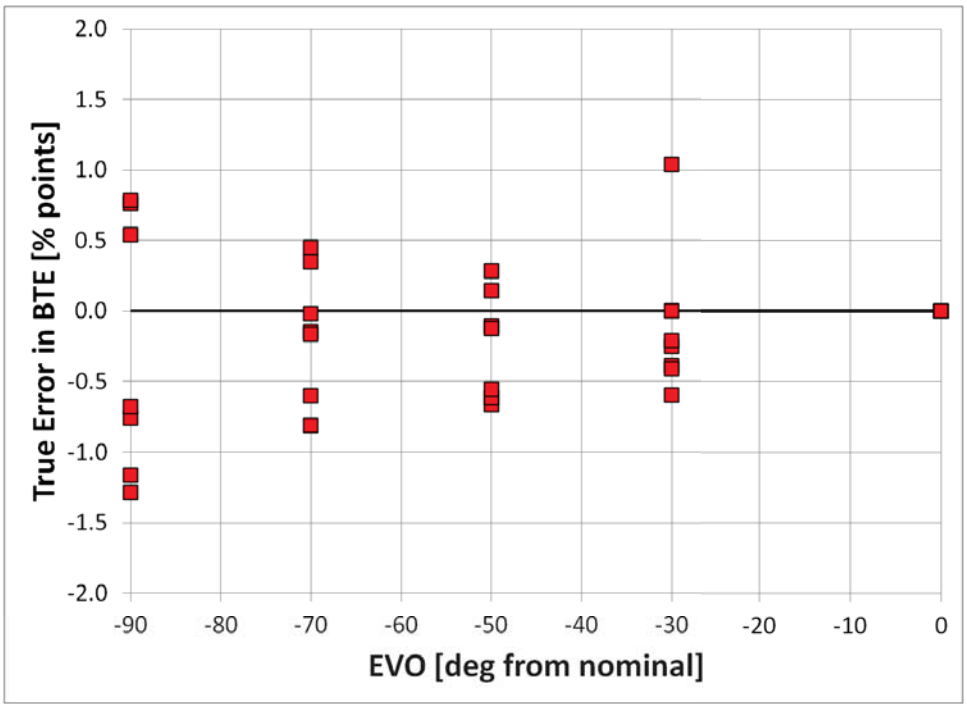

Figure 2.14. Actual residual error of predicted vs. actual BTE values.

$$\dot{m}_{air_{EEVO}} \simeq \dot{m}_{air_{NEVO}}. \tag{2.17}$$

Total heat transfer (to radiation and coolant) is not a direct measurement taken on the experimental testbed; however, heat loss values can be calculated with engine data and a first-law energy balance. $\dot{Q}$ values were calculated by rearranging equation 2.15 using measured TOT and $\dot{m}_f$ values from the EEVO sweeps. Fig. 2.17 shows these heat loss values versus EVO. This figure reveals that the heat transfer from the engine generally increases as EVO is advanced. This can be explained by realizing that as fueling increases the in-cylinder temperature also increases, resulting in more heat transfer. It was assumed that $\dot{Q}$ increases linearly with $\dot{m}_f$:

$$\dot{Q}_{EEVO} = C * \left(\frac{\dot{m}_{f_{NEVO}}}{f(EVO)} - \dot{m}_{f_{NEVO}} \right) + \dot{Q}_{NEVO}. \tag{2.18}$$

where C is a model fit parameter.

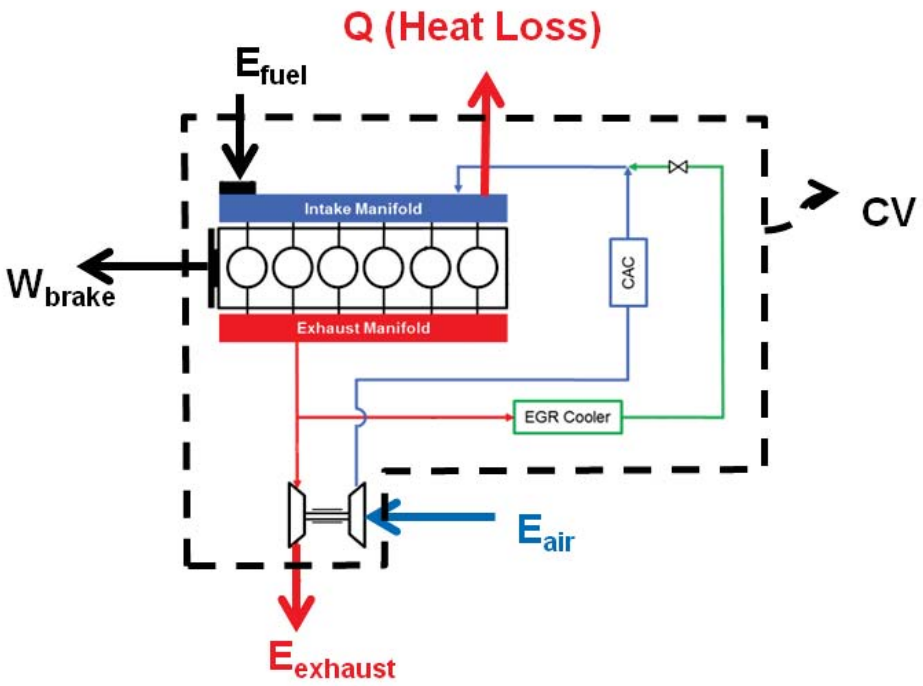

Figure 2.15. Schematic of engine as the control volume for energy balance.

Fig. 2.18 shows a one-to-one comparison of equation 2.18 predicted heat loss versus the actual heat loss. The residual percent and actual errors are shown in Figs. 2.19 and 2.20, respectively. The largest percent error is at condition 1 with ∼11.5% error at -90° EVO timing. Only two points have an error greater than 4 kW, and the majority have less than 5% error.

Applying the assumptions for $\dot{Q}_{EEVO}$ and $\dot{m}_{air}$ (equations 2.17 and 2.18) to equation 2.16 yields

$$TOT_{EEVO} = T_{ref} + \left(\frac{\frac{\dot{m}_{f_{NEVO}} * LHV}{f(EVO)} - \dot{W}_{b_{NEVO}} - \left(C * \left(\frac{\dot{m}_{f_{NEVO}}}{f(EVO)} - \dot{m}_{f_{NEVO}} \right) + \dot{Q}_{NEVO} \right)}{\left(\dot{m}_{air_{NEVO}} + \frac{\dot{m}_{f_{NEVO}}}{f(EVO)} \right) * c_p} \right). \tag{2.19}$$

where TOT_{EEVO} can be calculated based only on knowledge of EVO timing and engine variables at the nominal EVO timing, including brake work $\dot{W}_{b_{NEVO}}$, heat transfer $\dot{Q}_{NEVO}$, air flow rate $\dot{m}_{air_{NEVO}}$, and fuel mass flow rate $\dot{m}_{f_{NEVO}}$.

Turbine out temperature values were calculated using equation 2.19 and compared with the experimentally measured temperatures, as shown in Fig. 2.21. This one-to-

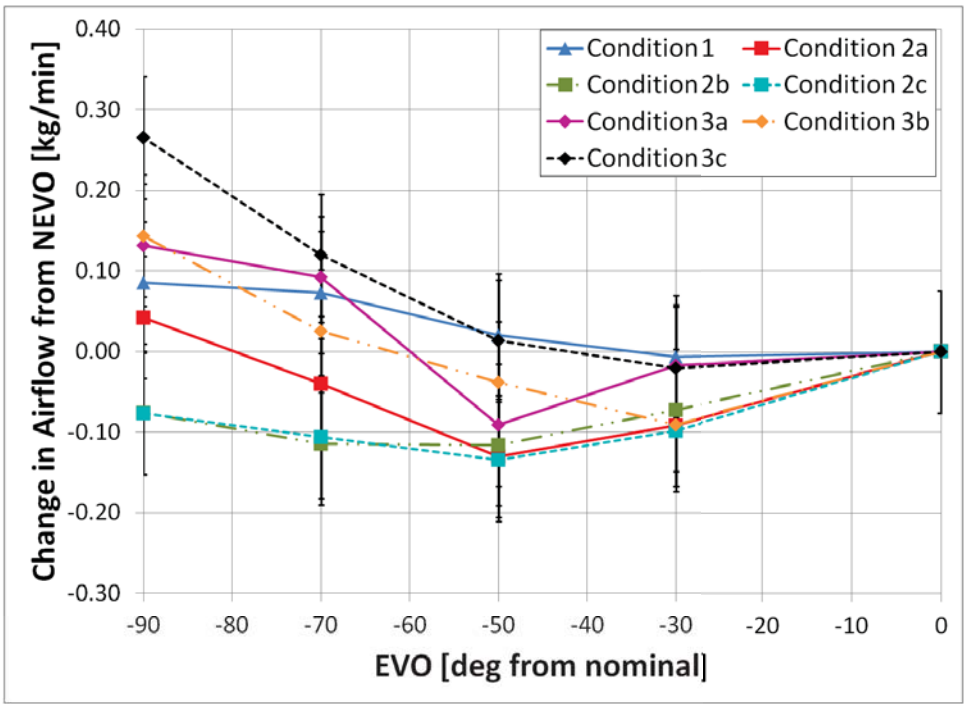

Figure 2.16. Fresh air flow values for experimental EEVO sweeps (see Table 2.2 for condition details).

one comparison demonstrates a good correlation with some amount of over-prediction at condition 1. The percent residual errors and actual residual errors are shown in Figs. 2.22 and 2.23. These show that the maximum error is at condition 1 with ∼16% error at an EVO of -90°, corresponding to an error of about 31°C. All other conditions are within 6% error across all EVO timings.

2.4 EEVO impact on other operating points

Models for the impact of EEVO on TOT and fuel consumption increase (equations 2.19 and 2.9, respectively) have been described and validated with data obtained from experiments. An analysis was conducted utilizing these expressions to predict the fuel penalty and TOT increase at conditions where experiments have not been conducted.

Fig. 2.24 shows TOT for steady-state engine operation with the baseline calibration and nominal valve timings for engine BMEP less than 7.6 bar. The bold black

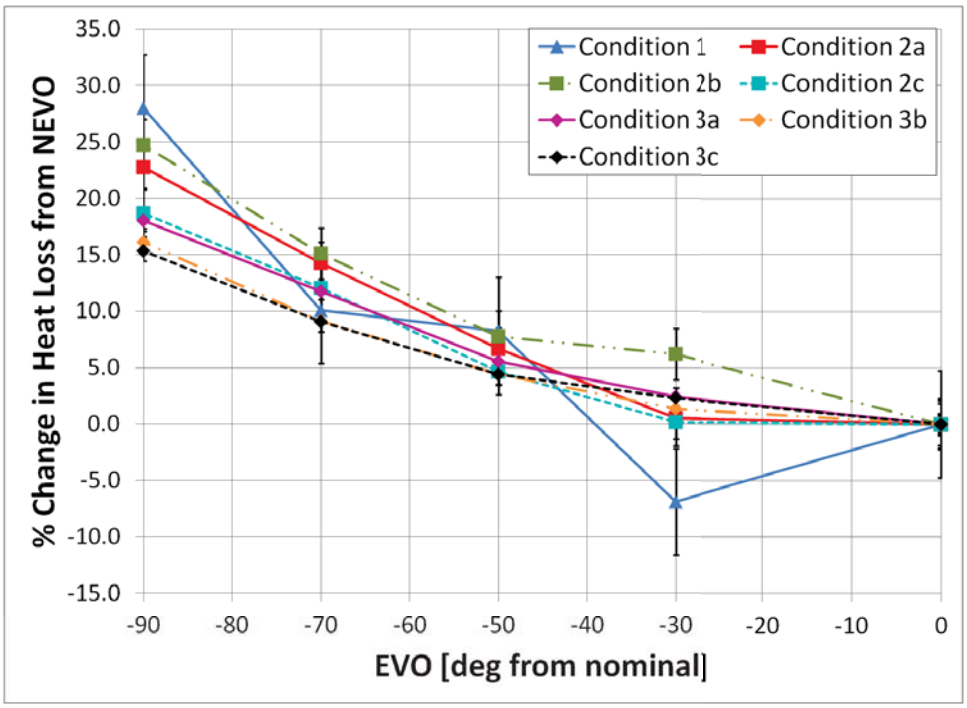

Figure 2.17. Heat loss values for experimental EEVO sweeps (see Table 2.2 for condition details).

line corresponds to a TOT of 250°C as a point of reference. This figure demonstrates that there is a significant potential benefit to thermal management at low loads.

Using equation 2.19, the projected TOT with an EVO 90° before nominal is shown Fig. 2.25. It is evident from Fig. 2.25 that the expected boundary for TOT greater than 250°C has been shifted down considerably on the speed/load map. This shows that EEVO has a significant benefit to aftertreatment thermal management at many operating conditions.

The change in TOT projected by the model is shown in Fig. 2.26. The model predicts a 30°C to 100°C increase in TOT with EVO 90° before nominal where, in general, the larger TOT increases are predicted at higher loads.

The "fuel cost" for this exhaust temperature benefit can also be predicted using equation 2.9 as shown in Fig. 2.27 with BTE given in percentage points for an EVO 90° before nominal. This analysis shows that the penalty is worse at lower speeds and

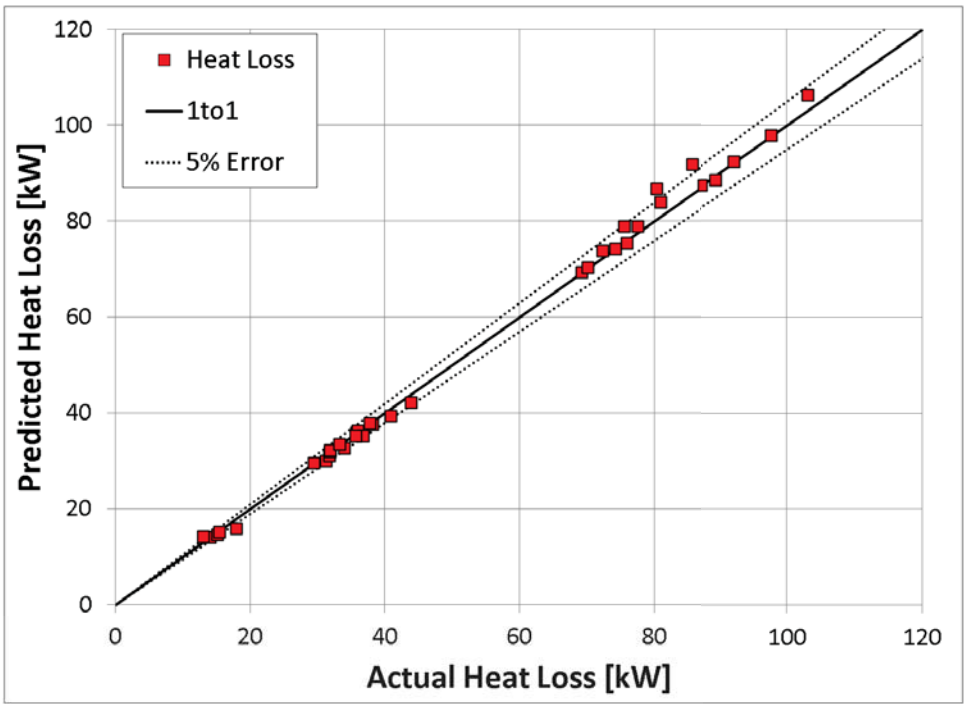

Figure 2.18. One-to-one comparison of predicted vs. actual heat loss values in kW.

higher loads (the conditions at which the engine is nominally more efficient) with a maximum decrease of about 5 BTE percentage points. The analysis projects that at higher speeds the temperature can be increased with a lesser penalty. The predicted BTE reduction at high speeds and low loads is about 2 BTE percentage points.

2.5 Summary

This chapter discusses an experimentally validated analysis strategy for the impact of early exhaust valve opening on turbine out temperature and brake thermal efficiency. Using data from experimental EEVO sweeps the impact of EEVO on the required fuel increase to maintain torque is modeled. This fueling model is utilized in a first law based analysis for the calculation of TOT based on EVO. Heat transfer is also modeled as a function of fuel increase to account for the increased heat lost as temperatures are elevated. These relationships are used to project what TOT can

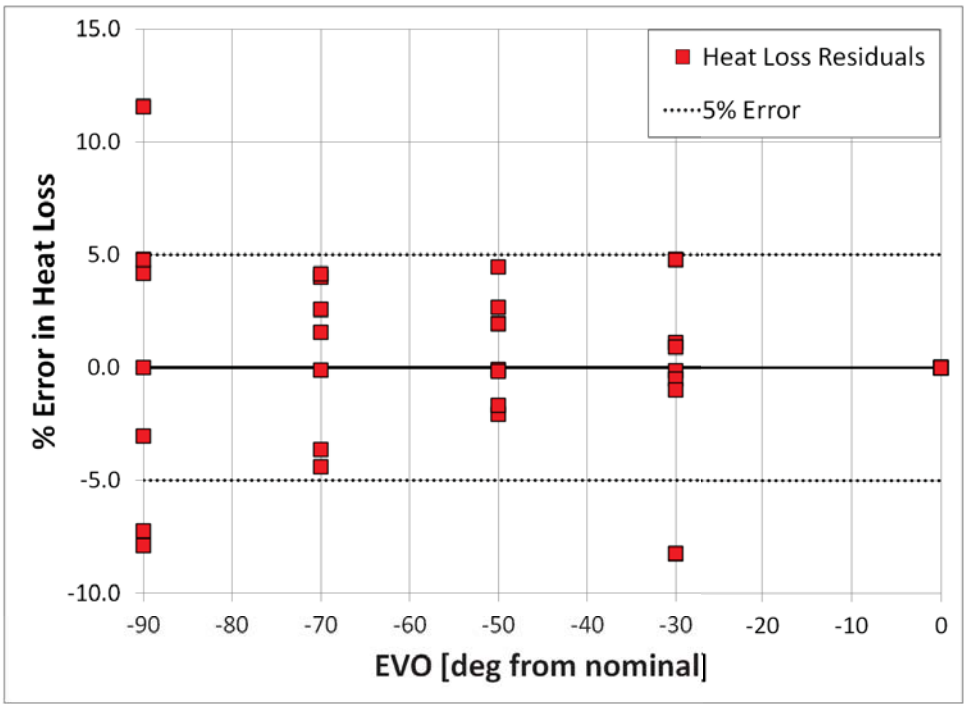

Figure 2.19. Residual percent error of predicted vs. actual heat loss values.

be achieved by advancing EVO as well as the resulting BTE penalty. The analysis predicts a ∼30°C to ∼100°C increase in TOT at the earliest EVO studied. This is sufficient to raise many low-load operating conditions to exhaust temperatures above 250°C for improved aftertreatment effectiveness. However, the model also predicts a significant fuel consumption penalty of ∼0.02 to ∼0.05 points BTE below nominal engine efficiency.

This study demonstrates EEVO as one method of utilizing VVA to accomplish TOT increase for aftertreatment thermal management. The preferred thermal management strategy would include the increase of both TOT and BTE; however, EEVO provides a significant trade-off between these parameters. In the next chapter, an analysis of the effects of cylinder deactivation on TOT and BTE will be discussed.

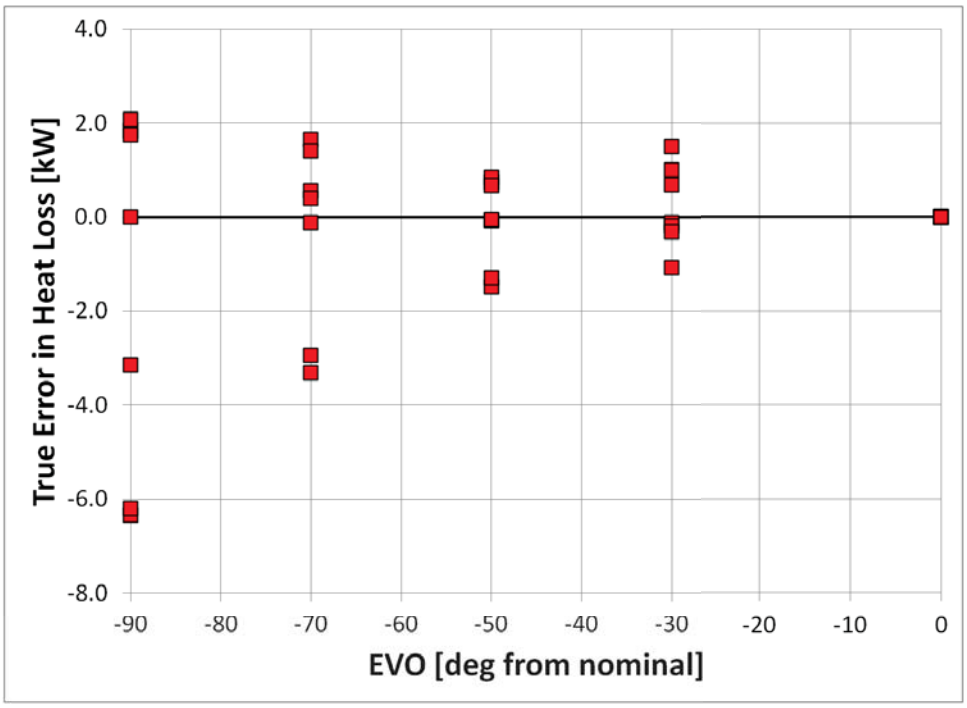

Figure 2.20. Actual residual errors of predicted vs. actual heat loss values in kW.

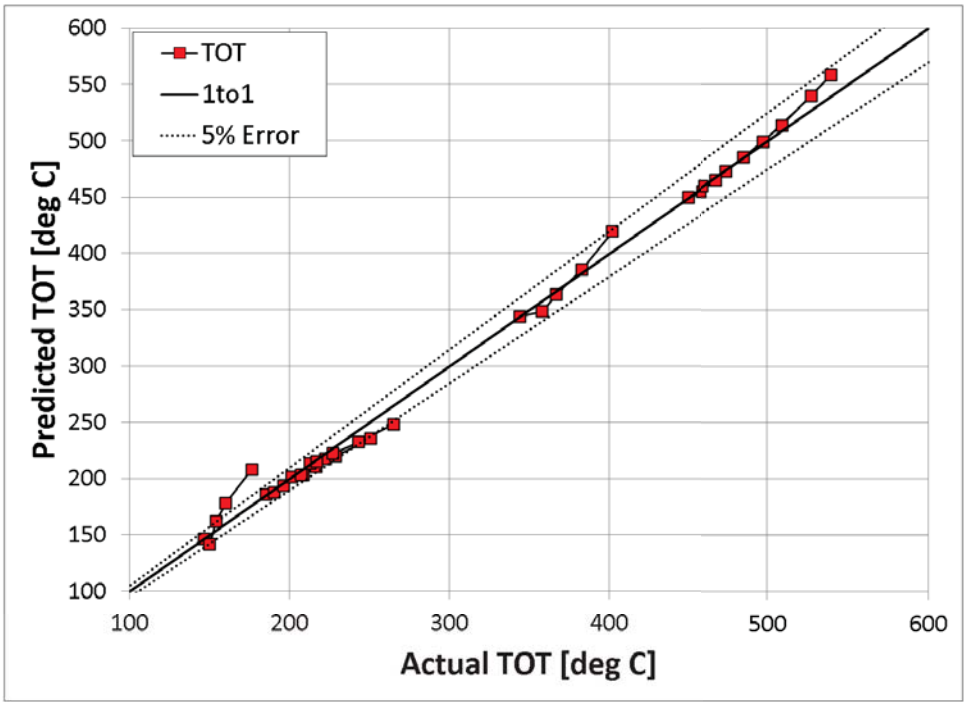

Figure 2.21. One-to-one comparison of predicted vs. actual turbine out temperature values in °C.

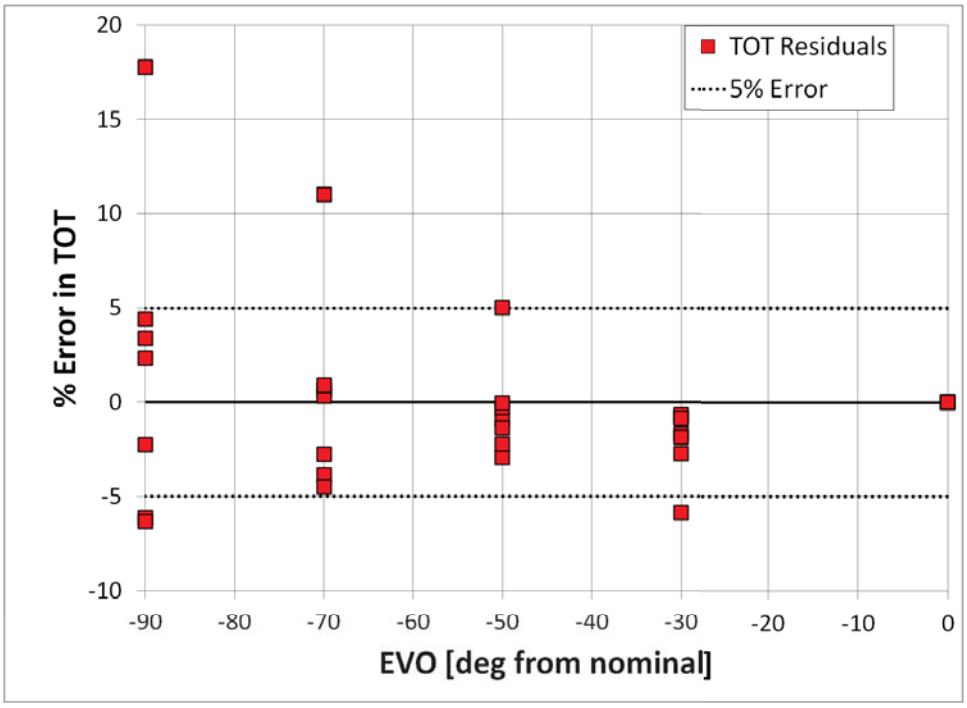

Figure 2.22. Residual percent error of predicted vs. actual turbine out temperature values.

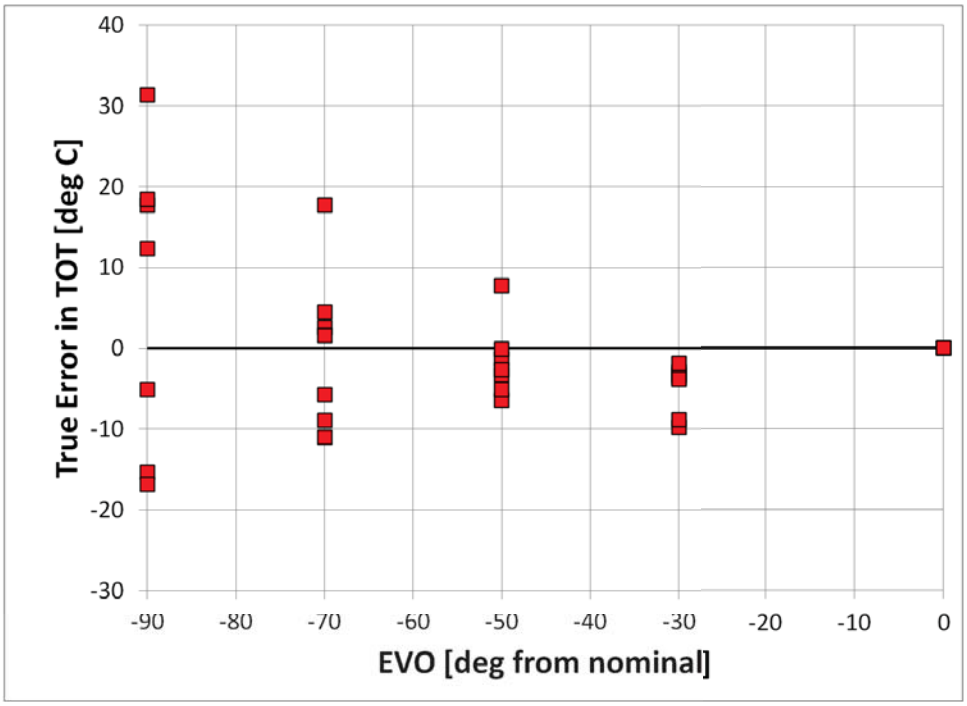

Figure 2.23. Actual residual errors of predicted vs. actual turbine out temperature values in °C.

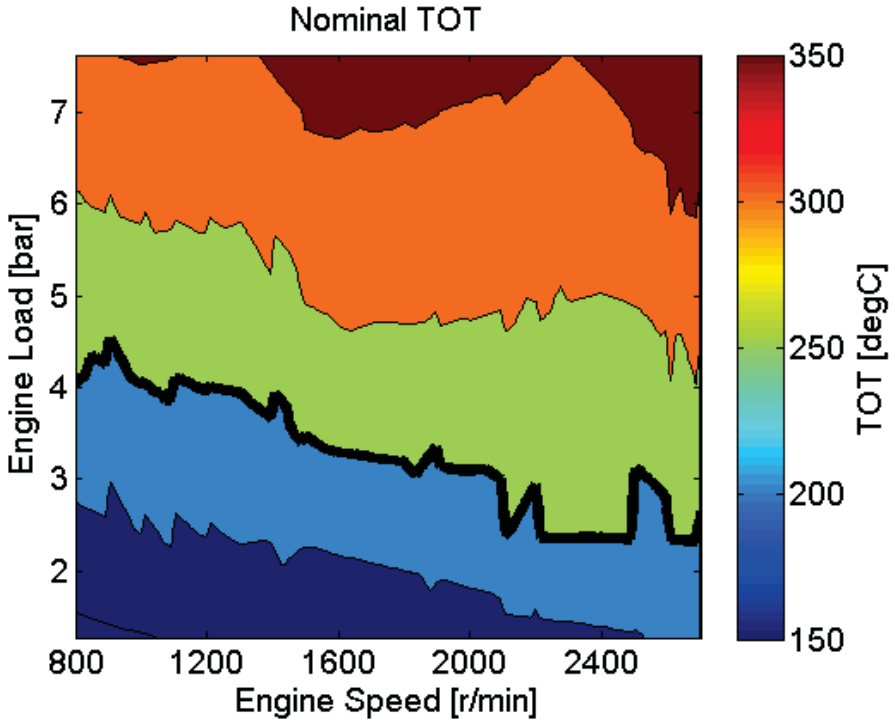

Figure 2.24. TOT under nominal engine operation.

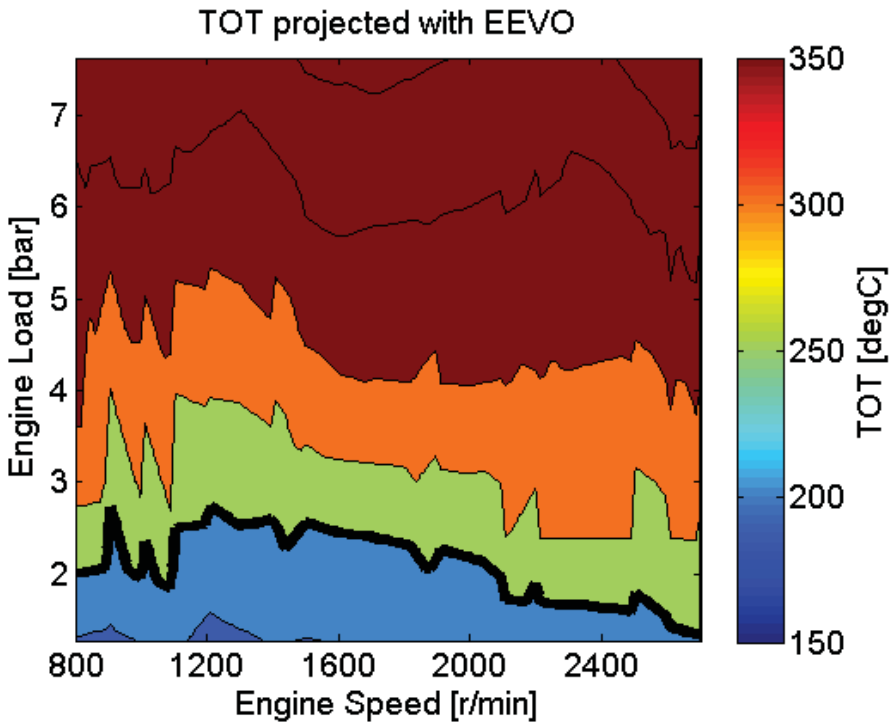

Figure 2.25. TOT projected with EVO -90° from nominal.

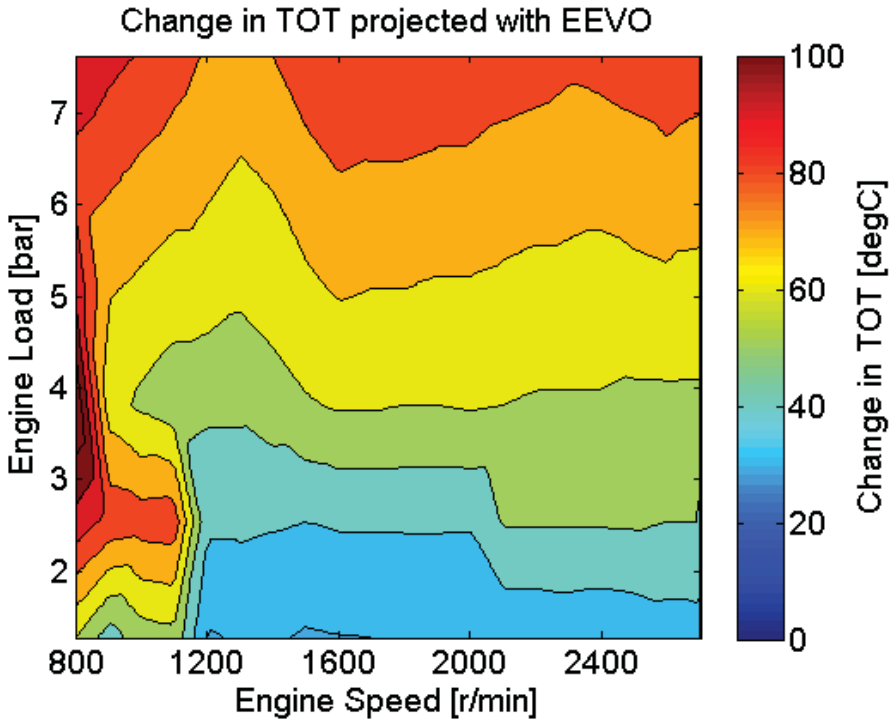

Figure 2.26. Change in TOT projected with EVO -90° from nominal.

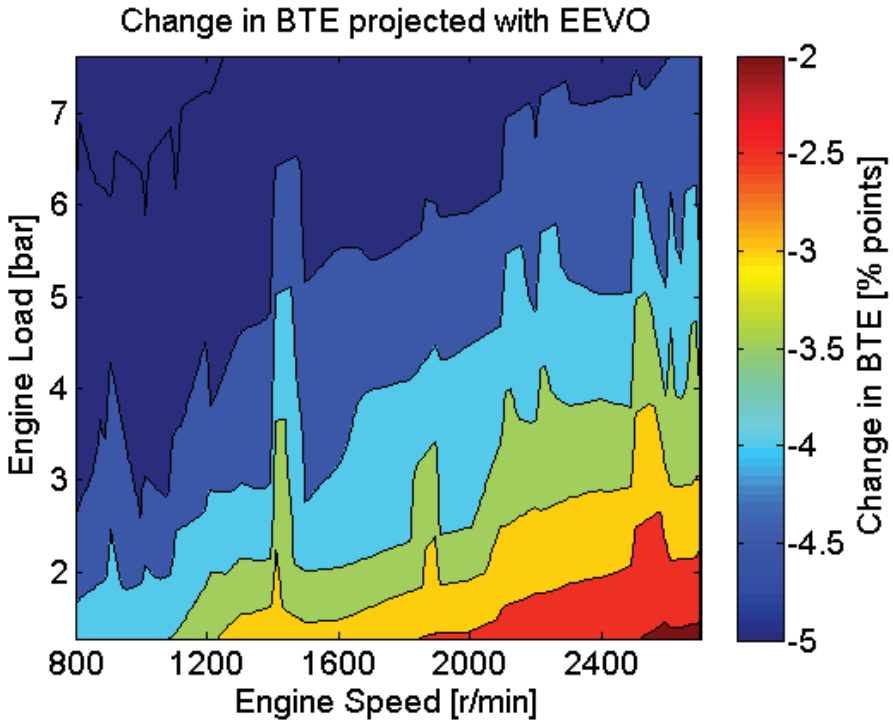

Figure 2.27. Change in BTE from nominal projected with EVO -90° from nominal.

3. ANALYSIS OF THE IMPACT OF CYLINDER DEACTIVATION AT LOADED AND UNLOADED IDLE ON THERMAL MANAGEMENT AND EFFICIENCY

Both unloaded and loaded idle are conditions at which trucks and other vehicles spend a significant amount of time and at which exhaust temperatures are low making afterftreatment thermal management difficult. Exhaust thermal management strategies often are accompanied by fuel consumption penalties, as was demonstrated in the previous chapter with EEVO operation. The ideal thermal management solution would increase temperature enough to keep the aftertreatment working effectively while minimizing the fuel consumption penalty. This chapter outlines a study of CDA at unloaded and loaded idle conditions and focuses on the quantification of exhaust temperature increase and potential fuel consumption benefit as a result of CDA operation.

3.1 Methodology

Two speed/load conditions were selected to study unloaded and loaded idle, respectively. Engines in trucks and other vehicles are often powering accessories and other equipment when idling. The load put on the engine can vary; however, 800rpm/100ft-lbs (136 N-m) (800/100) was selected to represent the loaded idle condition in this study. It is a point where TOT is too low for aftertreatment effectiveness (TOT $\approx$ 200°C) and where thermal management is important. Unloaded idle in this study is represented by 800rpm/11ft-lbs (15 N-m) (800/11). Unloaded idle could be represented as 800rpm/0ft-lbs (0 N-m), however, for simplification of experimental testing, the driveshaft was left connected to the engine and dynamometer, with the dynamometer disengaged. The 11 ft-lbs (15 N-m) represents the friction from leaving

the driveshaft attached. Each operating condition was studied in CDA and 6-cylinder operation. In this study, 3 of the 6 cylinders were deactivated for CDA operation.

The focus of this study was to explore the potential impact of CDA on fuel consumption and TOT. The experiments were constrained to three NOx targets at each operating condition. NOx was measured as brake specific NOx (BSNOx) in g/hp-hr (g/kWh) at the loaded condition. No emphasis was placed on brake power at the unloaded case; therefore, NOx rate was measured in mass per time (g/hr). The NOx targets selected were 1, 3, and 4 g/hp-h (1.3, 4.0, and 5.4 g/kWh) BSNOx and 20, 30 and 38 g/hr NOx at the loaded and unloaded conditions, respectively. These engine-out targets represent values that are consistent with meeting tailpipe NOx emission regulations with modern aftertreatment. In order to thoroughly understand the potential benefit of CDA, the following optimal trade-offs were investigated:

1. Minimize fuel consumption at specific NOx levels within constraints with traditional hardware (i.e. 6-cylinder operation).

2. Minimize fuel consumption at specific NOx levels within constraints with CDA (three cylinders deactivated).

3. Maximize TOT at specific NOx levels within constraints with CDA (three cylinders deactivated).

Trade-offs 1 and 2 are designed to show a comparison between 6-cylinder and CDA for potential benefit in fuel consumption. Trade-off 3 is meant to provide additional insight into the highest TOT that can be achieved by operating in CDA. All data presented in this paper and in subsequent figures were based upon one of these optimizations.

Two additional emissions constraints were imposed on all optimized results as listed in Tab. 3.1. These were selected based on the low speed (800 rpm) of the engine during these tests. These constraints are also designed to represent values that are consistent with meeting tailpipe emissions regulations.

Table 3.1. Emissions constraints.

Emission	Constraint Value
Unburned Hydrocarbons	200 ppm
PM (Smoke Number)	1.0 FSN

Table 3.2. Mechanical constraints.

Parameter	Maximum Constraint
Turbine In Temperature	760°C
Compressor Out Temperature	230°C
Turbo Speed	193 kRPM
Peak Cylinder Pressure	17.2 MPa
Exhaust Manifold Pressure	400 kPa (gauge)
Pressure Rise Rate	100 bar/sec

The results were also constrained by mechanical limits of the engine hardware, as are shown in Tab. 3.2. These limits represent the maximum pressures, temperatures, etc. at which the engine can operate. All work in this study was done at low loads at idle speed; therefore, no adjustments of operating conditions were needed to adhere to these limits.

3.2 Experimental Data Collection

The three trade-offs mentioned above were generated using constrained optimization utilizing on-engine experimental data. This data was obtained by performing a design of experiments (DOE) on the engine. Each DOE was a face centered central

composite design. The independent variables chosen for the DOEs were SOI (deg BTDC), rail pressure (bar), VGT position (% closed), and EGR position (% open). DOEs were run in both CDA and 6-cylinder mode. After each DOE was run on the test bed, the data was analyzed using Minitab software. Constrained optimization was performed for each trade-off at each NOx level to generate the trade-offs. The ranges of the independent variables were adjusted, and another iteration of DOE testing was performed if the optimized results returned inputs that were against the limits of the independent variable ranges specified in the DOEs.

Once the optimized results were found, those inputs were rerun on engine to validate the accuracy of the constrained optimization. Each optimized point was run once on engine for validation. Three consecutive measurements were taken for each operating condition (loaded and unloaded) and each mode of operation (6-cylinder and CDA) to be used for a measurement uncertainty analysis. This uncertainty is shown on all plots as error bars of +/- one standard deviation of each variable measured/calculated. All results discussed in this paper are from experimental validation of the optimized results.

3.3 Results and Discussion

3.3.1 Turbine Out Temperature

Loaded Idle

This optimization effort shows there is a substantial benefit of CDA with respect to TOT at 800/100. TOT for each of the three trade-off curves is shown in Fig. 3.1. Error bars are included on the plot; however, the uncertainty of TOT is too small to be visible. The optimized trade-off to which each set of points belongs is labeled in the legend. The mode of operation (6-cylinder or CDA) is also listed for reference. A comparison of the minimized brake specific fuel consumption (BSFC) curves (trade-offs 1 and 2) indicates that TOT increases from about 190°C to about 300°C in CDA.

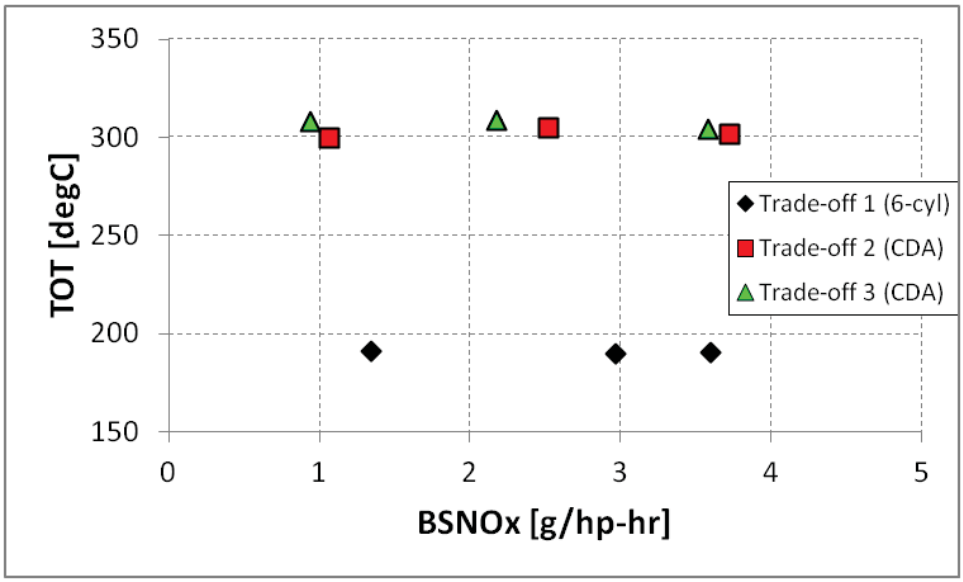

Figure 3.1. Turbine out temperature at 800/100.

This increase is independent of the BSNOx target. The optimization for maximum TOT with CDA (trade-off 3) yielded temperatures very similar to the minimum BSFC case. Maximum TOT observed was 308°C, at the 3 g/hp-hr BSNOx target. This shows that, while maximizing for TOT with CDA provides some additional increase in temperature, the major benefit is realized with CDA operation, even focused at minimizing BSFC. Nominal TOT at this operating point, as mentioned above, is too low for aftertreatment effectiveness. The major benefit here is realized because the TOTs in CDA are hot enough for most aftertreatment systems to work effectively.

The increase in TOT with CDA is mainly due to the reduction in the air-fuel ratio. The air-fuel ratios for each data point are displayed in Fig. 3.2. Note that the error bars are also very small for air-fuel ratio. The air-fuel ratio nominally in 6-cylinder mode is between 30-40. Fresh air flow increases as EGR is decreased to meet the higher BSNOx targets causing air-fuel ratios to be elevated for higher BSNOx levels. Charge flow is reduced with CDA because only half of the cylinders are "breathing." This causes a reduction in air-fuel ratio to about 20-25 in trade-off 2. Fueling is

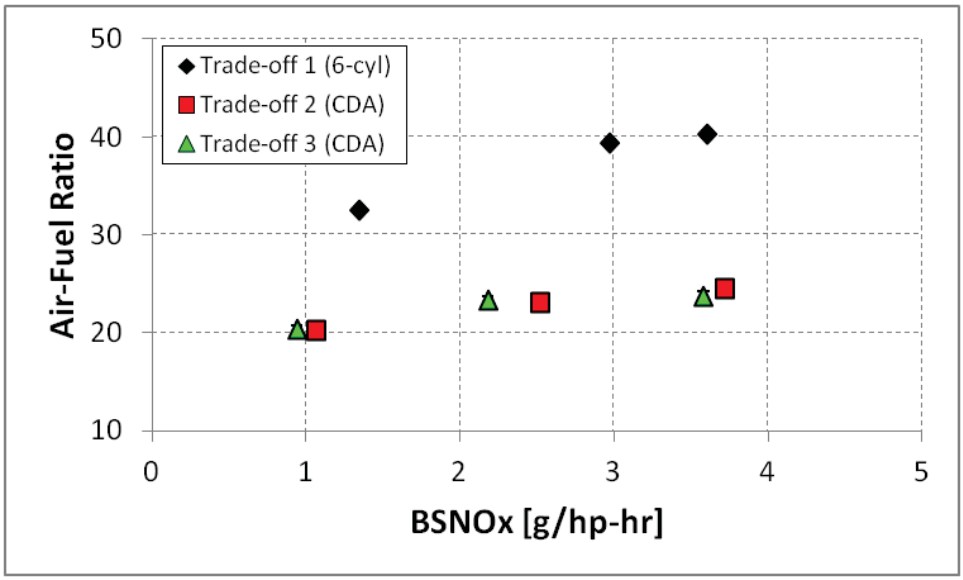

Figure 3.2. Air to fuel ratio at 800/100.

approximately doubled on a cylinder specific basis to maintain the torque with half the cylinders firing. These reduced air-fuel ratios in CDA are closer to, yet still above, the stoichiometric value of about 14.6 which causes combustion temperatures to increase. The increased in-cylinder temperatures lead directly to higher TOT. There is little difference in air-fuel ratio between trade-offs 2 and 3 which points to the similar TOTs measured at these points.

A first law-based analysis helps to verify why TOT is increased for CDA operation. Placing the control volume around the cylinders allows a calculation of the heat transfer from the engine block. The heat lost from the cylinders is shown in Fig. 3.3. There is no statistical distinction between trade-offs 2 and 3; however, the CDA points clearly show greater heat transfer than the 6-cylinder points at each BSNOx level. The greater heat loss in CDA is caused by higher in-cylinder temperatures.

There is an approximately 65% to 75% reduction in EGR flow in CDA mode. This causes the heat rejected through the EGR cooler to be less with CDA. The sum of the heat losses from the cylinders and the EGR loop is shown in Fig. 3.4. This plot

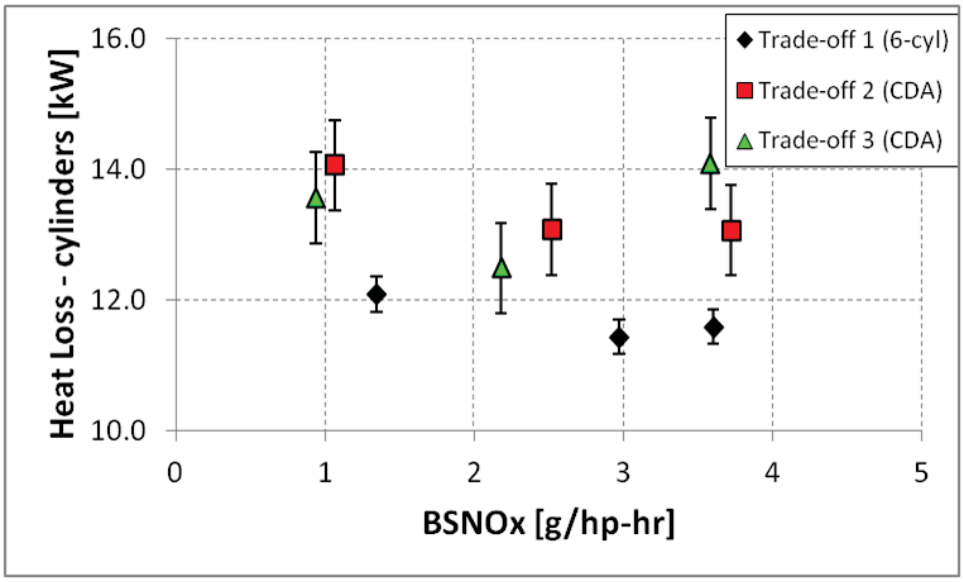

Figure 3.3. Heat loss from cylinders at 800/100.

shows that the heat loss is about the same for all points at each BSNOx target. The additional heat loss from the turbocharger is similar for all points and does not affect the relative difference in heat loss from that shown in Fig. 3.4. The combination of lower air-fuel ratios in CDA and no significant difference in heat transfer leads to greater TOTs with CDA.

Unloaded Idle

The condition at 800/11 or unloaded idle is also a point of thermal management concern because engines spend a considerable amount of time at idle, and the TOT is very low due to the small amount of fuel used. The optimized points show that TOT in CDA is also increased at 800/11 above nominal temperatures as shown in Fig. 3.5. The TOTs measured in 6-cylinder mode were approximately 117°C independent of the NOx rate target. Trade-off 2 shows an increase above trade-off 1 with TOT ranging from 131°C to 134°C. Optimizing for maximum TOT with CDA yielded TOTs about 3°C to 5°C above the minimized fuel consumption points, specifically

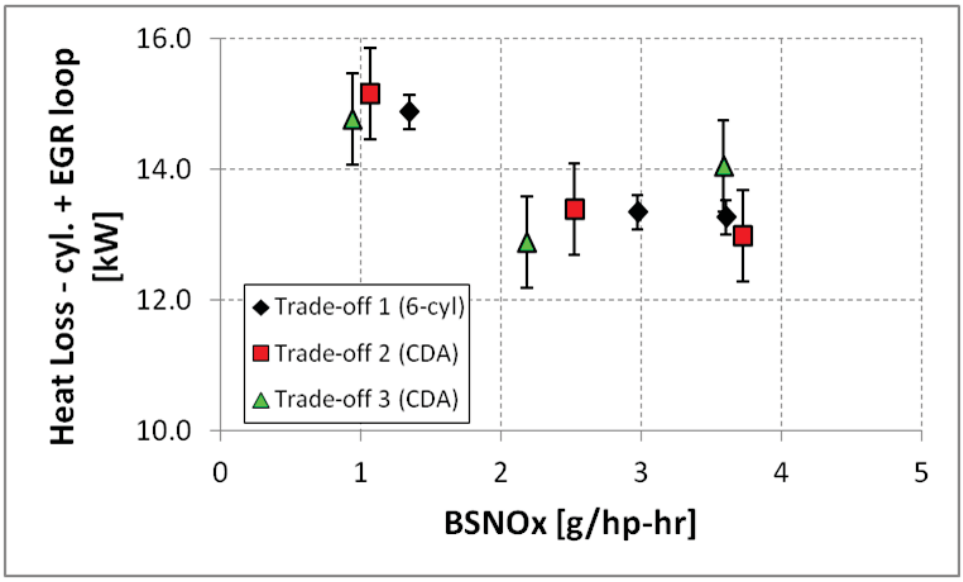

Figure 3.4. Heat loss from cylinders and EGR loop at 800/100.

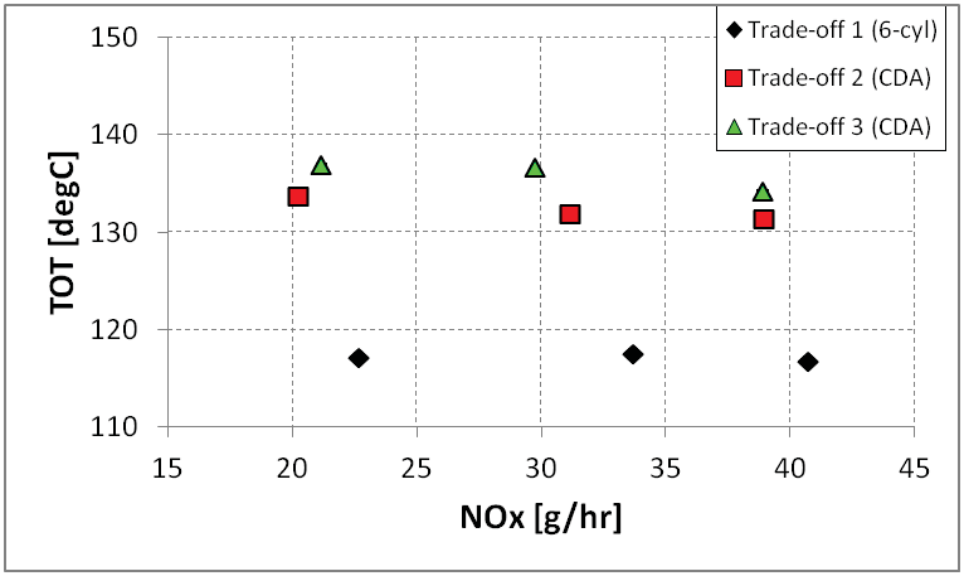

Figure 3.5. Turbine out temperature at 800/11.

134°C to 137°C. CDA can provide about a 20°C increase above nominal 6-cylinder operation.

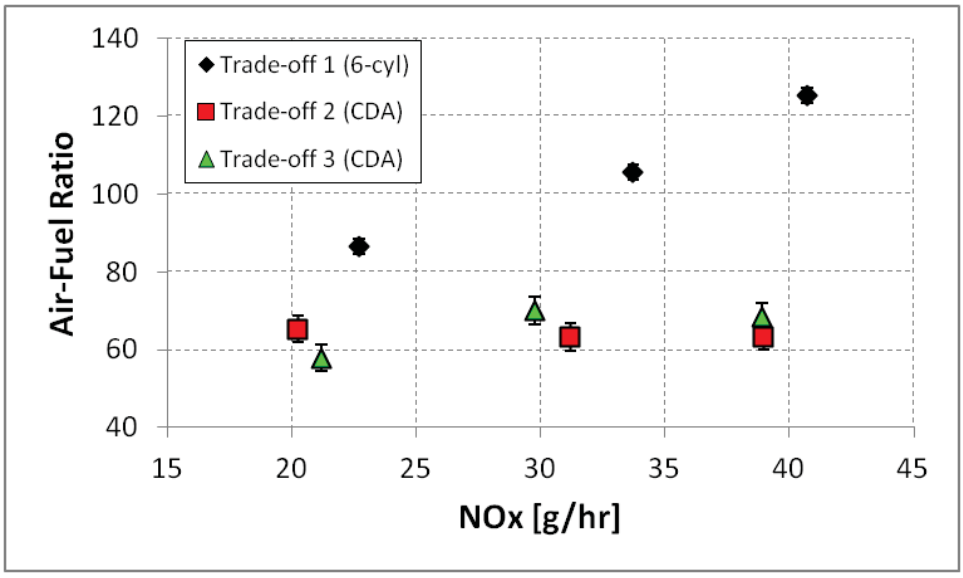

Figure 3.6. Air to fuel ratio at 800/11.

The increase in TOT is primarily due to the reduced air-fuel ratios in CDA, as was described for the loaded idle case. The air-fuel ratios for 800/11 are shown in Fig. 3.6. For trade-off 1, air-fuel ratios range from 85 at low NOx to 125 at the highest NOx target. This is due to the decrease of EGR used to meet the higher NOx targets. These high air-fuel ratios are a consequence of the small amount of fuel used at the unloaded idle condition. The air-fuel ratios for trade-offs 2 and 3 are around 60 to 70. There is not a significant variation between these two trade-off sets. It is expected that as the NOx level decreases, the TOT between 6-cylinder and CDA would be closer due to more similar air-fuel ratios. However, as shown in Fig. 3.5, the relative difference in TOT between 6-cylinder and CDA is almost constant across all NOx targets. This can be explained further by a comparison of heat transfer.

The heat loss from the cylinders is shown in Fig. 3.7. The heat lost in CDA mode is about 5.5 to 6.5 kW across all NOx levels. At the lower two NOx targets, 6-cylinder heat loss is about 20% to 25% higher. This is a different result than what was seen at the loaded case. The temperatures are similar between each mode with

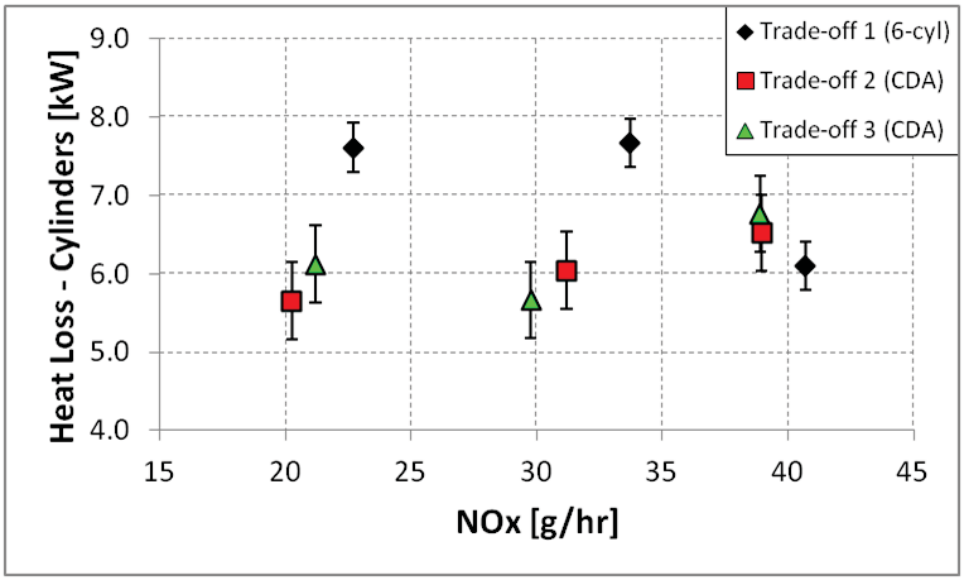

Figure 3.7. Cylinder heat loss at 800/11.

$\sim$20°C difference in the TOTs. There is also a higher surface area of firing cylinders which leads to greater heat transfer. Combustion temperatures at the higher NOx level are expected to be cooler which reduces the heat transfer.

There is also a reduction in EGR flow with CDA (45% to 65%) at the unloaded condition; however, the lower temperatures reduce the amount of heat transfer that occurs in the EGR cooler for both 6-cylinder and CDA operation. The heat loss in the EGR loop and the turbocharger are about equal for CDA and 6-cylinder mode meaning the relative difference in total engine heat transfer is similar to what is shown in Fig. 3.7. This difference in heat loss reveals why the difference in TOT is not much larger at 20 g/hr NOx than at 38 g/hr NOx. The combustion temperature is expected to be higher in 6-cylinder operation at 20 g/hr NOx but the heat transfer is also greater at 20 and 30 g/hr NOx to offset this difference.

3.3.2 Fuel Consumption

Loaded Idle

Figure 3.8 shows the BSFC trade-off results at 800/100 which indicate that while raising TOT (per Fig. 3.1), CDA consumes approximately equal fuel as 6-cylinder operation. The fuel consumption values are normalized to the 6-cylinder values at each NOx target. CDA values above 1 indicate that more fuel is consumed, while values below 1 demonstrate that less fuel is consumed. A comparison of trade-off 2 with trade-off 1 shows that optimizing for BSFC with CDA does not improve efficiency above 6-cylinder operation. There is a possible BSFC penalty of about 3% at 1 g/hp-hr BSNOx target. The BSFC is equal at the other two BSNOx targets; however, the error bars on the points demonstrate that there is no significant difference in fuel consumption. There was also very little difference in TOT between trade-offs 2 and 3. The approximately equal fueling between 6-cylinder operation and CDA means that there is no fuel consumption penalty to the increase in TOT obtained with CDA. This is a benefit as other strategies might cause a fuel consumption penalty in order to increase exhaust temperatures. In short, Figs. 3.1 and 3.8 demonstrate that at the loaded idle condition, deactivating 3 cylinders provides an increase in engine exhaust temperature from $\sim$200°C to 300°C with no fuel economy penalty.

It is worthwhile to consider why there is essentially no change in BSFC between CDA and 6-cylinder operation. One of the purposes of running with deactivated cylinders at low load is to avoid driving excess air through the engine that is not needed. This generally will increase the open cycle efficiency, which may in turn lead to higher brake thermal efficiencies. However, as shown in Fig. 3.9, 6-cylinder operation at the loaded condition is already near 100% open cycle efficiency. As such, at the optimized condition, CDA cannot provide a significant improvement to open cycle efficiency with 6-cylinder already operating near perfect open cycle efficiency.

There is also very little improvement in closed cycle efficiency, as shown in Fig. 3.10. Closed cycle efficiency is a measure of the efficiency of the power stroke (com-

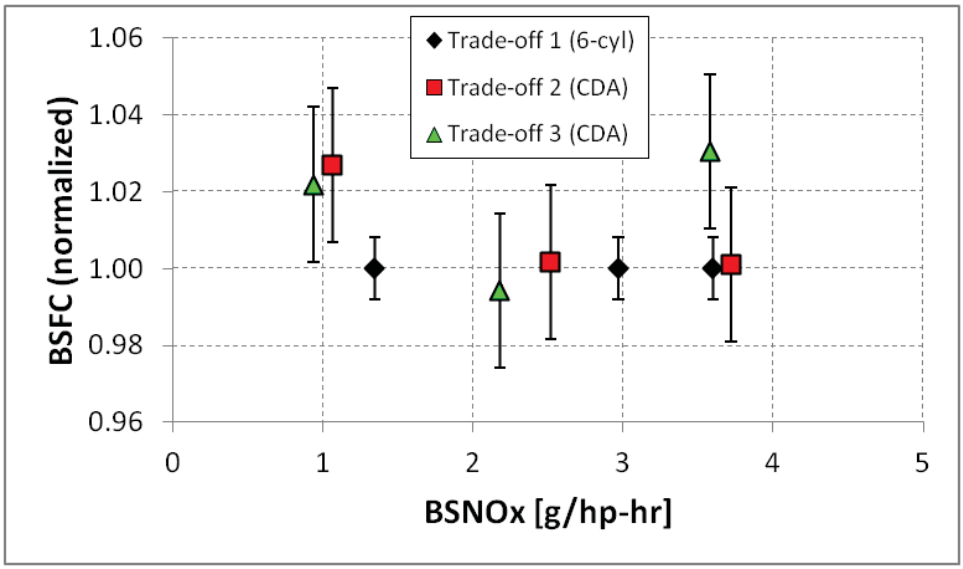

Figure 3.8. BSFC at 800/100.

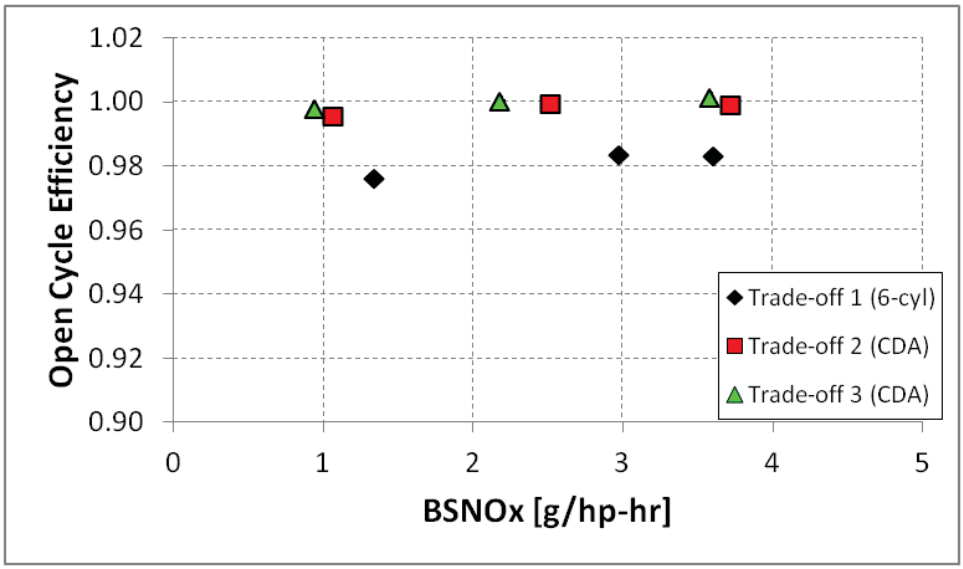

Figure 3.9. Open cycle efficiency at 800/100.

bustion and expansion) and is defined as the ratio of the power released from the injected fuel (measured at the piston) to the energy contained in the fuel. The fueling is approximately doubled in the active cylinders during CDA operation, increasing

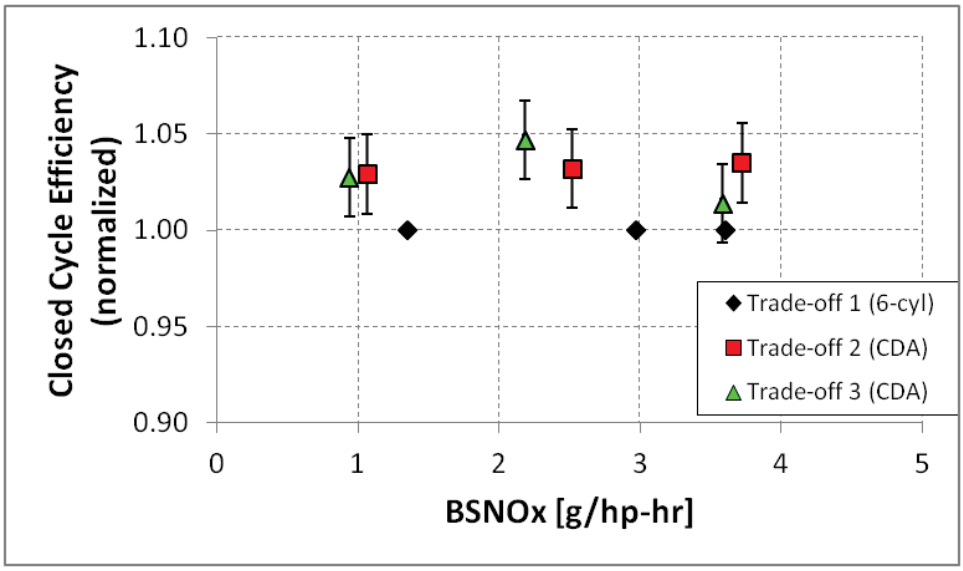

Figure 3.10. Closed cycle efficiency at 800/100.

the burned gas temperatures, which increases the heat transfer from the cylinders. Greater cylinder heat transfer has a negative impact on closed cycle efficiency, but despite this increase, CDA still has slightly higher closed cycle efficiency, due to aggressive heat release. This increase is realized independent of optimizing for BSFC or for TOT. There is less than 5% increase in closed cycle efficiency across all trade-offs and BSNOx levels.

It is worthwhile to note that, despite improved open and closed cycle efficiencies in CDA mode (per Figs. 3.9 and 3.10), there is no overall benefit to fuel consumption at this condition. This can be attributed to a decrease in mechanical efficiency for CDA; however, the specific cause of this reduction is not known.

Unloaded Idle

Fuel consumption in CDA has significant improvement at 800/11. Fuel consumption values, normalized to the 6-cylinder cases at each NOx target are shown in Fig. 3.11. Fuel consumption values below the 6-cylinder cases indicate that less fuel is

consumed. A comparison of trade-offs 1 and 2 show that optimizing for minimized fuel consumption yields much lower fuel consumption in CDA across all NOx targets. The maximum benefit measured was at 30 g/hr NOx with a 26% reduction in fuel consumption with CDA. The minimum fuel consumption benefit, observed at 38 g/hr NOx, is 15%. There is also a large benefit at 20 g/hr NOx. This reduction in fuel consumption also comes with an approximate 15°C increase in TOT, as described above.

Optimizing for maximum TOT in CDA also shows there is a benefit in fuel consumption, as shown with trade-off 3; however it requires slightly more fuel at these conditions than is measured for trade-off 2 points. This extra fuel is the cost for achieving the 3°C to 5°C increase over the optimized fuel consumption points in CDA. At 30 g/hr NOx target, however, there is still a 25% improvement in fuel consumption while achieving the maximum TOT increase of 20°C. Together, Figs. 3.5 and 3.11 demonstrate that at the unloaded idle condition, CDA provides an increase in exhaust temperature of about 20°C, from about 117°C to about 135°C, with a fuel consumption reduction of 15%-26%.

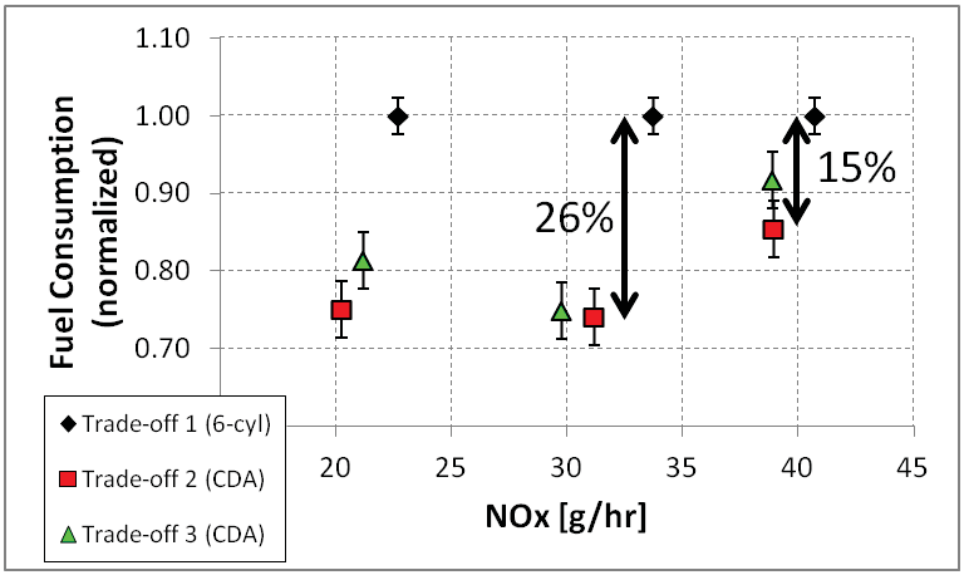

Figure 3.11. Fuel consumption at 800/11.

Deactivating cylinders, as mentioned above, reduces the charge flow which can reduce the pumping penalty and increase the open cycle efficiency. The engine pumps a great amount of excess air at unloaded idle, and as such, there is a large potential for efficiency improvement. The open cycle efficiency for 800/11 is shown in Fig. 3.12. The open cycle efficiency is approximately equal in CDA between trade-offs

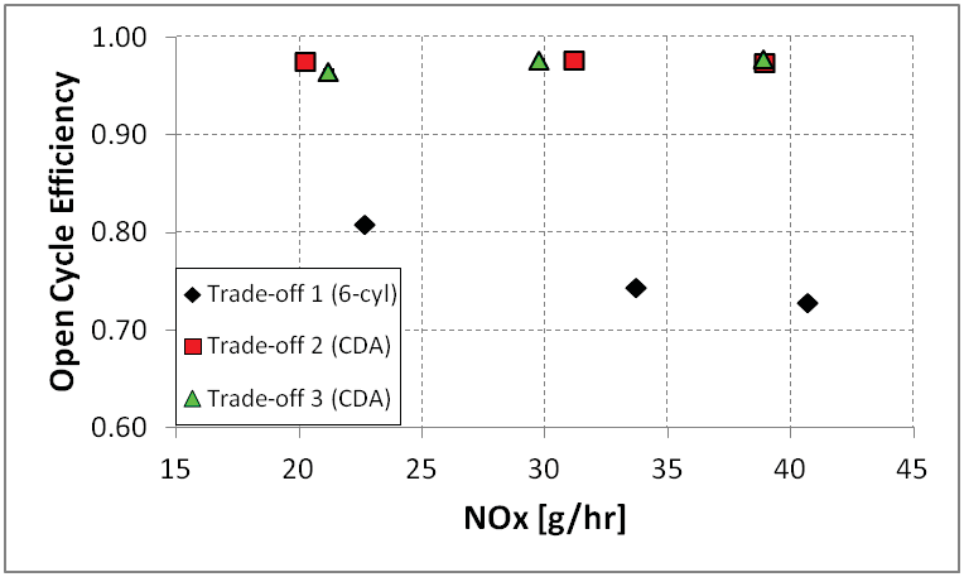

Figure 3.12. Open cycle efficiency at 800/11.

2 and 3. There is a 20% to 35% increase in open cycle efficiency with CDA. This improvement comes from a reduction in the charge flow by approximately half when half the cylinders are active. In addition, less EGR is needed in CDA to meet the same NOx targets as with 6-cylinders. This allows the VGT to be more open to drive less EGR, reducing the pumping penalty, and increasing the open cycle efficiency.

Closed cycle efficiency also is improved with CDA at unloaded idle. However, because of the reduction of EGR in CDA, the air flow is similar between both CDA and 6-cylinders for the lower NOx targets. This leads to similar air-fuel ratios. The in-cylinder temperatures are not very different, but in CDA mode, there is less surface

area for heat transfer to occur with only three cylinders active. As such, the heat lost from the cylinders is reduced with CDA, which improves closed cycle efficiency.

3.4 Summary

This chapter discusses an experimental based analysis of cylinder deactivation versus nominal 6-cylinder operation on a diesel engine with a focus on raising turbine out temperatures and improving fuel consumption at both loaded and unloaded idle conditions. A constrained optimization was performed utilizing data obtained from design of experiments. The optimization was performed for minimizing fuel consumption or BSFC with both 6-cylinder operation and CDA and maximizing TOT with CDA. The results of the optimization were validated on the experimental testbed.

CDA provides the largest benefit in TOT at the loaded idle case (800/100). Optimizing either for maximum TOT or minimum BSFC showed that CDA can achieve more than 115°C increase in TOT while consuming approximately the same amount of fuel as with 6-cylinder operation. This provides enough TOT increase for improved effectiveness for many aftertreatment systems while avoiding a fuel consumption penalty.

CDA enables a significant fuel consumption improvement at unloaded idle (800/11). Optimizing for minimum fuel consumption yields 15% to 26% reduction in fuel consumption with CDA depending on the NOx target under consideration. An increase in TOT of about 20°C is also realized with CDA at the unloaded condition. This is significant given the fact that this increase comes with a major reduction in fuel consumption. Work is continuing with other VVA functions to explore means to further increase TOT. However, CDA alone provides significant benefit to TOT at loaded idle and improvement to fuel consumption and TOT at unloaded idle. The stated efficiency comparisons between 6-cylinder and CDA operation do not account for the extra fuel that would be required to maintain adequate TOTs to support the aftertreatment.

The results of this study make CDA appear to be an attractive option for aftertreatment thermal management at low load. However, engines are often operated transiently, transitioning from low to higher load. The airflow needs to be increased to operate at higher loads. The reduced airflow from CDA can potentially challenge the operation of CDA during transient operation. The following chapter will discuss the associated challenges of CDA.

4. CHARACTERIZATION OF CHALLENGES OF CYLINDER DEACTIVATION FOR TRANSIENT LOAD PERFORMANCE

This chapter discuses the thermal management and efficiency potential benefit of three cylinder deactivation on a diesel engine operating at cruising speed. Additionally, a transient study is performed to characterize the potential challenge for load performance of the engine during CDA operation. The transient load performance limitation comes from the reduced airflow caused by the deactivation of half the cylinders.

4.1 Steady State Load Sweeps

This first section discusses an effort to quantify the benefits of operating CDA in a diesel engine at several different loads. For more detail on this effort, the reader is referred to [30].

4.1.1 Steady State Data Collection

The steady-state data was taken at 1200 rpm, which is a typical cruising speed for on-highway trucks and heavy-duty vehicles. On-highway vehicles spend the majority of time at cruising speed conditions; therefore, emissions control and aftertreatment thermal management are very important considerations at these conditions. Any benefit in thermal management as a result of CDA would be significant.

Load sweeps (from low to high load) were performed in order to investigate the potential benefits and tradeoffs of TOT and fuel consumption at various operating conditions. BMEP was increased starting from 1.27 bar, and data was taken every 1.27 bar until a constraint was reached. Data was taken at each operating point after allowing the engine to reach a steady-state condition.

Three load sweeps were performed with CDA, each with a specific BSNOx level targeted, specifically 1.5, 3, and 4 g/hp-hr BSNOx. The 6 cylinder fueling inputs such as SOI, Rail Pressure, Pilot Quantity and Timing, Post Quantity and Timing at twice the load were used as guides for fueling inputs in CDA. EGR and VGT were varied as required to meet NOx targets. SOI was also modified at the higher loads to help meet the NOx targets.

One load sweep in 6-cylinder operation was performed for a baseline comparison. NOx was targeted between 3 and 4 g/hp-hr to keep the NOx comparable with the CDA cases. The fueling inputs for the 6-cylinder cases were based on the baseline engine calibration.

Note that the results presented here do not represent optimized operating conditions; however, the screening effort performed on the experimental engine provides an approximation of the potential benefit with respect to the nominal 6-cylinder operation. This analysis will be used to quantify the ability of CDA to increase TOT and then to examine its effect on engine efficiency.

4.1.2 Steady State Results

The TOT results are shown in Fig. 4.1. The BMEP is displayed on the x-axis. The 6-cylinder results with each NOx target CDA load sweep results are shown with different symbols as shown in the legend. At 1.5 g/hp-hr, the maximum achievable load was approximately 7.6 bar. At 3 g/hp-hr, the maximum achievable load was approximately 8.0 bar, and at 4 g/hp-hr, the maximum achievable load was approximately 8.3 bar. As the NOx target is decreased, more EGR is required, resulting in a decrease in AFR, which increases the turbine inlet temperature, the limiting factor in all three cases.

The experimental results indicate that CDA is effective at raising exhaust temperatures significantly at every BMEP. The CDA points have similar TOTs with some variation due to different EGR rates used to meet the specific NOx targets.

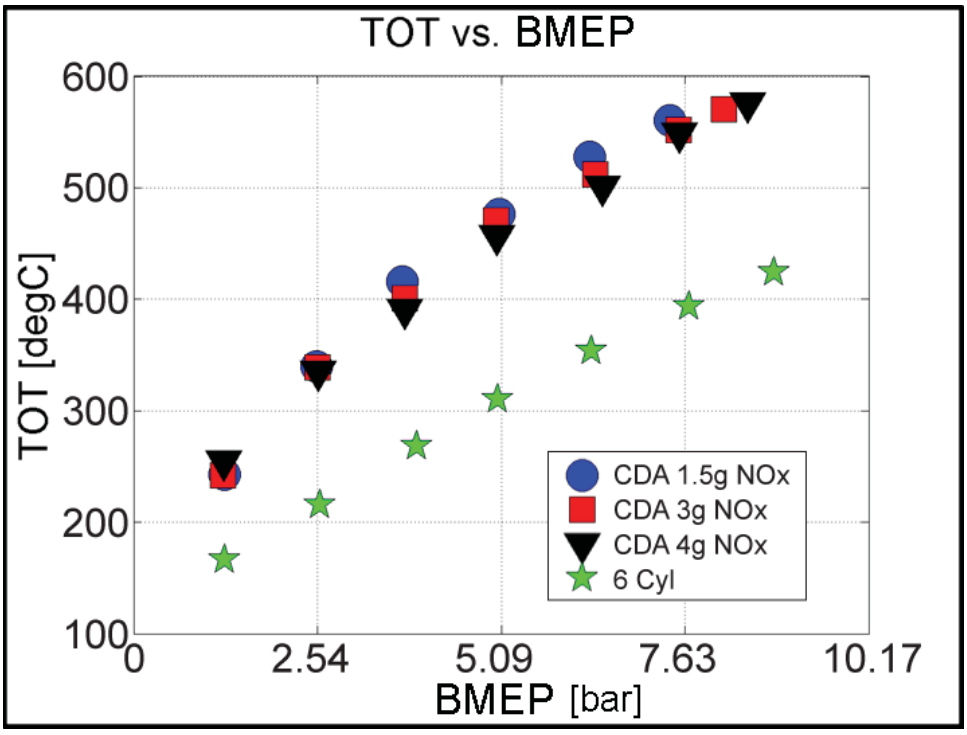

Figure 4.1. Turbine out temperature results of load sweeps at 1200 rpm.

At 1.27 bar, the TOTs with CDA have an approximate 88°C increase, from 166°C in 6-cylinder operation to 254°C with CDA. This is enough temperature increase for significant improvement in aftertreatment catalyst effectiveness. The elevated temperature in CDA is also approximately equivalent to the TOT with 6 active cylinders at 3.8 bar. The TOT increase from CDA is about 174°C (from 354°C in 6-cylinder operation to about 528°C with CDA) at 6.4 bar. The temperature increase at this load would allow for active regeneration of a DPF. The increase at any load is beneficial for increased heat-up of the aftertreatment from cold conditions.

The TOT increase is primarily a result of reduced AFR, as shown in Fig. 4.2. 6 cylinder AFR is between 70 at low load to about 25 at the maximum BMEP studied. The charge flow is reduced by about half when three cylinders are deactivated. This leads to reduced airflow and, therefore, AFR. As the NOx targets are decreased, more EGR is used which displaces the fresh air causing an even greater reduction in the

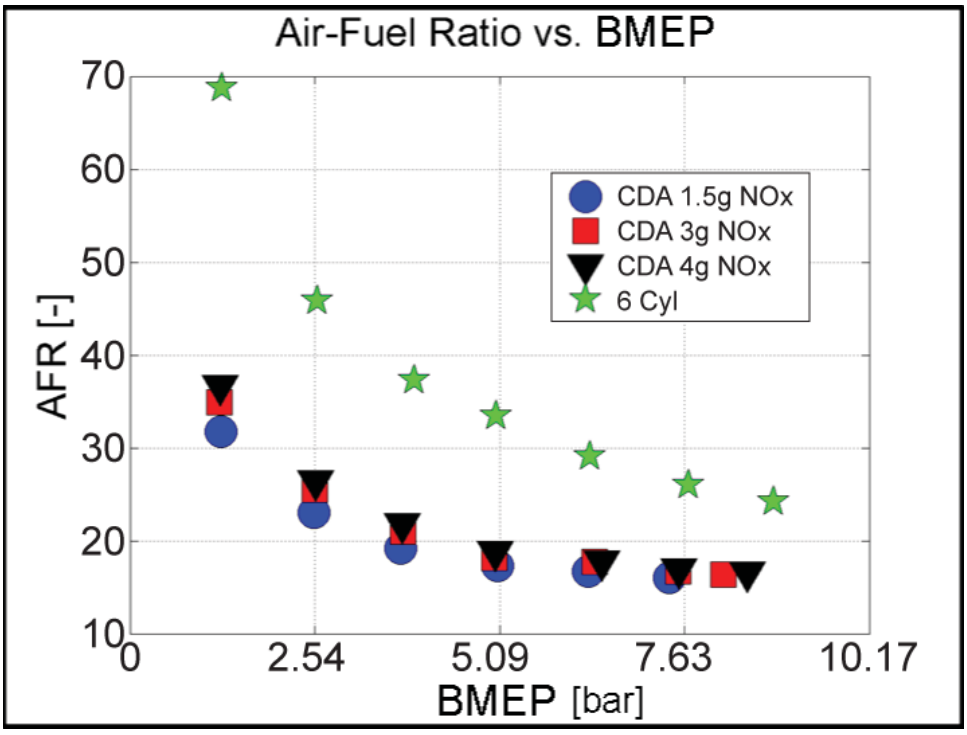

Figure 4.2. Air-fuel ratio results of load sweeps at 1200 rpm.

AFR. As the AFR approaches the stoichiometric value of 14.7, TOT continues to increase significantly.

The impact of CDA on overall BTE is an important factor when determining the effectiveness of the thermal management strategy. BTE results normalized to the maximum 6-cylinder value, are shown in Fig. 4.3. There is an improvement in BTE at 1.3 bar by 5% to 7%. It is worth noting that this efficiency increase also comes with a significant TOT benefit, as described above. By 2.5 bar, the efficiency is approximately equivalent, while CDA still provides a significant TOT benefit. However, at high loads, there is a BTE penalty which is worse for the lower NOx targets. At 7.6 bar, the BTE penalty for the TOT increase realized is about 10% to 15% reduction from the baseline efficiency.

The BTE increase for CDA at low loads is due to an improvement in open cycle efficiency (OCE), as shown in Fig. 4.4. At the lower loads, the exhaust and intake

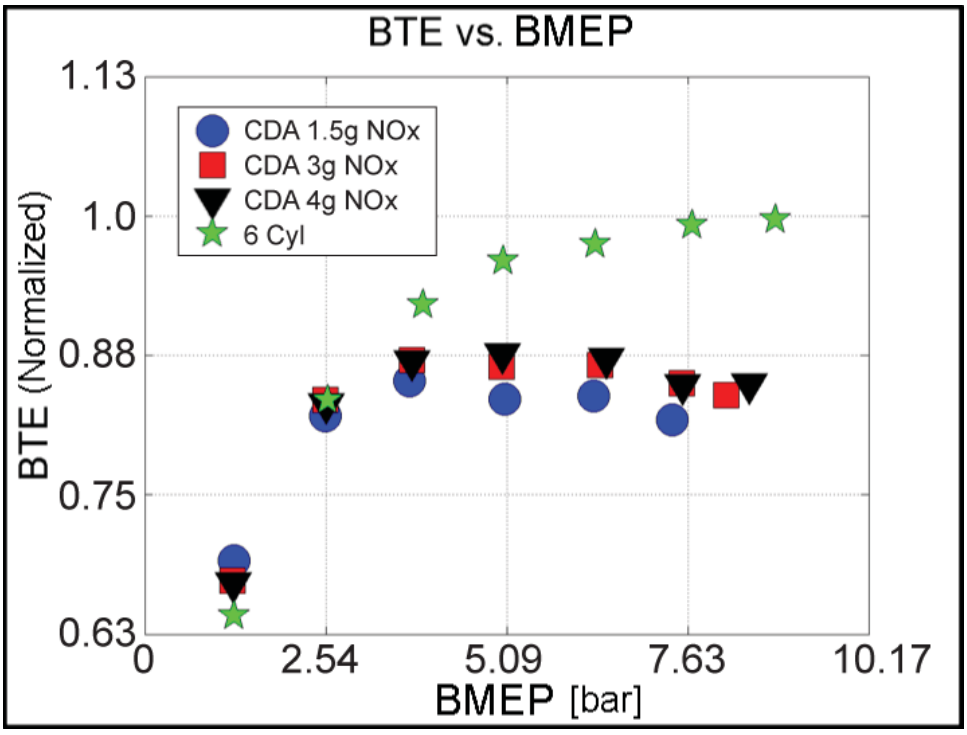

Figure 4.3. Brake thermal efficiency results of load sweeps at 1200 rpm.

manifold pressures are both close to atmospheric, and the VGT is fully open, minimizing the pumping work. At 1.3 bar, there is a 5% increase to OCE. However, this improvement disappears at high loads where higher EGR fractions are required. To meet the requirements, the VGT is closed to build up exhaust manifold pressure driving EGR flow, and increasing the pumping work required.

The closed cycle efficiency (CCE) of the engine is shown in Fig. 4.5, and follows a similar trend as open cycle efficiency. At 1.3 bar, there is an improvement in CCE caused by main injection placement in CDA closer to top dead center (TDC). As the centroid of the heat release rate approaches TDC, combustion becomes more efficient, improving CCE. From 3.8 bar and above, there is a reduction in CCE, due to the delay in main injection timings that are required at higher loads in order to meet the BSNOx targets.

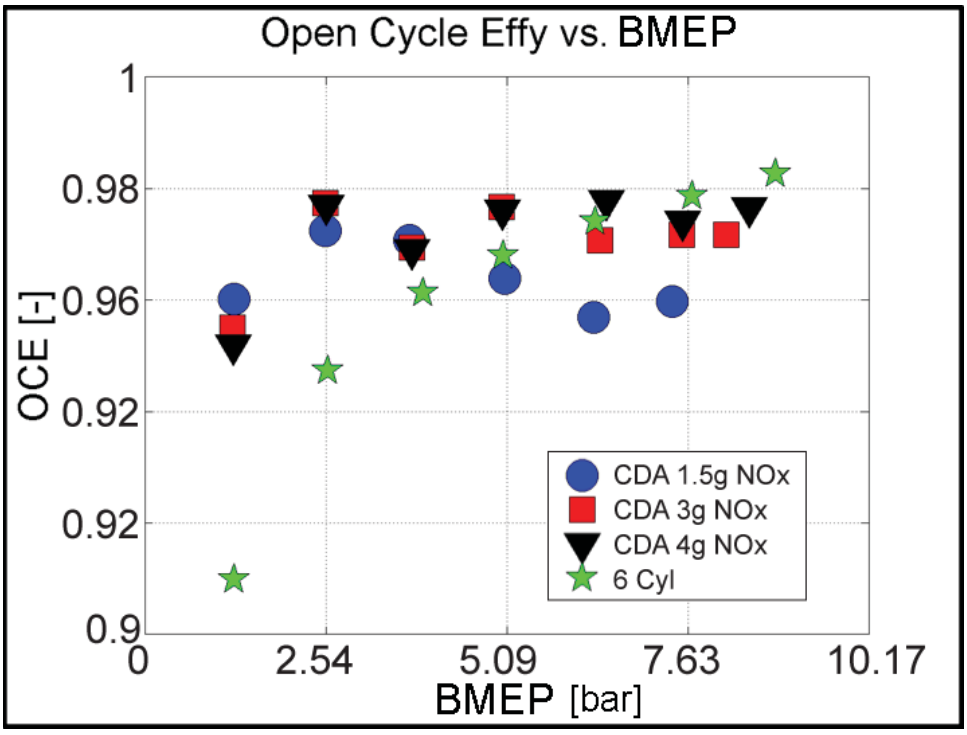

Figure 4.4. Open cycle efficiency results of load sweeps at 1200 rpm.

An example of the delayed heat release is shown in Fig. 4.6. The heat release rates for both 6 and 3 cylinder operation are shown for 7.6 bar at 3 g/hp-hr BSNOx. The crank angle degree (CAD) is displayed on the x-axis. The injector current is also shown in dashed lines for reference. As the injections are pushed later for CDA, the centroid of the heat release is delayed resulting in a reduction in the closed cycle efficiency.

CDA is very effective in raising TOT higher across the load range up to about 7.6 bar as a result of decreased airflow and, therefore, AFR. Therefore, when considering relevant NOx targets, CDA can improve aftertreatment performance up to approximately 7.6 bar (per Fig. 4.1), but there will be an efficiency penalty above 2.5 bar (per Fig. 4.3).

This analysis shows there are significant steady state benefits to CDA operation, especially in TOT, as a result of reduced airflow. However, during transient oper-

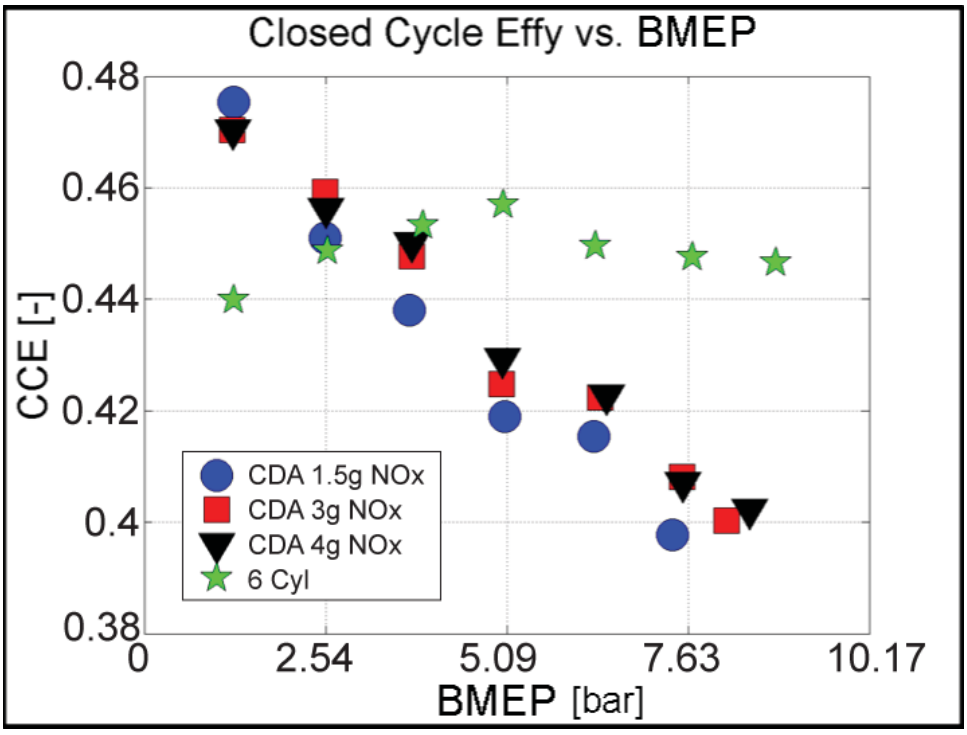

Figure 4.5. Closed cycle efficiency results of load sweeps at 1200 rpm.

ation from low to high loads the reduced airflows achieved during CDA may limit the load responsiveness of the engine. The next section describes an experimental characterization of the limitations of the transient response of an engine operating CDA.

4.2 Transient Analysis

This section describes an analysis that compares the load response required by the federal test procedure (FTP) with the engine response to a load transition in both CDA and 6-cylinder operation.

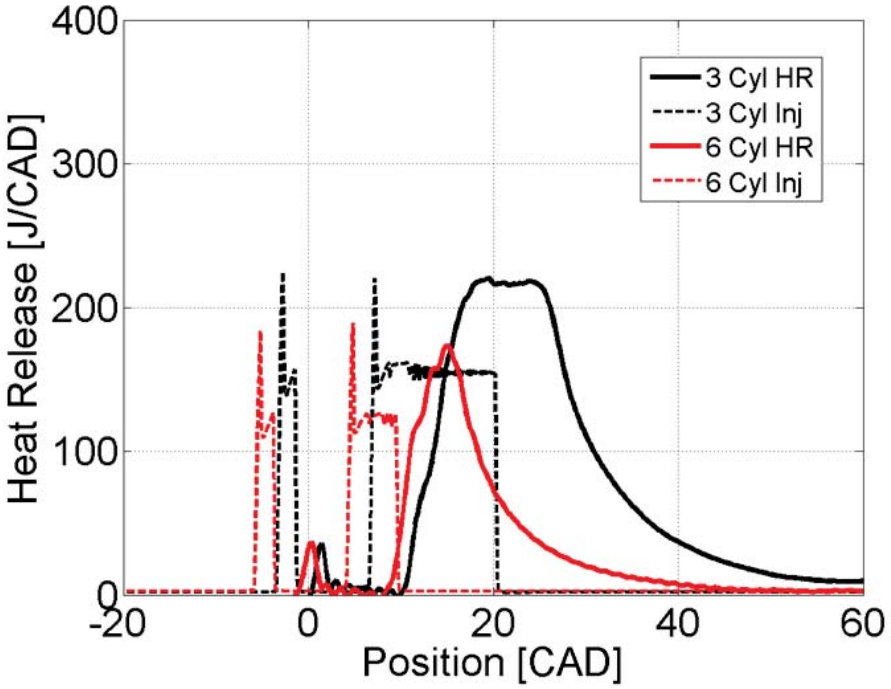

Figure 4.6. Heat release rate profiles and injector current for 6 and 3 cylinder operation at 7.6 bar at 3 g/hp-hr BSNOx.

4.2.1 Methodology

The FTP is a regulatory emissions testing standard designed to replicate various driving cycles in urban and freeway conditions. This procedure, as a dynamic drive cycle test, contains a series of engine load and speed transitions. On-road vehicles must meet the emissions requirements outlined by this procedure when subjected to this test. The load transitions represented in the FTP are also representative of the load response that would be required of an engine. This cycle requires an approximately constant speed load transition from near zero load to about 6.3 bar BMEP within approximately one second. In this study, any experiments that do not meet this response while maintaining other emissions limits were determined to be unable to meet the FTP.

4.2.2 Transient Data Collection

These experiments were attempted at both idle speed (800 rpm) and at cruising speed (1200 rpm). At 800 rpm, the engine cannot be operated with CDA higher than 6.1 bar due to the reduced airflow leading to stoichiometric combustion conditions. Therefore, it was concluded that the test engine cannot meet the torque response required by the FTP at 800 rpm with CDA operation.

At 1200 rpm, the experiments were performed by setting the engine to low load (1.3 bar) and transitioning to 6.4 bar. The setpoints for all inputs at each load were obtained from the steady state load sweep experiments described in the previous section. The CDA inputs were taken from the data points targeting 3 g/hp-hr BSNOx. The start of injection, rail pressure, VGT, and EGR actuators were given a step change command at the time of transition. Multiple methods were used throughout this study to transition the commanded total fueling amount from the low to high values. The fueling command was stepped for the initial experiments. In order to maximize the load response while maintaining proper soot limits, linear ramp and variable fueling strategies were utilized, as will be described later.

It is important to observe emissions limits to maintain a fair comparison between CDA and 6-cylinder operation and the FTP. The assumed transient smoke limit for this effort was 1.5 filter smoke number (FSN). Also, it was assumed that the AFR is to remain above the stoichiometric condition.

Due to the inability to operate the engine with CDA at 800 rpm at a sufficient load to meet the FTP requirements, no data from 800 rpm will be presented here. However, it is noted that CDA operation is limited at lower speed in transient operation. The following section will discuss the results of experiments at 1200 rpm. It will be shown that there is also a challenge in meeting a reasonable torque response at 1200 rpm with CDA operation.

4.2.3 Transient Results

The initial experiments involved a step change of all inputs, including fueling amount. This was performed in both 6-cylinder and CDA operation. The BMEP, AFR, and soot responses are each shown in Fig. 4.7. The commanded fueling for each experiment is also shown for reference. The fueling command is normalized to values of zero to one with zero being the initial value and one being the fueling consistent with the higher load condition. Experiments are time aligned such that the point of transition is set to 0.5 seconds. BMEP is from the load measured at the dynamometer. The AFR is calculated from the measured airflow through the LFE and commanded fueling quantity. The soot response is from an AVL Micro Soot 483 Analyzer. There is almost no noticeable change in soot for the 6-cylinder baseline experiment. Even with a step fueling change, the AFR only reduced to $\sim$20. A step fueling strategy for 6-cylinder operation represents the fastest possible transition while maintaining acceptable limits. However, a step fueling input with CDA yielded soot much greater than the assumed 1.5 FSN limit. Note that the calculation for FSN from soot concentration does not resister at numbers above 5 FSN. This soot response comes from an AFR below 10 and also inhibits the load response. As such, the engine needs a different fueling method for the load transition during CDA operation.

In order to reduce the soot generation during a load transition with CDA a linear ramp fueling input strategy was explored. This was used as an effort to allow the airflow to increase faster than the fueling in order to keep the AFR high enough to avoid excessive soot generation. While the fueling input strategy was modified, all other inputs were stepped to the new values at the time of transition. The fueling ramp rate was specified in milligrams per stroke per second (mg/st/sec). Experiments were conducted with various ramp rates until the soot response was within the limit. Fig. 4.8 shows the response of two different ramp rates compared with the 6-cylinder baseline step fueling case. The amount of time it took to reach the higher fueling setpoint is displayed next to the fueling strategy label in the legend. As shown in

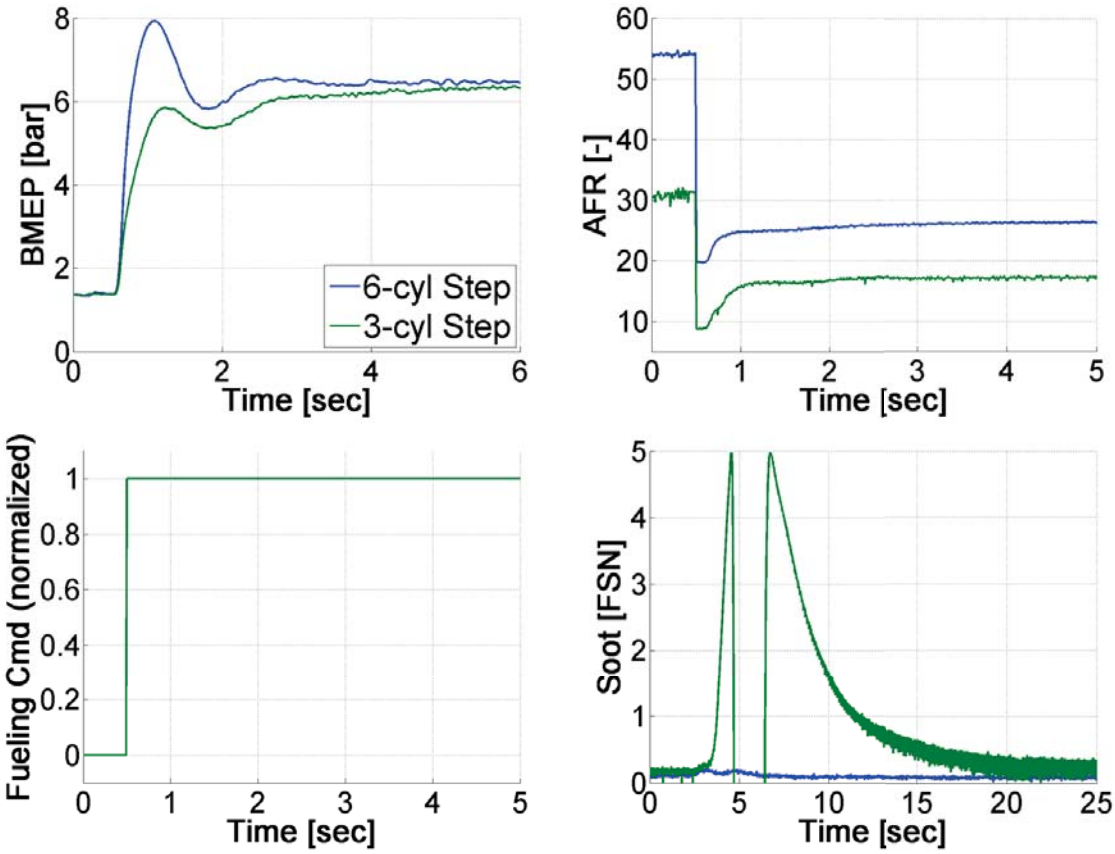

Figure 4.7. Transient responses showing BMEP, AFR, fueling, and soot for 6 and 3 cylinder step fueling.

the plots, the fueling ramp rate must be quite slow to maintain a soot level below 1.5 FSN. The fastest transition time with a ramp fueling input is ∼2.8 seconds. This is much slower than the FTP which requires a load transition in approximately 1 second.

A variable fueling strategy was implemented as a means to reduce the soot generation during a load transition. This fueling strategy was designed as a series of linear ramps with the ability to change the ramp rate three times during the transition period. Examples of these variable fueling profiles are shown in Fig. 4.9. These experiments were variations on the ramp fueling experiment with a 2.33 second transition time and a soot peak greater than the 1.5 limit. Each fueling profile used

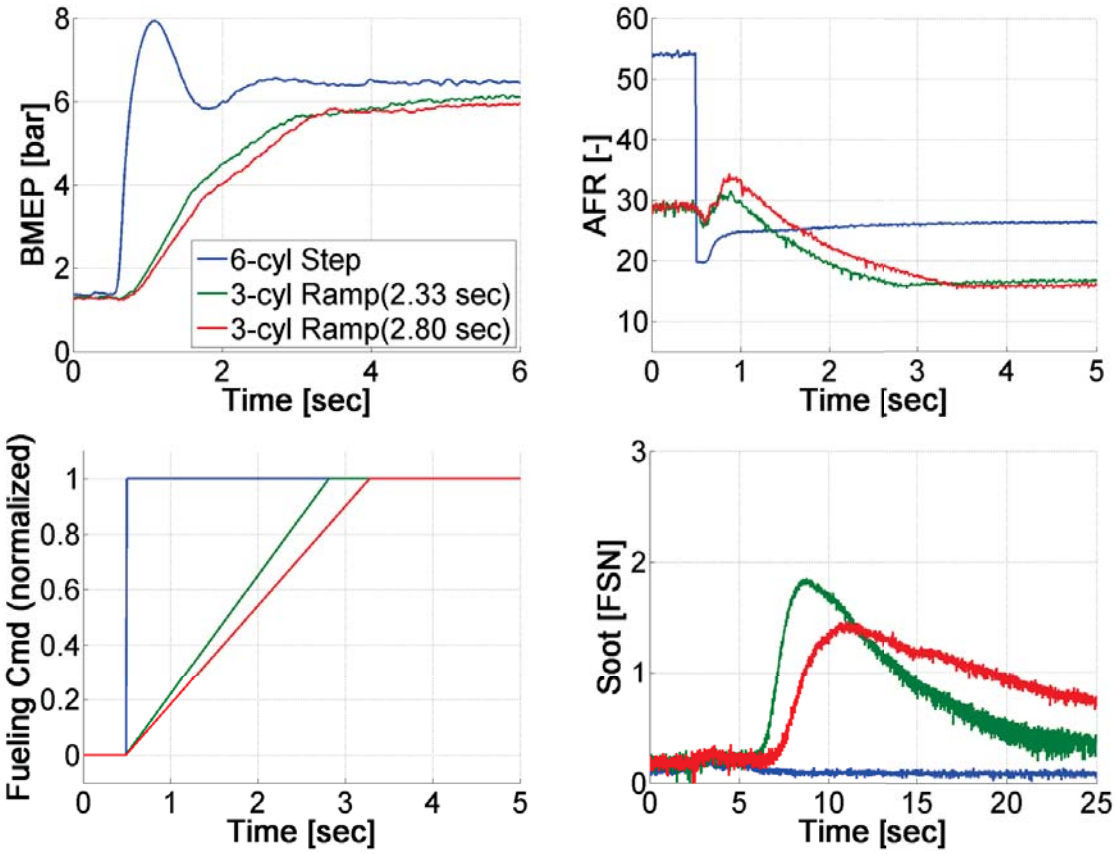

Figure 4.8. Transient responses showing BMEP, AFR, fueling, and soot for 6 cylinder step and 3 cylinder ramp fueling.

was varied in an attempt to reduce the peak soot concentration. It was found that no fueling profile could significantly reduce the soot measured from the linear ramp fueling case. This was due to the low AFR that occurs as the fueling reaches the maximum value. The results indicate that the way to increase the minimum AFR is to slow down the ramp rate or increase the time to transition between the operating conditions. As shown in the BMEP plot, no variable fueling strategy could improve the overall load response.

Since the transition cannot be made within a reasonable time at such a low steady state AFR, transient experiments were conducted with a transition to the high load condition (6.3 bar) with a higher steady state AFR. This was accomplished by remov-

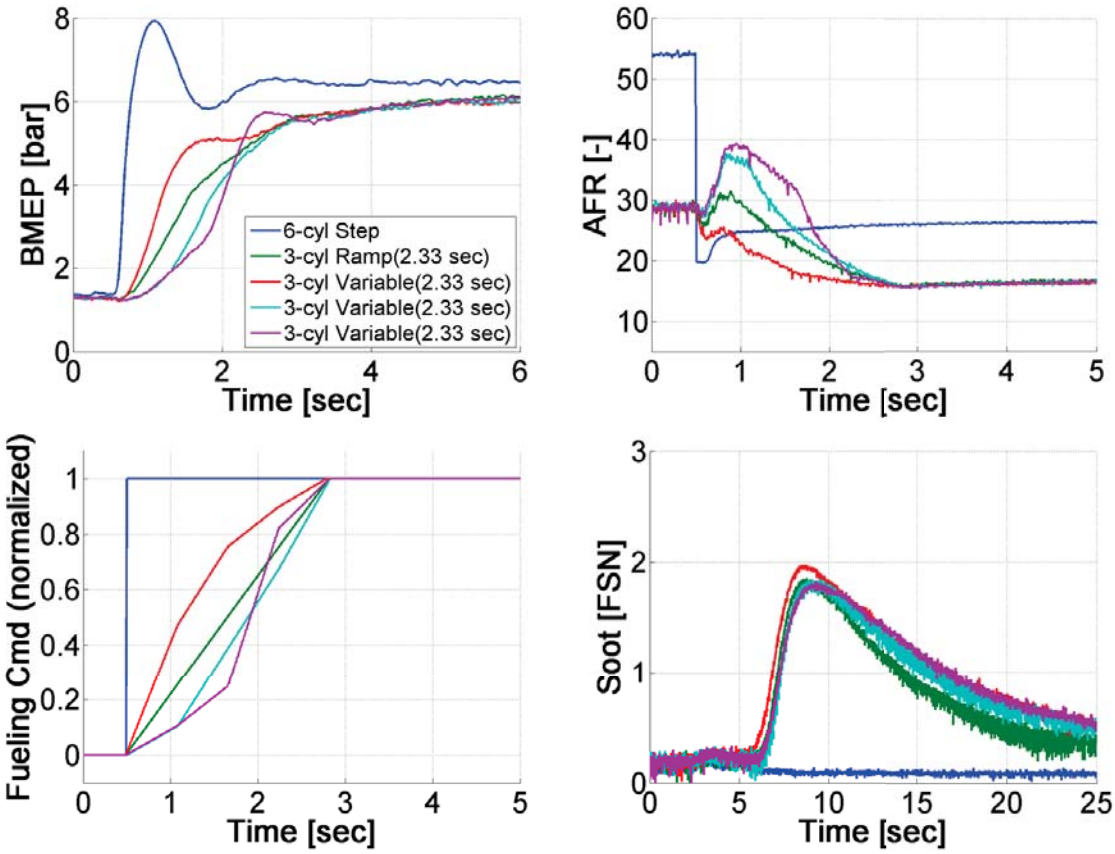

Figure 4.9. Transient responses showing BMEP, AFR, fueling, and soot for 6 cylinder step and 3 cylinder variable fueling.

ing the EGR at the higher load point by setting the EGR valve position to zero at the time of transition. This change allows airflow to increase to a higher value. The reduction of EGR also increases the NOx, which no longer is kept within the target range as discussed in the first section. to achieve 6.3 bar reduced which also increases AFR. The elimination of EGR causes the steady state AFR to increase from ∼18 to ∼21.

A ramp fueling strategy was again used to explore the potential responses for the case with "relaxed" (i.e. higher) high load AFR. Fig. 4.10 shows the responses of two additional experiments in comparison to the ramp fueling experiment at a steady state AFR of 18 previously shown. As shown, the fueling ramp rate was increased

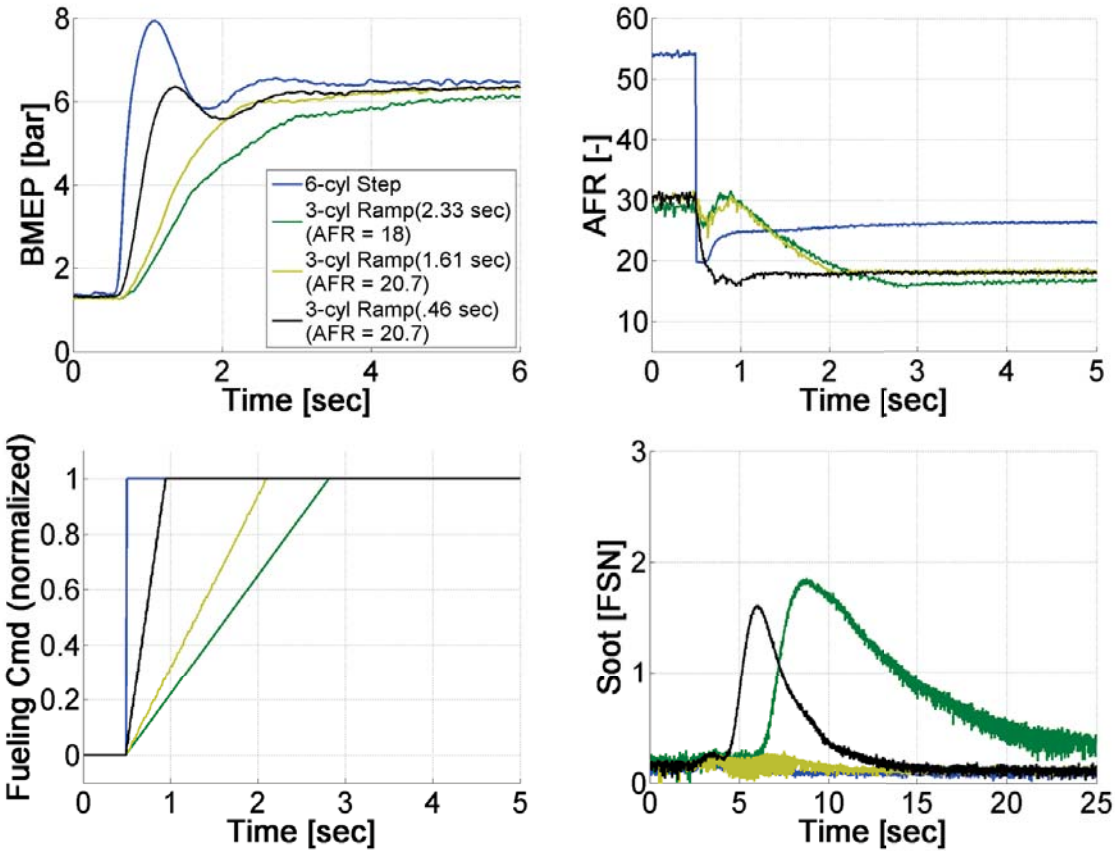

Figure 4.10. Transient responses showing BMEP, AFR, fueling, and soot for 6 cylinder step and 3 cylinder ramp fueling at an elevated steady state AFR of 20.7.

until the 1.5 FSN soot limit was violated and resulted in a reduction in the transition time from 2.33 to 0.46 seconds.

A variable fueling strategy was again used to attempt to reduce the soot response with a transition time of 0.46 seconds. Two of these responses are shown in Fig. 4.11. The fueling profiles were designed to start with slower ramp rates and end with elevated ramp rates to allow time for the airflow to increase. The experiment shown in red indicates that a variable fueling strategy may be enough to reduce the soot peak to a value below 1.5 FSN. This shows that 0.46 seconds is approximately the fastest fueling transition time possible between the two given load setpoints while

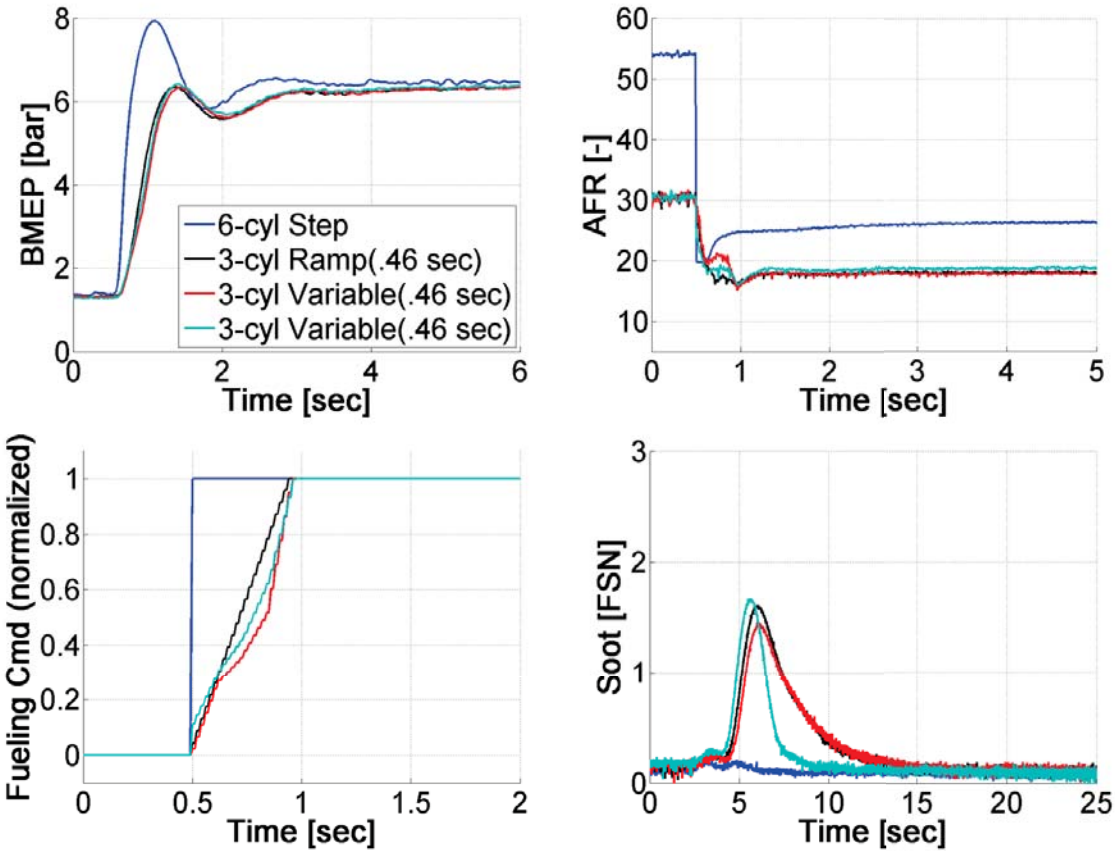

Figure 4.11. Transient responses showing BMEP, AFR, fueling, and soot for 6 cylinder step and 3 cylinder variable fueling at an elevated steady state AFR of 20.7.

maintaining a reasonable soot response. As shown in the BMEP plot, this effect of varying the fueling ramp rates is small on the load response.

As described above, in order to reduce the load transition time, the steady state AFR was increased at the 6.3 bar operating condition. This causes negative effects on TOT and BSNOx. The TOT at 6.3 bar was reduced ~60°C from 512°C to 480°C. This represents a significant drawback because thermal management is the primary advantage for operating CDA at this condition. In addition, as mentioned above, the BSNOx target is not met at the elevated AFR point; BSNOx increases from 3.2 to 10.3 g/hp-hr.

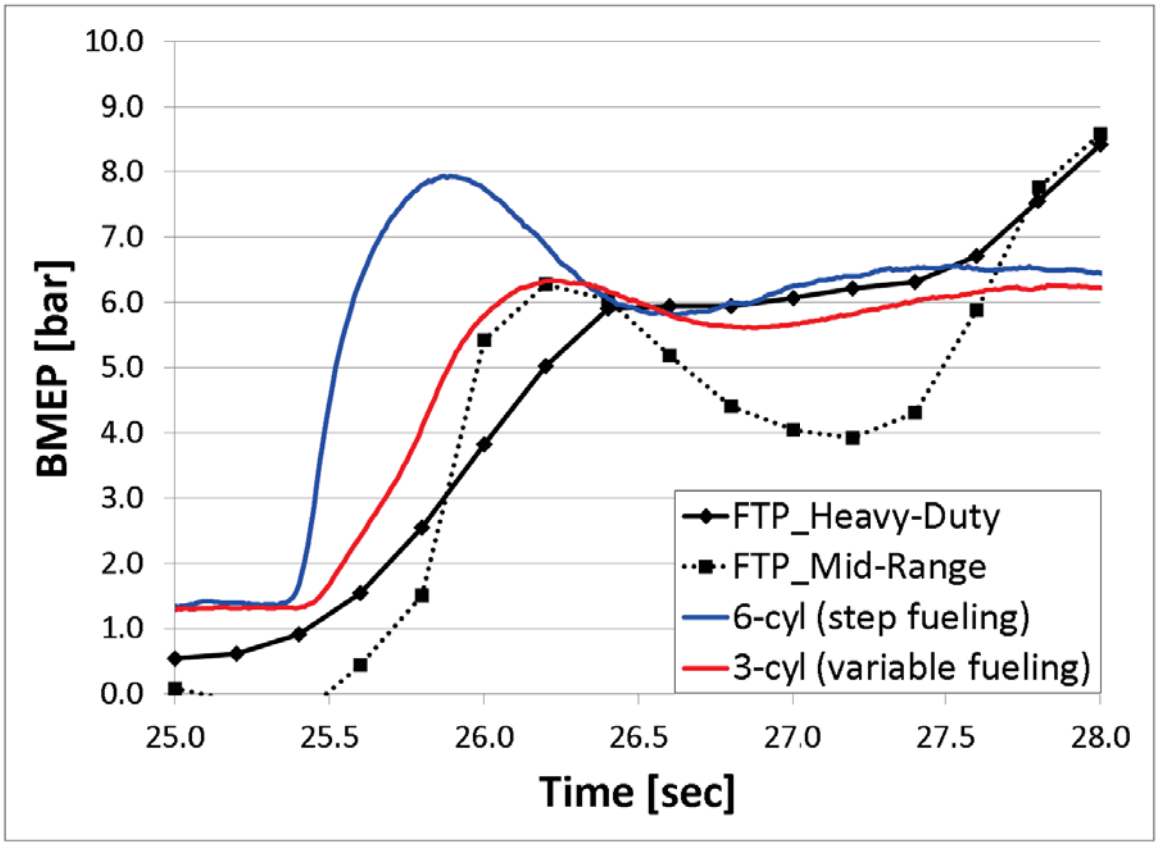

Figure 4.12. Comparison of 6 and 3 cylinder load responses with both heavy-duty and mid-range FTP cycles.

The CDA load response using a variable fueling strategy as well as the 6-cylinder step fueling experiment were compared to a typical load transition in the FTP, as shown in Fig. 4.12. The experimental load responses were compared with both the heavy-duty and mid-range cycles. The start of transition was assumed to be at 25.3 seconds into the FTP. The 6-cylinder BMEP response rate is more than adequate for the required load transitions. The CDA load response is consistent with the heavy-duty FTP cycle but not the medium duty one.

4.3 Summary

In this chapter, experimental results were discussed for both steady state and transient operation of a diesel engine utilizing cylinder deactivation. The steady state experiments involved a load sweep at 1200 rpm. These results showed promising benefits to CDA both for thermal management as well as efficiency at low load. CDA yields a TOT increase by more than 88°C at 1.3 bar and about 160°C at 6.4 bar. In addition, BTE is increased by 5% to 7% at 1.3 bar.

The reduced airflow that comes from deactivating three cylinders was shown to cause issues when attempting to meet the load transitions required by the FTP. It was observed that at 800 rpm CDA cannot be run at high enough load to meet the first load transition of the FTP. At 1200 rpm, it was found that the mid-range FTP cycle cannot be met with any fueling strategy or by relaxing the benefit of CDA at higher loads via higher steady state AFRs. However, the heavy-duty cycle can be met by increasing the steady state AFR at 6.3 bar from ∼18 to ∼21, decreasing the TOT by 60°C. Also, NOx is increased from 3.2 to 10.3 g/hp-hr with a decrease in EGR to raise the airflow.

5. CONCLUSIONS AND FUTURE WORK

5.1 Conclusions

Modern diesel aftertreatment systems are effective in reducing emissions, however they must operate at sufficiently high temperatures. Thermal management is a means to provide these systems with the heat energy they need for efficient operation. The objective of this work was to explore the potential benefits of two strategies involving variable valve actuation for aftertreatment thermal management, namely early exhaust valve opening and cylinder deactivation. This effort describes the quantification of the benefits and penalties of exhaust temperature and fuel economy, respectively. In addition, the potential challenges for CDA during transient operation were also investigated.

The first technology discussed in this work was EEVO. This section described how a model was developed for determining the impact of EEVO on both turbine out temperature and brake thermal efficiency. This work utilizes a first-law energy balance analysis with data from experimental EEVO sweeps to develop generalizations about how temperature and fuel consumption are increased as EVO is advanced. The model was validated at a wide range of engine speeds, from 800 rpm to 2200 rpm and at loads up to about 7 bar. The model analysis shows that EEVO can cause a significant increase in exhaust temperature; however, the fuel consumption penalty is also large.

Due to the significant fuel consumption penalty observed as a result of EEVO, CDA was studied in the following chapter. The focus of the work in this section was at idle (both loaded and unloaded) at which condition thermal management has room for significant temperature and efficiency improvements. This experimental based effort utilized design of experiments and constrained optimization to compare the exhaust temperature benefit and the corresponding efficiency impact relative to the optimized

6-cylinder case. The results showed enough temperature increase for aftertreatment effectiveness at loaded idle with no fuel economy penalty. The temperature increase was not significant at unloaded idle, but CDA operation showed to have a large fuel economy benefit.

CDA shows to be a promising thermal management strategy; deactivating three of six cylinders yields a large exhaust temperature increase with fuel consumption reduction at low loads. The next section discussed an experimental load sweep screening effort at cruising speed and all possible loads. The operating conditions studied in this work were then utilized in a transient analysis of how CDA load response compares with the FTP during a load transition. Results of the load sweep screening are consistent with the optimization work completed focusing on CDA operation at idle. Specifically, there is an efficiency improvement with CDA at loads below 1.3 bar, with a significant exhaust temperature increase at all loads. However, there was found to be drawback to CDA during transient operation. The tests showed that the test engine could not meet the load response required by the FTP at either 800 rpm or 1200 rpm with operating conditions focused on maximizing exhaust temperature. A relaxed air-fuel ratio condition allowed for experiments to meet a heavy-duty FTP cycle load response within emissions limits. These results indicate a tradeoff between maximizing thermal management benefits and allowing for fast transient load transitions.

The results of the work presented in this thesis indicate that at steady state low load operation CDA is an ideal aftertreatment thermal management strategy due to the large temperature gains with improved fuel economy. However, this strategy cannot be used at higher loads and may not be sufficient for transient operation. For aftertreatment warm up over a variety of drive cycles, other thermal management strategies may be needed, if the transient challenges with CDA cannot be solved.

5.2 Future Work

Thermal management of aftertreatment is not a simple problem. It is dynamic with multiple systems that need to work together, each with high efficiency, in order to increase overall system efficiency. There are a plethora of strategies that have been researched which are effective in raising exhaust gas temperatures for improved thermal management. Some of these methods are more efficient than others, and some are more suited to particular applications or drive cycles. Since all strategies have some tradeoffs between efficiency and temperature, it is important to know which strategy will provide adequate thermal management benefit with the smallest fuel consumption penalty. It is imperative that the aftertreatment system operate at near maximum efficiency. The thermal management strategy that can enable this most efficiently has potential to improve the efficiency of the whole system.

This thesis described a detailed analysis for EEVO and CDA. The steady state benefits in temperature and the associated benefits/penalties in brake thermal efficiency have been discussed. Future work will include the comparison of these two strategies over a transient drive cycle to determine the effectiveness of each on heating up the catalysts in the aftertreatment system. The conclusions made in this thesis could inform a simulation analysis to be performed with transient aftertreatment temperature models. Both EEVO and CDA should be compared with more conventional thermal management strategies, especially those that are use in modern production engines. In addition, multiple VVA based strategies could be combined to further improve the benefits observed in this work. This would inform if implementation of either strategy (or both) would help to improve overall vehicle efficiency.

The fourth chapter of this thesis also describes the challenges for transient operation of CDA. Future work could involve research into potential solutions to this transient problem. One simple strategy could be the transition to fewer deactivated cylinders. This would increase airflow quickly and has the potential to allow for faster transition times. However, this just allows for a load increase after CDA operation. If

CDA is desired even after a load transition other solutions will need to be developed. Some potential solutions that could be involved in future work are electrification of the turbo-machinery, powertrain hybridization, or supercharging.

LIST OF REFERENCES

LIST OF REFERENCES

[1] Steve Charlton, Thomas Dollmeyer, and Thomas Grana. Meeting the us heavy-duty epa 2010 standards and providing increased value for the customer. *SAE International Journal of Commercial Vehicles*, 3(1):101–110, 2010.

[2] Donald W Stanton. Systematic development of highly efficient and clean engines to meet future commercial vehicle greenhouse gas regulations. *Diesel Engine*, 2013:05–16, 2013.

[3] *Meeting EPA 2010*. http://www.factsaboutscr.com/scr/engine-control-standards.aspx, June 2008.

[4] Timothy V Johnson. Vehicular emissions in review. *SAE International Journal of Engines*, 5(2):216–234, 2012.

[5] Mojghan Naseri, Raymond Conway, Howard Hess, and Ceren Aydin. Development of emission control systems to enable high nox conversion on heavy duty diesel engines. 2014.

[6] Donald Stanton, Stephen Charlton, and Phani Vajapeyazula. Diesel engine technologies enabling powertrain optimization to meet us greenhouse gas emissions. *SAE International Journal of Engines*, 6(3):1757–1770, 2013.

[7] Jeffrey Seger, Long-Kung Hwang, Josh Shao, Thomas Grana, and Steve Charlton. Systems engineering approach for the design of a low carbon, fuel efficient, diesel engine powertrains for commercial vehicles. Technical report, SAE Technical Paper, 2011.

[8] Stephan Stadlbauer, Harald Waschl, Alexander Schilling, and Luigi del Re. Doc temperature control for low temperature operating ranges with post and main injection actuation. Technical report, SAE Technical Paper, 2013.

[9] X Song, H Surenahalli, J Naber, G Parker, et al. Experimental and modeling study of a diesel oxidation catalyst (doc) under transient and cpf active regeneration conditions. *Diesel Engine*, 2007:10–01.

[10] Ronny Allanson, Phillip Blakeman, Barry Cooper, Howard Hess, Peter Silcock, and Andrew Walker. Optimising the low temperature performance and regeneration efficiency of the continuously regenerating diesel particulate filter (cr-dpf) system. *Development*, 2012:05–10, 2002.

[11] Matthias Bouchez and Jean Baptiste Dementhon. Strategies for the control of particulate trap regeneration. *SAE transactions*, 109(4):220–226, 2000.

[12] AP Walker. Controlling particulate emissions from diesel vehicles. *Topics in catalysis*, 28(1-4):165–170, 2004.

[13] Christine Lambert, Robert Hammerle, Ralph McGill, Maadi Khair, and Christopher Sharp. Technical advantages of urea scr for light-duty and heavy-duty diesel vehicle applications. *SAE transactions*, 113(4):580–589, 2004.

[14] Manfred Koebel, Martin Elsener, and Michael Kleemann. Urea-scr: a promising technique to reduce nox emissions from automotive diesel engines. *Catalysis Today*, 59(3):335–345, 2000.

[15] James Girard, Giovanni Cavataio, Rachel Snow, and Christine Lambert. Combined fe-cu scr systems with optimized ammonia to nox ratio for diesel nox control. *SAE International Journal of Fuels and Lubricants*, 1(1):603–610, 2009.

[16] Harald Fessler and Marco Genova. An electro-hydraulic lost motion vva system for a 3.0 liter diesel engine. *SAE transactions*, 113(3):1639–1649, 2004.

[17] Paramjot Singh, Abishek M Thalagavara, Jeffrey D Naber, John H Johnson, and Susan T Bagley. *An experimental study of active regeneration of an advanced catalyzed particulate filter by diesel fuel injection upstream of an oxidation catalyst.* PhD thesis, Michigan Technological University, 2006.

[18] Jim Parks, Shean Huff, Mike Kass, and John Storey. Characterization of in-cylinder techniques for thermal management of diesel aftertreatment. *studies*, 10:11, 2007.

[19] A Mayer, Th Lutz, Chr Lämmle, M Wyser, and F Legerer. Engine intake throttling for active regeneration of diesel particle filters. *Development*, 2005:24–082, 2003.

[20] T Akiyoshi, H Torisaka, H Yokota, T Shimizu, et al. Development of efficient urea-scr systems for epa 2010-compliant medium duty diesel vehicles. *Diesel Engine*, 2012:06–18.

[21] Chang Hwan Kim, Michael Paratore, Eugene Gonze, Charles Solbrig, and Stuart Smith. Electrically heated catalysts for cold-start emissions in diesel aftertreatment. Technical report, SAE Technical Paper, 2012.

[22] John A Schwoerer, Krishna Kumar, Brian Ruggiero, and Bruce Swanbon. Lost-motion vva systems for enabling next generation diesel engine efficiency and after-treatment optimization. *Training*, 2013:10–14, 2010.

[23] GB Parvate-Patil, H Hong, and B Gordon. Analysis of variable valve timing events and their effects on single cylinder diesel engine. *SAE transactions*, 113(3):1510–1519, 2004.

[24] William De Ojeda. Effect of variable valve timing on diesel combustion characteristics. *SAE paper*, pages 01–1124, 2010.

[25] Akash Garg, Mark Magee, Chuan Ding, Leighton Roberts, and Greg Shaver. Exhaust thermal management using cylinder throttling via intake valve closing timing modulation. Manuscript submitted for publication, 2013.

[26] Sebastian Gehrke, Dávid Kovács, Peter Eilts, Alexander Rempel, and Peter Eckert. Investigation of vva-based exhaust management strategies by means of a hd single cylinder research engine and rapid prototyping systems. *SAE International Journal of Commercial Vehicles*, 6(1):47–61, 2013.

[27] Anders Wickström. *Variable valve actuation strategies for exhaust thermal management on a HD diesel engine.* Master's thesis, Stockholm, Sweeden, 2012.

[28] S Honardar, H Busch, T Schnorbus, C Severin, et al. Exhaust temperature management for diesel engines assessment of engine concepts and calibration strategies with regard to fuel penalty. *Measurement*, 2012:04–13, 2011.

[29] Ryo Kitabatake, Akihiko Minato, Naoki Inukai, and Naoki Shimazaki. Simultaneous improvement of fuel consumption and exhaust emissions on a multicylinder camless engine. *SAE International Journal of Engines*, 4(1):1225–1234, 2011.

[30] Mark Magee. *Exhaust Thermal Management Using Cylinder Deactivation.* Master's thesis, Purdue University, West Lafayette, Indiana, 2013.